AN ABSTRACT OF THE THESIS OF

William Stanley French (Name) for the Doctor of Philosophy (Degree)

in Geophysics (Degree) presented on October 14, 1969 (Date)

Title: EARTHQUAKE WAVES FOLLOWING THE P_n PHASE AND THEIR INDICATIONS OF FOCAL DEPTH AND CRUSTAL STRUCTURES IN THE PACIFIC NORTHWEST STATES

Abstract approved Peter Dehlinger

The nature of "Post-P_n" phases on seismograms, which includes several distinct phases which arrive for about 10 seconds after P_n but before the P^* phase, were investigated theoretically and then verified on seismograms from local earthquakes in the Pacific Northwest states. The analysis applies to earthquakes occurring within the crust and recorded at epicentral distances from 150 to 1000 km. Eight different mechanisms that would account for the Post-P_n waves were hypothesized and compared with numerous earthquake recordings for their acceptability.

The only mechanism which satisfactorily explains the observed data, and in fact can be shown theoretically to produce synthetic seismograms that are in remarkable agreement with earthquake seismograms, consists of various head waves reflected at the surface

or converted at the Mohorovicic discontinuity. From theoretical analyses it is possible to identify the paths of the various second arrival head waves, the two most prominent being an $\uparrow S_1 P_1 P_2 P_1$ (sP_n) and an $\downarrow S_1 P_2 P_1$ wave. By measuring time intervals between the various identified second arrivals and P_n, it is possible to determine focal depths of small crustal shocks with marked accuracy, using seismograms from only a few (even one) recording station and no knowledge of origin time. It is also possible to obtain estimates on crustal thicknesses beneath either the source or station, or both (depending on the particular phases identified), from these analyses.

The theory developed was used to determine focal depths of rather small earthquakes in the Pacific Northwest area. Depths ranged from 4 to 16 km in seven shocks (magnitude range $3\frac{1}{2}$ to 5) that occurred in 1962 and 1963.

Earthquake Waves Following the P_n Phase and Their Indications of Focal Depth and Crustal Structures in the Pacific Northwest States

by

William Stanley French

A THESIS

submitted to

Oregon State University

in partial fulfillment of
the requirements for the
degree of

Doctor of Philosophy

June 1970

APPROVED:

Redacted for Privacy

Professor of Geophysics
in charge of major

Redacted for Privacy

Chairman of Department of Oceanography

Redacted for Privacy

Dean of Graduate School

Date thesis is presented October 14, 1969

Typed by Nancy Kerley for William Stanley French

ACKNOWLEDGMENTS

This research was performed under the direction of Dr. Peter Dehlinger, Professor of Geophysics at Oregon State University.[1] I am grateful to Dr. Dehlinger for initiating and suggesting this project, for many helpful discussions during the research, and for critically editing the manuscript.

Appreciation is extended to my colleague Dr. R. W. Couch for the many discussions we held concerning parts of this research.

---

[1] Present address: Director, Institute of Marine Sciences, The University of Connecticut.

TABLE OF CONTENTS

TABLE OF CONTENTS (continued)

LIST OF TABLES

LIST OF FIGURES

LIST OF FIGURES (continued)

LIST OF FIGURES (continued)

EARTHQUAKE WAVES FOLLOWING THE P_n PHASE AND THEIR INDICATIONS OF FOCAL DEPTH AND CRUSTAL STRUCTURES IN THE PACIFIC NORTHWEST STATES

INTRODUCTION

Analyses of the times required for seismic energy to traverse various paths within the earth provide diagnostic information about average physical properties of the materials composing the earth. The data available for analysis consist of recordings of earth motion at stations on or near the surface of the earth. These recordings are made at various epicentral distances, i.e. surface distance between source and receiver. In the case of artificial seismic sources (e.g. chemical or nuclear explosions), the distances are usually known precisely. This is not the case for natural seismic sources, where epicentral distances must be determined from the recordings themselves. In both cases, however, the ray paths traversed between source and receiver must be determined from recordings at surface stations.

In seismology, a "phase" is any distinctive activity or wave group on a recording of the vibrations at the earth's surface. Time-distance charts are constructed by plotting the arrival times of the phases as a function of epicentral distance. The origin time of the earthquake can be determined by various standard methods, and this time has been used as the time origin on the recordings. The

time-distance charts and the individual seismograms can be examined to determine if any of the phases are correlative from one epicentral distance to the next. Such correlations are based upon the character or shape of the wave forms and on the smoothness of the curve connecting the arrival times of phases recorded at different distances. The time-distance or travel-time curves have been found to exhibit individual characteristics for every region. These curves represent constraints which must be satisfied by models of the structure of the earth.

It is usually the case that phases are observed on seismograms which are not associated with any of the plotted travel-time curves. Certain of these heretofore uncorrelated phases are the subject of this thesis. The specific phases of interest will be discussed shortly.

Local travel-time curves were constructed by Dehlinger et al. (1965) for earthquakes that occurred in the Pacific Northwest states. The observed travel-time data were found to fit two distinct sets of curves. One set was characteristic of waves that were recorded in the region west of the Cascade Range, while a different set was characteristic of waves recorded east of these mountains. The sparsity of seismic stations in the Pacific Northwest states did not allow detailed recording in the epicentral range from 0 to 120 km. Quite adequate station coverage was obtained for epicenters between 120 and 1000 km.

Travel-time curves for the P_n and P* phases in the region east of the Cascade Range were found to obey the following relations:

$$T_{P_n} = 6.62 + \Delta/7.96$$

$$T_{P^*} = 3.55 + \Delta/6.60$$

T_{P_n} and T_{P^*} are times, in seconds, required for these two phases to travel from the earthquake source to a station at an epicentral distance Δ, measured in kilometers.

Statistical tests applied to the travel-time data verified that the assumption of a linear expression for the P_n phase was justified. The linearity of the travel-time curve leads to the usual interpretation that the P_n phase is a head wave associated with the crust-mantle boundary. The P* phase is assumed to be a head wave associated with an intermediate crustal discontinuity (described in Richter, 1958, p. 284).

It is seen from the above expressions that the P_n and P* phases arrive simultaneously at an epicentral distance of 118.4 km, and that differences in their arrival times vary linearly with epicentral distance. Thus, the P* phase arrives 22.9 seconds later than the P_n phase at a distance of 1000 km. As is well known, however, seismograms exhibit the arrival of seismic energy between the arrival times of the P_n and P* phases; this recorded energy is not associated with other refracting layers in the earth, and it must have other explanations regarding its origin. In particular, it was

noted during the construction of the travel-time curves that the initial P_n motion on seismograms is usually followed by a second phase arriving 3± 2 seconds after P_n. The amplitude of this second phase may be 3 to 4 times larger than that of P_n (e.g., Dehlinger, 1964; Dehlinger and French, 1965). A further examination of seismograms of local earthquakes in the Pacific Northwest states indicated that there are usually several distinct onsets of seismic energy between the arrivals of the P_n and P* phases; these phases will be referred to collectively as "Post-P_n phases." The first phase after P_n will be referred to as the "Post-P_n" phase, the next as the "Second Post-P_n" phase, etc.

An investigation of these "Post-P_n phases" is needed to determine the nature of these waves and to decide whether they might be diagnostic in determining earthquake focal depths, earthquake source mechanisms, or crustal structures in the source or recording regions.

PURPOSE OF THE INVESTIGATION

The purpose of this investigation is to examine various hypotheses concerning the origin of the Post-P_n phases on the recordings of local earthquakes in the Pacific Northwest states. The epicentral-distance range of interest will be from 120 to 1000 km as the P_n phase is the first arrival on recordings made in this range. The P_n phase has been extensively studied and provides a sound basis for examining phases which travel with velocities nearly equal to that of the P_n phase.

The first large amplitude phase following P_n, the Post-P_n phase, is of particular interest. However, it is also necessary to consider later phases in view of the possibility that several events may be related.

Finally, the theory developed on the origin of Post-P_n waves will be used to analyze data for specific earthquakes.

PREVIOUS WORK AND PRELIMINARY CONSIDERATIONS

Seismometers of various degrees of sophistication have been used to record vibrations of the surface of the earth since about 1880. The origins of various phases on the recordings of earth motion, including the Post-P_n phases, have been the subject of many investigations. Investigations relating to the Post-P_n phases are described in this study under the following subjects:

1) Instrumental effects,

2) Reflected phases,

3) Signal-generated noise,

4) Second source motion,

5) Wave conversions by crustal discontinuities,

6) Head wave multiples.

This investigation is concerned only with Post-P_n phases recorded in the epicentral range from 120 to 1000 km. Clearly, explanations of second arrivals in this range must also be consistent with observations of such phases at both shorter and longer distances. Therefore, the results cited below include some analyses of recordings made outside of the 120 to 1000 km epicentral distance range.

Instrumental Effects

Seismometers consist of a mass suspended on either a vertical or horizontal spring within a seismometer case. The seismometer case follows the vibrations of the earth, and the differential motion between the case and suspended mass is usually converted into an electrical signal. In modern seismometers this conversion is accomplished by either the movement of a coil in a fixed magnetic field (electromagnetic or moving-coil seismometer) or by changing the air gap in a magnetic circuit on which a fixed pick-up coil has been mounted (variable-reluctance seismometer). The resultant electrical signal is then used as the input to a galvanometer or other recording device. The galvanometer employes an optical lever with subsequent recording along with time fiducials on a photographic film or paper attached to a constantly rotating drum. Both the moving-coil and variable-reluctance seismometers utilize electrical damping of the mass and of the recording galvanometer. The complete instrumentation is referred to as the seismograph and the continuous record of earth motion as the seismogram.

The theoretical response of an electromagnetic seismograph has been derived by Hagiwara (1958). The calculations were carried out for a simple harmonic input of infinite duration. The resulting seismogram is a simple harmonic record of the same frequency as

the input ground motion, but with a change in amplitude and a change in phase. Both the amplitude and phase of the seismometer output depend upon the input frequency.

The amplitude and phase response functions vary continuously with variation in input frequency. The amplitude response function has a single maximum which depends upon the instrumental parameters. The maximum response represents a maximum instrument magnification which occurs at the resonance frequency. Frequencies above and below the resonance frequency have lower instrumental magnifications. It is therefore to be expected that large displacements on a record of complex ground motion will occur when frequency components near the resonance frequency interfere constructively. This instrumental resonance has been observed on seismograms (see, e.g., Richter, 1958, p. 215).

Ideally, records can be deconvolved to eliminate instrumental effects, but the digitization of large numbers of analog records with subsequent numerical calculation is not tractable without specialized equipment. Therefore, the many existing analog records must be analyzed directly, and instrumental effects which alter the appearance of the records must be understood. As earthquakes are transient phenomena, the instrumental effects on the onset of a causal signal must be considered.

Hagedoorn (1964) has found experimentally that when a starting

sine wave with a frequency near the resonance frequency is passed through a seismograph, the amplitude of the first half cycle on the resultant record is smaller by half than the amplitude of the second half cycle. This "cramping" effect is also displayed by a theoretical calculation of Sarmah (1966). Sarmah numerically filtered a theoretical pulse through the response function of a short-period Benioff seismograph. His results are reproduced in Figure 1. This figure shows that the recorded onset time corresponds to the actual ground motion onset time, but, because of the effect of the instrument, the largest recorded amplitude occurs at 0.4 second later. Thus, when interpreting seismograms it is necessary that true arrivals are distinguished from large amplitudes which are a result of the instrument itself through instrumental resonance or second cycle enhancement.

Finally, general considerations of the theory of seismometers indicate that the seismogram can be a record of ground displacement, velocity, or acceleration, depending upon whether the signal period is much less than, nearly equal to or much greater than the natural period of the seismometer pendulum (see, e.g., Richter, 1958, p. 215). Seismograms thus represent a recording of ground motion modified in a complex manner by the instrumental reaction to the different frequency components of the signal. In general, modern seismographs are designed to provide essentially a record of the velocity

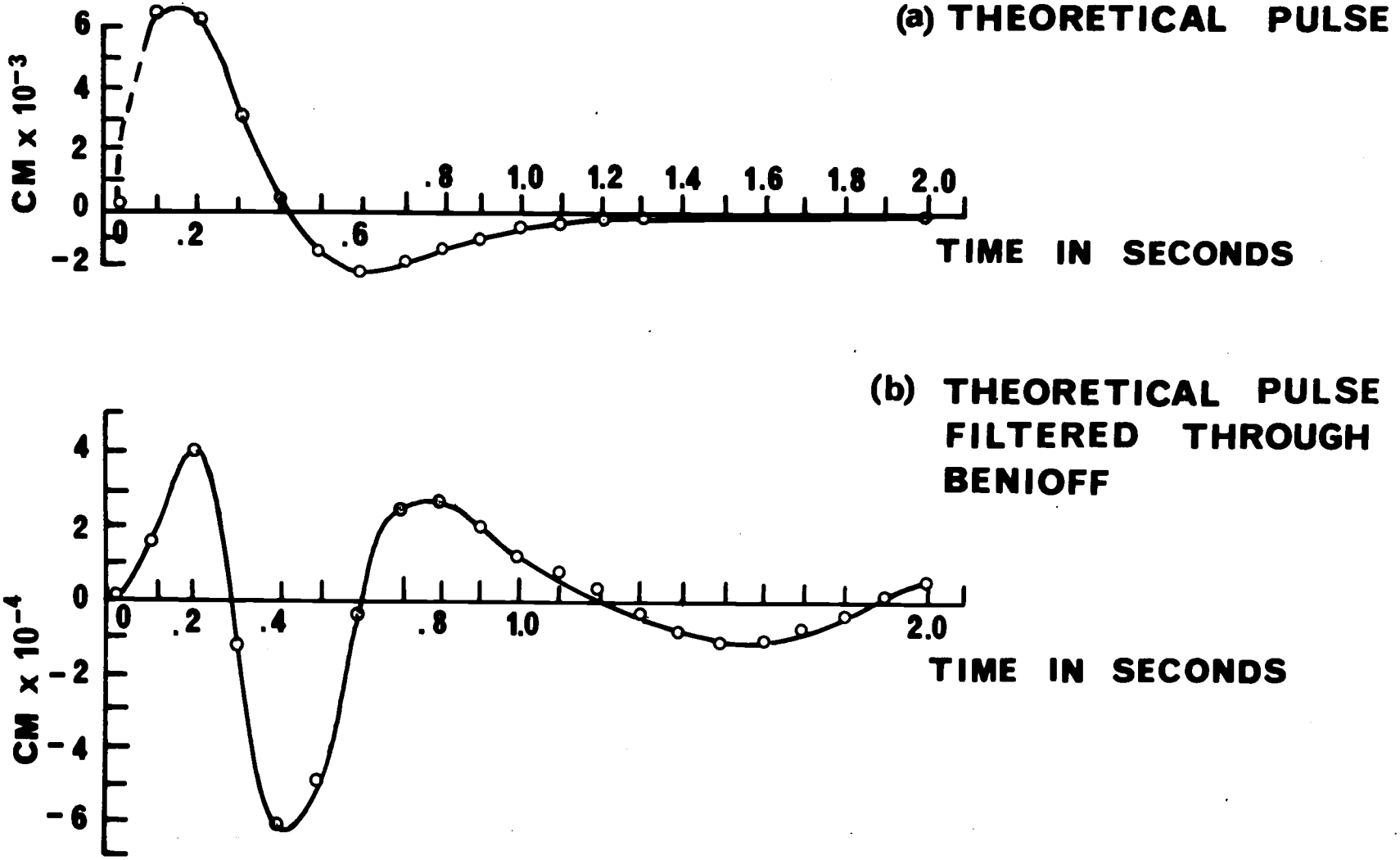

Figure 1. Instrumental effect upon the input signal. Reproduced from Sarmah, 1967.

of ground motion.

Reflected Phases

The most extensive experimental study of second arrivals was published by Gutenberg (1951), wherein he examined the recordings of 50 southern California earthquakes in the epicentral range of 0 to 1000 km. Gutenberg assumed a focal depth of 16 km for all of the earthquakes. By using a crustal and subcrustal model which was consistent with previous earthquake and explosion studies, he was able to account for many of the observed second arrivals. These arrivals were considered to be reflections and refractions from seismic discontinuities within the crust and upper mantle. He also described a phase, P_x, for which he could find no satisfactory explanation. The P_x phase followed P_n by a few seconds for epicentral distances from 150 to 900 km. Gutenberg found that the P_x-P_n time interval varied from 1 to 4 seconds, and that P_x occasionally appeared with an amplitude about five times that of P_n. On some records he was unable to find P_x while on two records he found two phases near the P_x time. There seemed to be a slight increase in the P_x-P_n time interval from about 150 to 300 km, but there was no change in time interval for distances between 367 and 818 km. It was not possible to explain the small P_x-P_n time interval at the larger distances in terms of reflections or refractions from an additional discontinuity.

Gutenberg therefore suggested that P_x may actually be the result of several different waves.

In addition to the P_x phase, some of the later second arrivals considered by Gutenberg to be reflections and refractions are in want of an explanation as the crustal model used by Gutenberg is now obsolete. Finally, Gutenberg's use of a constant focal depth for all the shocks is no longer a tenable assumption.

Signal-Generated Noise

It has been shown by the use of model seismology (Tatel, 1954; Tatel and Tuve, 1955) that blocks of materials on the surface of a layered medium can produce surface waves from incident body waves. Also, buried geologic features may act as acoustic inhomogenieties resulting in the transfer of body-wave energy to surface-wave motion. The recorded second arrivals resulting from this conversion of the primary signal to the slower surface-wave motion by local inhomogenieties are usually referred to as signal-generated noise. When the inhomogeniety is a geologic feature with dimensions of several kilometers located near the recording station, the signal-generated noise may arrive within a few seconds after the onset of the primary signal.

This effect was observed by Key (1967) while studying the records of the Eskdalemuir, Scotland, seismic array of a Kamchatka event.

The records from several instruments of this array are reproduced in Figure 2. A single trace of Figure 2 would represent the information of a single three-component station. It is seen that a second phase arrives some 3 to 7 seconds after the onset of the first arrival. If only a single trace were available for examination, this second arrival could easily be interpreted as body-wave energy which has traveled by a different ray path than the first arrival. When the records from the complete array are compared, however, the second phase is seen to traverse the array with a much lower apparent velocity than that of the first arrival. Key identified the second phase as being locally produced by virtue of its phase velocity across the array and by the fact that its phase velocity and propagation direction were constant despite changes in the approach azimuth of the P signals of over 50°. Key also found that the particle motion for the second phase was elliptical, indicating that it has the character of a Rayleigh wave. The first two properties of signal-generated noise require an array for detection, but the character of the particle motion can be determined from a single three-component seismic station.

Second Source Motion

Multiple Shocks

The actual time dependence of the acoustic radiation at the focus of an earthquake is not well known. According to Bullen (1963, p. 78),

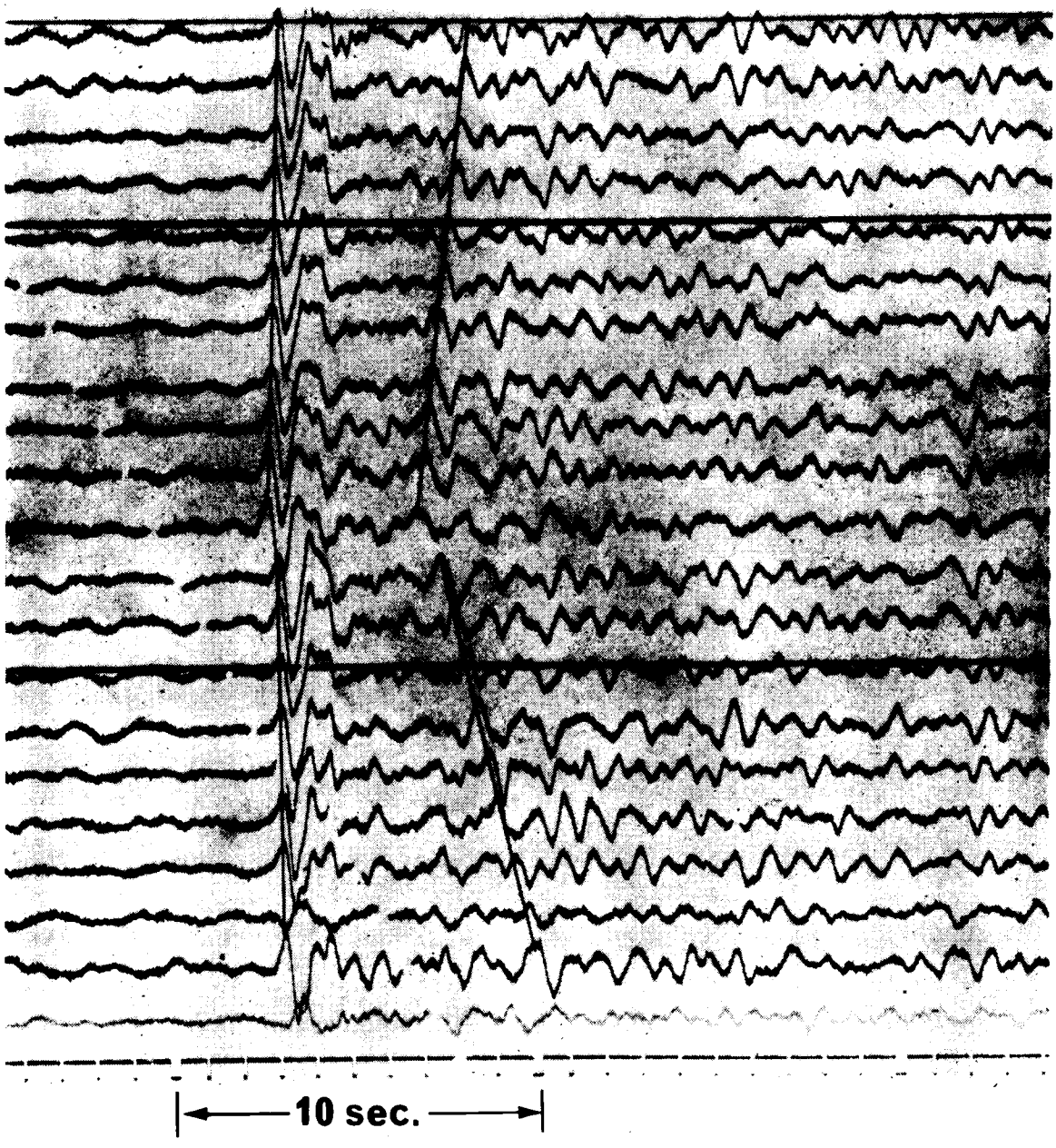

Figure 2. Vertical component seismograms of a Kamchatka event recorded at the seismic array in Eskdalemuir, Scotland. Reproduced from Key, 1967.

the main energy of most earthquakes is released over a short duration. Bullen describes the events at the source as: "conditions approximate to the occurence of an instantaneous initial impulse, followed by a swift displacement and return to near the undisturbed position, all taking place within a few seconds at most." He also reports that the existence of multiple shocks, i.e., the first disturbance repeating itself several times, was suggested by Stoneley. Stoneley showed that the Mongolian earthquake of August 10, 1931 could be interpreted as consisting of two shocks of comparable intensity. The two shocks were separated by a time interval of 33 seconds, with possibly two other shocks in between.

Other examples of multiple shocks have been reported. A recent multiple shock interpretation was given by Wyss and Brune (1967) for the Alaskan earthquake of March 28, 1964. Seismogram phases at 9, 19, and 44 seconds after the first P wave were considered to be the result of separate shocks occurring at 35, 66, and 165 km, respectively, south of the main epicenter. They state: "From the analysis it appears that a reasonable source model is a rupture or a shear wave spreading out from the epicenter which triggers off more or less distinct events." This interpretation is of importance here as the time between the first and second shock is 9 seconds and is nearly equal to the interval between the phases observed for the smaller crustal shocks in the Pacific Northwest

states.

Multiple shock interpretations are based on the observation that several seismic phases on a single record are duplicated after a constant time delay. The time delay may not be the same for seismograms recorded at different source-to-station azimuths, however, when the focus of the second disturbance is separated in space as well as in time from that of the initial disturbance. This was observed in the case of the Alaskan shock mentioned above.

Source Dynamics

In addition to the triggered-failure concept of second source motion (multiple shocks) Savage (1965) has proposed the ideas of the "stopping phase" and the "breakout phase." From model experiments utilizing thermally induced fractures in glass plates, Savage proposed a second emission of seismic energy from a fault-model earthquake corresponding to the time of termination of a fracture. He termed this phenomenon the "stopping phase." Also, a second emission of seismic energy should occur if the fracture encounters a free surface. Savage referred to this as the "breakout phase." He explained that the first motion of the "breakout phase" is in the same direction as that of the first arrival, whereas the ordinary "stopping phase" exhibits an opposite direction of initial movement. He comments: "This is to be expected since the free surface relieves the

constraints which oppose the fracture displacement whereas the ordinary stopping of a fracture implies the dominance of these constraints."

In his paper, Savage cites examples of strain recordings (records of the very long period motion of the earth - from a few minutes to several hours) which show displacements consistent with a stopping phase interpretation. There is a considerable difference, however, between the source dynamics hypothesized by Savage and by Bullen. Savage's failure model is that of a crack spreading with a somewhat constant velocity over what will eventually be the complete rupture surface. According to Savage, the velocity of rupture is of the order of 3 km/sec, while the fault lengths vary from perhaps 70 km to 1500 km (Savage, 1965). The rupture duration time would thus vary from some tens of seconds to several minutes. The time interval between the initial phase and the stopping phase would have a similar variation. For shocks whose fault dimensions are only a few kilometers, this time interval may be a few seconds.

The breakout phase requires that the rupture encounter the surface of the earth and therefore depends upon the rupture velocity, the dip of the fault plane and the depth of the initial point of failure. Savage used as a possible example of the breakout phase the observations and results of Ryall (1962) for the Hebgen Lake, Montana, earthquake of August 18, 1959. This earthquake displayed the required

surface faulting, and the seismograms showed a large, clear event 5 to 8 sec after the arrival of the first P wave. The amplitude of the second event was always larger than that of the first, the directions of initial motion for the two events were always the same, and the time interval between the two events was larger by 2 or 3 sec for stations to the north of the epicenter than for stations to the south. Savage stated that the first two observations are consistent with a "breakout phase" (indicating a focal depth of less than 13 km), but that the third observation is not consistent as fault-plane solutions and surface observations show the dip to be to the south.

Wave Conversion by Crustal Discontinuities

When a compressional or shear wave is incident upon a surface separating two media of different acoustical parameters, the energy in the incident wave is partitioned among the transmitted compressional and shear waves and the reflected compressional and shear waves. Thus, a single wave in a layered crust may produce several daughter waves. This multiplicity may occur either within the crust near the source or within the crust in the vicinity of the recording station.

Partitioning of the energy of an upward traveling compressional wave by discontinuities beneath the recording station has been proposed in certain areas as an explanation of second arrivals.

Matuzawa et al. (1928, 1929) were the first to use this explanation for second arrivals as observed on earthquake seismograms recorded in Japan. They accounted for several large second arrivals which were recorded principally on horizontal instruments. The earliest of these second arrivals was delayed by only 1.5 seconds with respect to the initial motion on the seismograms, and the second phases were observed for local shocks of all focal depths. Russian investigators, notably Andreev (1957a, 1957b), have identified large amplitude second arrivals on horizontal seismograms as being P to S converted waves (P-S exchange waves in their terminology); the conversion is interpreted to have occurred at intermediate crustal discontinuities. Both local and teleseismic earthquakes were used by Andreev, and the short period instruments recording the waves had response curves similar to the short-period Benioff systems.

Schwind et al. (1960) have provisionally interpreted second arrivals with amplitudes several times that of the initial P wave as P to S converted waves at the receiving site from a large chemical explosion. The observed arrival times compared favorably with calculated ones, using the crustal layering for the area in Utah as determined by the seismic refraction studies of Berg et al. (1959). Particle-motion diagrams were consistent with the interpretation of the phases as shear arrivals.

Head Wave Multiples

From a geometrical optics point of view, there are a number of possibilities for seismic arrivals which have travel-time curves that are parallel to and are displaced by only a few seconds from the P_n travel-time curve. The causes of this travel-time multiplicity can be categorized as follows:

(a) source reflections and conversions,

(b) conversions at the Mohorovicic discontinuity under the station,

(c) true multiples,

along with the effects at internal crustal discontinuities mentioned earlier. These categories are defined by their ray paths for a single layered crust in Figure 3. The letters S and P, respectively, indicate that the corresponding ray segment is traversed with the shear-wave velocity or the compressional-wave velocity of the medium. The complete ray path from source to station is obtained by connecting any of the source possibilities, (a), with one or more of the transmission possibilities, (c), and terminating the path with either of the station possibilities, (b). The situation would be compounded in a multilayered crust.

Of the number of possible ray paths in Figure 3, a few have been considered in the literature. The existence of arrivals produced

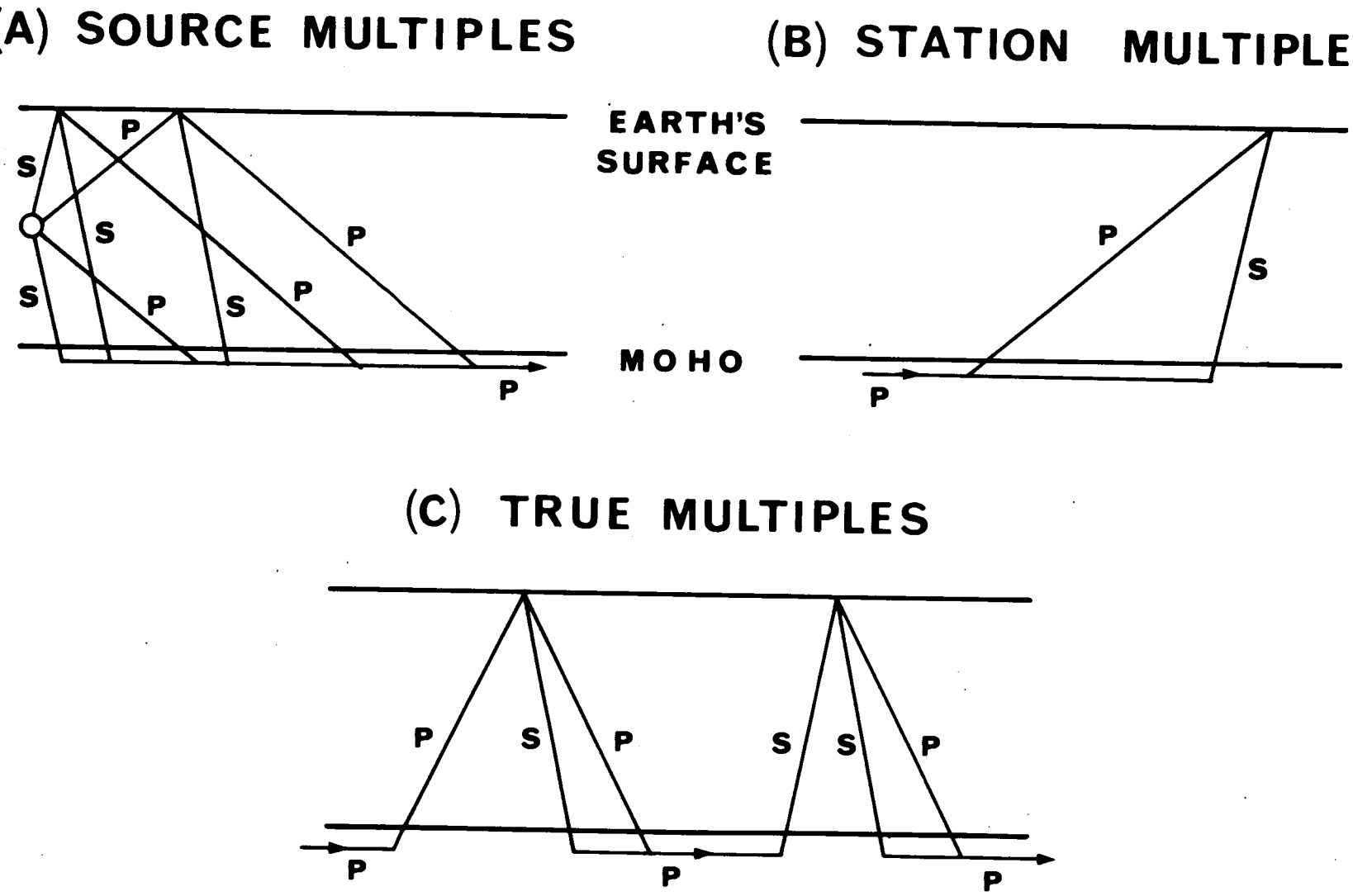

Figure 3. Origins of head wave multiples.

by (c) is well documented by the model experiments of Nakamura (1966). His results indicate that the amplitude of the refracted-reflection taking place near the source and the amplitude of the reflected-refraction occurring near the station can be of appreciable size. Those paths whose reflection points are further from the source or the station are of secondary importance. Nakamura's model with the uniform one layer crust produced a second arrival whose amplitude was as much as 1.3 times that of the principal head wave.

Multiples resulting from mechanisms (a) and (b) in Figure 3 have been somewhat neglected in the literature, due in part to the fact that the more detailed head-wave studies have been carried out using chemical or nuclear explosive sources at or near the free surface. Thus, the large energy shear waves which are generated by earthquakes are not assumed to be present, and the nearness of the free surface does not afford a large enough time delay for the surface reflections to be adequately defined on the records in the period range of interest in earthquake studies. Furthermore, there is a lack of knowledge in a form applicable to experimental seismology concerning the amplitudes of head waves which inovlve a conversion of wave type--even though the theory has been developed to a considerable degree. The few references to wave interpretations based on (a) and (b) in Figure 3, which can be cited, are based primarily on

travel-time considerations.

Interest has been expressed in the sP_n wave, an S wave reflected from the earth's surface above the source, which then travels as a P_n wave, as its identification would be valuable in determining focal depths. This possibility was suggested by Dehlinger and French (1965), and the wave so generated was also discussed by Kondorskaya (1956). Both papers pointed out the observational fact that shear waves recorded at stations near the epicenter are usually more energetic than compressional waves. It was suggested that the sP_n wave should be recorded because of the large coefficient for an S to P reflection at a free surface in the incidence angle range required for subsequent critical refraction at the Moho. Relations giving focal depths as functions of sP_n-P_n time intervals were presented in both papers. Kondorskaya was principally concerned with large subcrustal shocks recorded at teleseismic distances, and the experimental evidence presented was for those cases. The use of sP_n in local crustal shocks was presented only as a theoretical possibility. Dehlinger and French, on the other hand, emphasized the use of the S to P surface reflected wave for the investigation of crustal shocks in the P_n epicentral distance range and indicated provisional identification of the sP_n wave on records of shocks in the Pacific Northwest states. They found the focal depth determinations by the sP_n technique for shocks in the Pacific Northwest states to be quite

reasonable. Focal depths determined by this method for certain shocks in central California were reasonably consistent with depths determined by Turcotte (1964), using conventional techniques.

In a recent refraction study by Hall and Brisbin (1965) in western Manitoba, two seismic discontinuities were distinguished - the Conrad and the Mohorovicic discontinuities. Using a two-layer crustal model and travel-time considerations, they were able to explain certain second arrivals on their records in terms of a combination of paths (a) and (b) in Figure 3, along with conversions at the intercrustal discontinuity. The head wave types which they observed were P*, $S_1P_2P_1$, $S_1P_2S_1$, S*, P_n, $P_1S_2P_3S_2P_1$, $S_1S_2P_3S_2S_1$, $S_1P_2P_3P_2S_1$, $S_1S_2P_3P_2S_1$, and $P_1S_2P_3S_2S_1$. (The subscript indicates the layer traversed by the ray, except for the central terms of each label which represents head wave propagation.) Energy considerations were not discussed in this paper.

An earlier example of a second arrival resulting from (b) can be found in Grant and West (1965, p. 103) where the records and results of Dobrin et al. (1951) are reproduced with the tentative identification of PPS from travel-time considerations.

MATERIALS USED

Recording Stations

The nature of this study sets timing requirements on the measurement of intervals between successive arrivals. As the time intervals are of the order of a second to a few seconds, it would be desirable to read times to 0.1 second. This accuracy would also allow measurement of the wave periods which are typically between 0.4 and 1 second. A matched set of instruments, with one measuring vertical ground motion and two measuring perpendicular components of horizontal motion, are desirable. The motion of the ground at the station can then be reproduced.

The World-Wide Standard Seismic (WWSS) stations have a matched set of instruments. The recording drums of the short-period instruments operate at 60 mm/min, which is a rather condensed time scale for the accuracy required. Second arrivals can be seen on the records of the WWSS stations, but the records do not provide the resoltuion for the small time interval or period measurements. Photographic enlargement of the records has not been of any value.

The Long-Range Seismic Measurement (LRSM) stations, operated as part of the Vela Uniform Project of the Advanced

Research Projects Agency, also have a matched set of short-period instruments. These instruments record on 35 mm film and provide a time scale of 6 mm/sec when the film is viewed on a X24 microfilm viewer. Hence, LRSM stations have the desired time resolution, and measurements can be taken visually from the microfilm reader using a millimeter scale. In addition, LRSM stations record higher frequency motion than WWSS stations, and thus provide a better resoltuion of closely spaced pulses.

Data from the LRSM stations are considered more reliable, but WWSS stations were also used. Records from stations other than LRSM or WWSS stations were used when necessary for adequate station coverage. These include stations from the seismic network operated by the University of California at Berkeley and the seismic array at Baker, Oregon, which is a Geneva-type station of the Vela Uniform Project.

Pertinent station information is listed in Table 1.

Earthquakes

The records of 25 earthquakes in the Pacific Northwest states were examined. Only nine of these were found to provide recordings useful for this study. The remaining earthquakes were discarded as the station records were not of sufficient quality to provide information concerning the first ten seconds following the first arriving

Table 1. Seismograph station information.

Station	Type	Code	Coordinates
Arcata, California	U. Calif.	ARC	40 52 36.0 N 124 04 30.0 W
Bellingham, Washington		BLL	48 44 20.0 N 122 29 05.0 W
Berkeley, California (Haviland)	U. Calif.	BRK	37 52 24.0 N 122 15 36.0 W
Berkeley, California (Strawberry)	WWSS	BKS	37 52 36.0 N 122 14 06.0 W
Baker, Oregon	Geneva	BKR	44 50 56.0 N 117 18 20.0 W
Bozeman, Montana		BOZ	45 36 00.0 N 111 38 00.0 W
Corvallis, Oregon	WWSS	COR	44 35 08.6 N 123 18 11.5 W
Hailey, Idaho	LRSM	HLY	43 38 50.0 N 114 15 02.0 W
Hungry Horse, Montana		HHM	48 20 58.0 N 114 01 39.0 W
Longmire, Washington	WWSS	LON	46 45 00.0 N 121 48 36.0 W
Mt. Hamilton, California	U. Calif.	MHC	37 20 30.0 N 121 38 30.0 W
Mina, Nevada	LRSM	MNA	38 26 10.0 N 118 08 53.0 W
Mineral, California	U. Calif.	MIN	40 20 42.0 N 121 36 18.0 W
Palo Alto, California		PAC	37 25 00.0 N 122 10 54.0 W
Pendleton, Oregon	LRSM	PND	45 36 40.0 N 118 53 02.0 W
Penticton, B. C.		PNT	49 19 00.0 N 119 37 00.0 W

Table 1. (continued)

Station	Type	Code	Coordinates
Reno, Nevada	U. Calif.	REN	39 32 24.0 N 119 48 47.0 W
Seattle, Washington		SEA	47 39 18.0 N 122 18 30.0 W
Shasta, California	U. Calif.	SHS	40 41 42.0 N 122 23 30.0 W
Tonasket, Washington	LRSM	TON	48 47 38.0 N 119 35 16.0 W
Tumwater, Washington		TUM	47 00 54.0 N 122 54 30.0 W
Victoria, B. C.		VIC	48 31 10.0 N 123 24 55.0 W
Vineyard, California	U. Calif.	VIN	36 45 00.0 N 121 23 18.0 W
Winnemucca, Nevada	LRSM	WMC	41 21 02.0 N 117 27 30.0 W

waves. The poor record quality resulted from unfavorable combinations of earthquake magnitudes and station magnifications, along with the usual noise and instrumentation problems encountered in earthquake studies.

The epicentral locations and origin times for the earthquakes used are listed in Table 2. The data for those earthquakes marked with an asterisk were published by Dehlinger et al. (1965), and the data for the remaining earthquakes in the table were taken from the "Preliminary Determination of Epicenters" cards published by the U. S. Coast and Geodetic Survey.

Table 2. Earthquake epicenters and origin times.

Date	Hr. Min. Sec.	Latitude	Longitude
*August 23, 1962	19:29:13.4	41 47 N	124 15 W
*November 6, 1962	03:36:43.0	45 36 N	122 39 W
*January 6, 1963	18:07:42.9	44 51 N	112 05 W
*January 24, 1963	21:43:11.8	47 29 N	122 01 W
*January 27, 1963	15:24:41.9	44 10 N	114 25 W
*December 27, 1963	02:36:18.5	45 38 N	123 23 W
		Oceanic Shocks	
October 14, 1962	10:14:27.7	38 43 N	124 00 W
June 25, 1963	08:26:21.7	44 12 N	129 00 W
August 22, 1963	09:27:07.3	42 06 N	126 12 W

Crustal Structure

The earthquakes and stations listed above lie in three structural provinces: the oceanic province off Oregon and northern California, and two continental provinces - one west and the other east of the Cascade Range.

The structure of the oceanic province was based on seismic refraction work by Shor et al. (1968). The structure of the two continental provinces was suggested by Dehlinger et al. (1965) in connection with their studies of earthquakes and gravity anomalies in the areas. Further, the crustal structure in the province east of the Cascade Mountains was examined through seismic refraction measurements by Pakiser and Hill (1963). A study by Chiburis (1965) of Rayleigh-wave dispersion provides additional constraints for the structure of the continental provinces.

All of the above seismic data, along with the reliable gravity data collected by investigators at Oregon State University (Thiruvathukal, 1968), have been utilized in the construction of the composite crustal and subcrustal cross-section shown in Figure 4 (reproduced from Dehlinger et al., 1968). This figure will be used as the basis for numerical calculations.

Figure 5 displays appropriate one-layer models representing an average for the structure shown in Figure 4. The crustal velocity

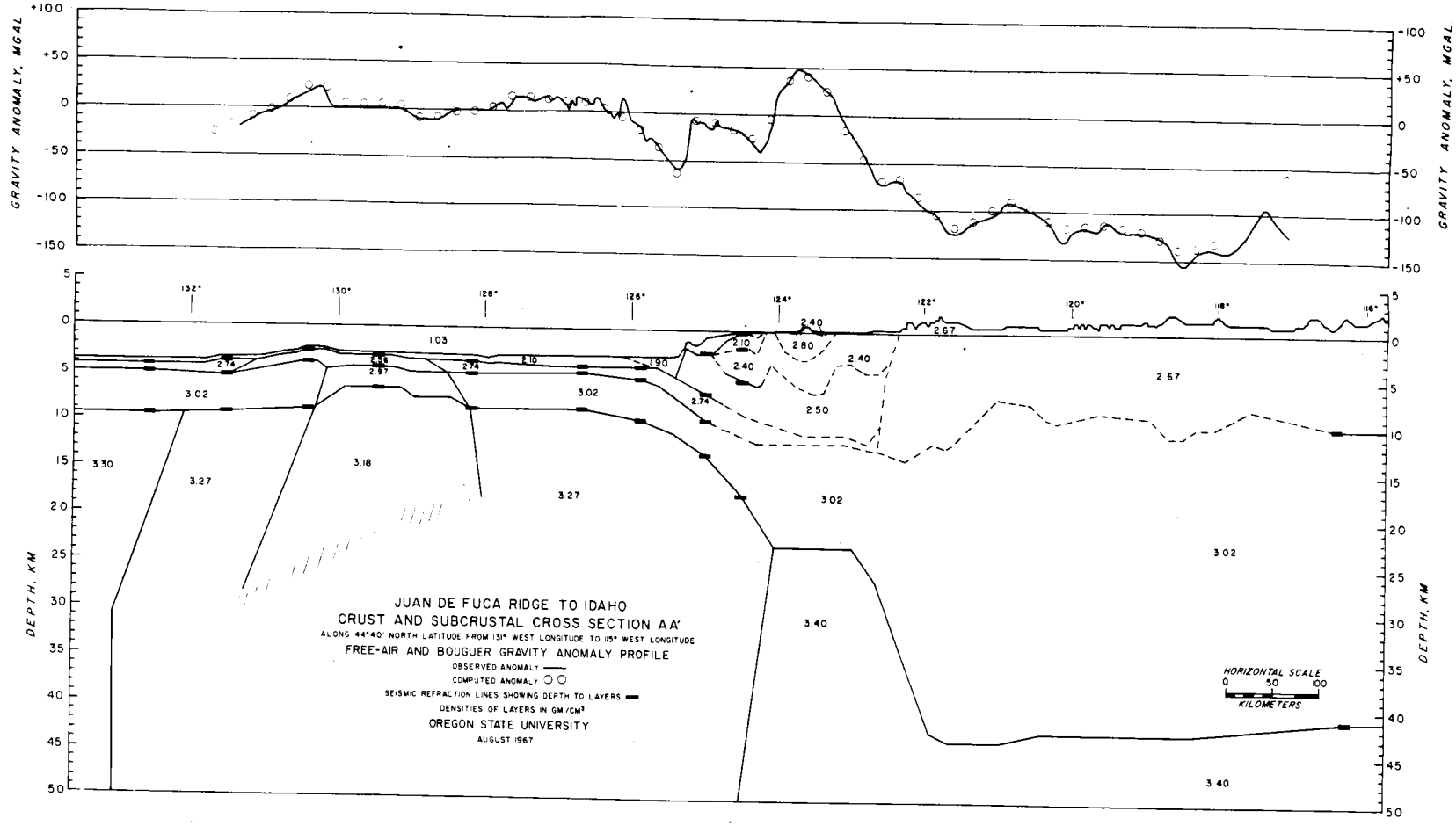

Figure 4. Crustal structure in the Pacific Northwest states. Reproduced from Dehlinger et al. (1968).

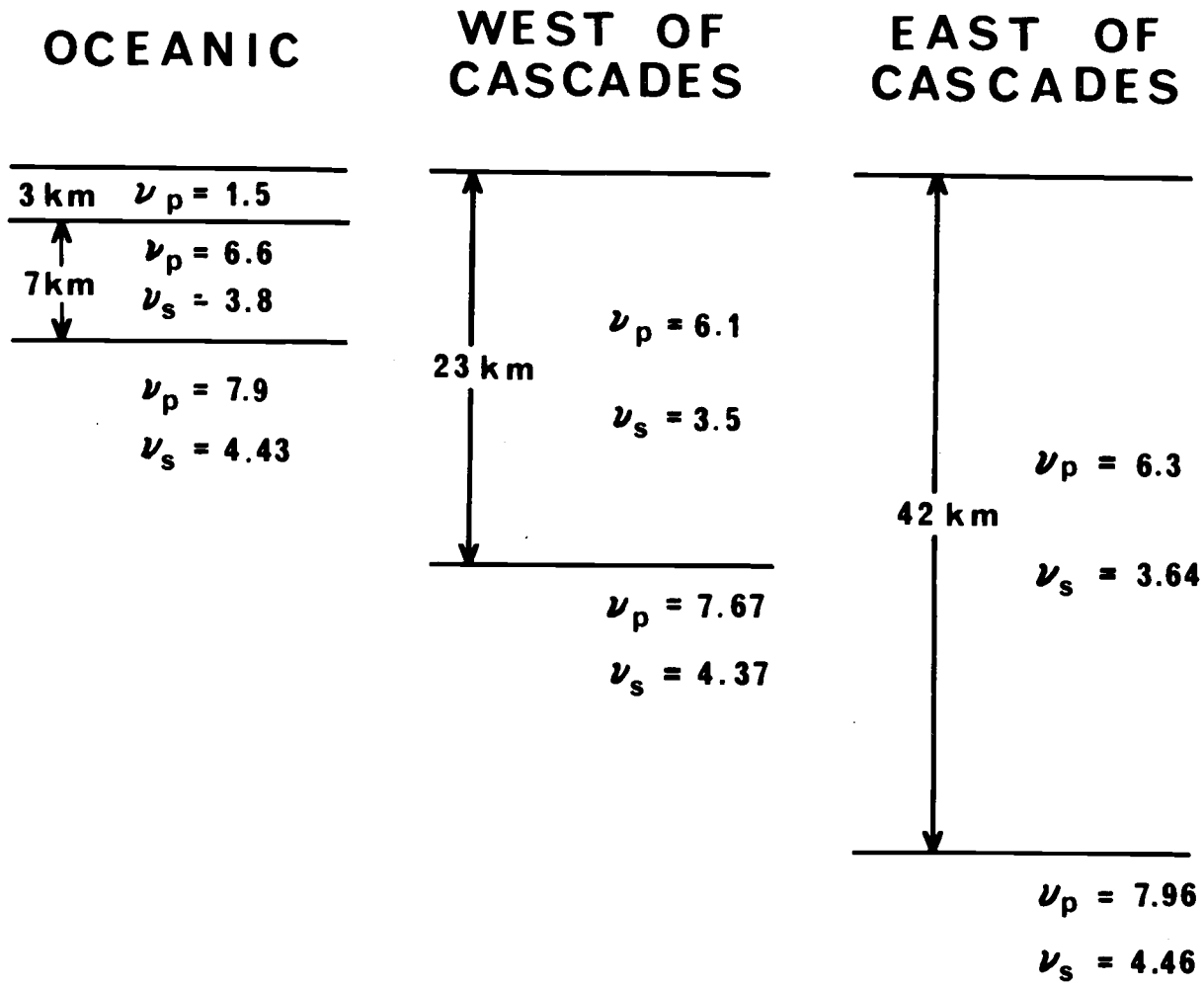

Figure 5. One-layer crustal models for the three provinces in the Pacific Northwest states.

of 6.1 km/sec in the western continental province should probably be increased to 6.3 km/sec (Dehlinger, personal communication), but it will be shown that this change does not affect the following results.

OBSERVATIONS OF THE "POST-P_n" WAVE

As a second phase whose amplitude was larger than that of the P_n phase was observed to follow the P_n phase by a few seconds on most of the records of Pacific Northwest earthquakes, it was initially suspected that this arrival resulted from the same phenomenological cause for all earthquakes. Thus, one phase was defined, tentatively called the "Post-P_n" phase, using the terminology of Dehlinger and French (1965), as the first discernable onset following P_n on those seismograms for which P_n is the first arrival and the epicentral distance is sufficiently large that P^* does not afford an explanation of the second arrival. This sets the epicentral distance between about 200 and 1000 km. With this definition as a guideline, statistical data concerning the "Post-P_n" phase were gathered for the stations and earthquakes listed in Tables 1 and 2. Data collected consisted of time intervals between the arrivals of P_n and Post-P_n, ratios of amplitudes of the first half cycle of Post-P_n to P_n, relative directions of first motion of Post-P_n to P_n, and ratios of the apparent periods of Post-P_n to P_n. The data collected are presented in Table 3, and the following generalizations can be made from the results.

(1) The time interval between "Post-P_n" and P_n is nearly constant for any one shock, but varies for different shocks

recorded at the same set of stations. For example, the interval may be from 1.5 to 2.5 seconds for one shock (see Table 3 for the shock of 8-23-62), but 3 to 4.5 seconds for another shock (11-6-62 or 10-14-62). There seems to be no systematic dependence of the time interval upon epicentral distance.

(2) Amplitudes of "Post-P_n" were usually 2 to 5 times the amplitude of the P_n wave on all three components of the short-period system, although some were larger and others smaller. There seems to be no systematic dependence of the "Post-P_n" to P_n amplitude ratio upon the epicentral distance.

(3) Average periods of the "Post-P_n" and P_n waves were approximately the same, both being between 0.4 and 1.3 seconds. In the instances where there were differences, "Post-P_n" tended to be shorter.

(4) Whether the first motion of P_n and "Post-P_n" had the same or opposite directions appeared to depend upon azimuth.

(5) It was not possible to determine whether the first arrival, assumed to be P_n, was indeed the same wave at all stations recording a given earthquake as the appearance of the onset of the motion seemed to change with azimuth. Figure 6 shows short-period vertical seismograms recorded at two stations in Nevada for which ray asimuths were only 16° apart. A quite remarkable in-phase correlation is observed, almost wave for

Table 3. "Post-P_n" data.

Station and Instrument	Epicentral Distance (KM)	Time Interval after P_n (SEC)	(Post-P_n)/P_n Ratios		Periods
			Amplitude	First Motions	
		Land Shocks			
		August 23, 1962			
MIN	271				
V		Amplitudes too large			
NS		1 + ?	-	same?	-
EW		1 + ?	-	same?	-
BKS	469				
V		Amplitudes too large			
NS		1.8	2 1/2	same	-
EW		1.8	2 1/2	same	-
USF	474				
V		Amplitudes too large			
NS		2	2	same?	.6
EW		1.5	2	same?	1
PAC	520				
V		2	1	same	-
NS		1.8	2	opp	-
MHC	544				
V		Amplitudes too large			
NS		2.2	3	opp	.7
EW		2.0	3	opp	1
WMC	561				
V		Amplitudes too large			
R		" " "			
T		" " "			
LON	575				
V		Second arrival not evident			
NS		" " " "			
EW		" " " "			
PND	597				
V		2	5	opp	1
R		2	4	opp	1
T		2	4	opp	1
VIN	614				
V		No record			
NS		1.5	6	opp	-
EW		1.3	8	opp	1
HLY	835				
V		2	100?	same	2
R		2.2	100?	same?	1
T		2	70?	same	1

Table 3. (Continued)

Station and Instrument	Epicentral Distance (KM)	Time Interval after P_n (SEC)	(Post-P_n)/P_n Ratios		Periods
			Amplitude	First Motions	
		November 6, 1962			
BKR	425				
V		3 + ?			
NS		3 + ?	Recorded amplitudes very large		
EW		3 + ?			
WMC	632				
V		3.7	6	-	-
R		3.3	-	-	-
T		3 + ?	-	-	-
HLY	698				
V		3.5	3	same	-
R		4	9	-	-
T		3.7	-	-	-
		January 24, 1963			
PTC	269				
V		2.2	3	-	-
NS		2.8	3	opp	-
EW		2.7	4	opp	-
PND	313				
V		Amplitudes too large			
R		1 + ?	-	-	-
T		1 + ?	-	same?	-
HLY	735				
V		1.7	-	opp?	.7
R		1.8	-	opp?	.5
T		1.8	3	same	.7
MNA	593				
V		2	1	same	1
R		2	1	same	1
T		2	2	same?	1
WMC	768				
V		3	2 1/2	opp	.7
R		3	2 1/2	same	1
T		2.5	-	-	-
		December 27, 1963			
LON	180				
V		Record not clear			
NS		2?	3	-	-
EW		Amplitude too large			

Table 3. (Continued)

Station and Instrument	Epicentral Distance (KM)	Time Interval after P_n (SEC)	$(Post\text{-}P_n)/P_n$ Ratios		Periods
			Amplitude	First Motions	
SEA	237				
V		3?	2	same?	-
NS		Amplitudes too small			
EW		" " "			
VIC	329				
V		3 1/2?	-	-	-
NS		Amplitudes too small			
EW		3	2	-	-
BLL	348				
V		2.5	2	opp	1
NS		Amplitudes too small			
EW		" " "			
TON	454				
V		2.2	2	opp?	-
NS		Amplitudes too small			
EW		2.1	3	-	-
		January 6, 1963			
PND	541				
V		Amplitudes too large			
R		1?	22	-	1
T		1	10	opp	1
WMC	585				
V		1.5	8	-	-
R		1.5	-	-	-
T		2	2	-	1
LON	778				
V		2 1/2?	3/4	-	-
NS		2 1/2	3/4	same	-
EW		Second arrival not evident			
		January 27, 1963			
BOZ	240				
V		Amplitudes too large			
NS		3 1/2	1 1/2	-	-
EW		Amplitudes too large			
HHM	466				
V		4?	-	-	-
NS		3.5	1 1/2	-	-
EW		Amplitudes too small			
LON	646				
V		3.5	2	opp?	-
NS		3	2	same	-
EW		3.8	3	-	-

Table 3. (Continued)

Station and Instrument	Epicentral Distance (KM)	Time Interval after P_n (SEC)	$(Post\text{-}P_n)/P_n$ Ratios		Periods
			Amplitude	First Motions	
		Oceanic Shocks			
		October 14, 1962			
PAC	214				
V		Amplitudes too large			
NS		3?	-	-	-
EW		3	2	same?	-
BRK	218				
V		4.5	4	opp	1
NS		4.5	-	-	-
EW		4.5	-	opp?	1
MHC	256				
V		Amplitudes too large			
NS		3 1/2	1	-	-
EW		3 1/2	1	-	-
VIN	316				
V		No record			
NS		2.7	4	-	-
EW		1?	2	-	1
REN	374				
V		5	2	opp?	-
NS		4 1/2	4	-	-
EW		4 1/2	4	-	-
WMC	631				
V		2 1/4	2	-	1
R		2	2	same?	1
T		2	2	-	1
PND	876				
V		Second arrival not evident			
R		" " " "			
T		" " " "			
BKR	881				
V		3 1/2	7	opp	1.3
NS		Records not available			
EW		" " "			
HLY	984				
V		2.8	2 1/2	same?	1
R		Amplitudes too small			
T		2 1/2 + ?	1 1/2	-	-

Table 3. (Continued)

Station and Instrument	Epicentral Distance (KM)	Time Interval after P_n (SEC)	$(Post\text{-}P_n)/P_n$ Ratios		Periods
			Amplitude	First Motions	
		June 25, 1963			
SHS	669				
V		1.5	2	same?	-
NS		No records			
EW		" "			
LON	629				
V		1 1/2	2?	same?	-
NS		Second arrival not evident			
EW		" " " "			
PND	814				
V		Second arrival not evident			
R		Amplitudes too small			
T		1.6	2	opp?	1 1/2
WMC	996				
V		1.9	1	same	-
R		1.9	1 1/2	same	-
T		1.9	1	same	-
HLY	1184				
V		1.5	3	opp?	3/4
R		1 1/2	-	-	-
T		1 1/2	2	opp	3/4
		August 22, 1963			
SHS	350				
V		Second arrival not evident			
NS		" " " "			
EW		" " " "			
ARC	217				
V		1.6	2	same	-
NS		1.6	1 1/2	-	-
EW		1.6	1	-	-
MIN	427				
V		1.5	12	opp	-
NS		1.5	-	-	-
EW		1.5	-	-	-
PAC	615				
V		Second arrival not evident			
NS		" " " "			
EW		" " " "			

Table 3. (Continued)

Station and Instrument	Epicentral Distance (KM)	Time Interval after P_n (SEC)	(Post-P_n)/P_n Ratios		Periods
			Amplitude	First Motions	
WMC	732				
V		1 1/2	4 1/2	same?	1
R		1 1/2	-	-	-
T		1 1/2	-	-	-
HLY	993				
V		1 1/2	-	-	-
R		1 1/2	-	-	-
T		1 1/2	7	opp?	1

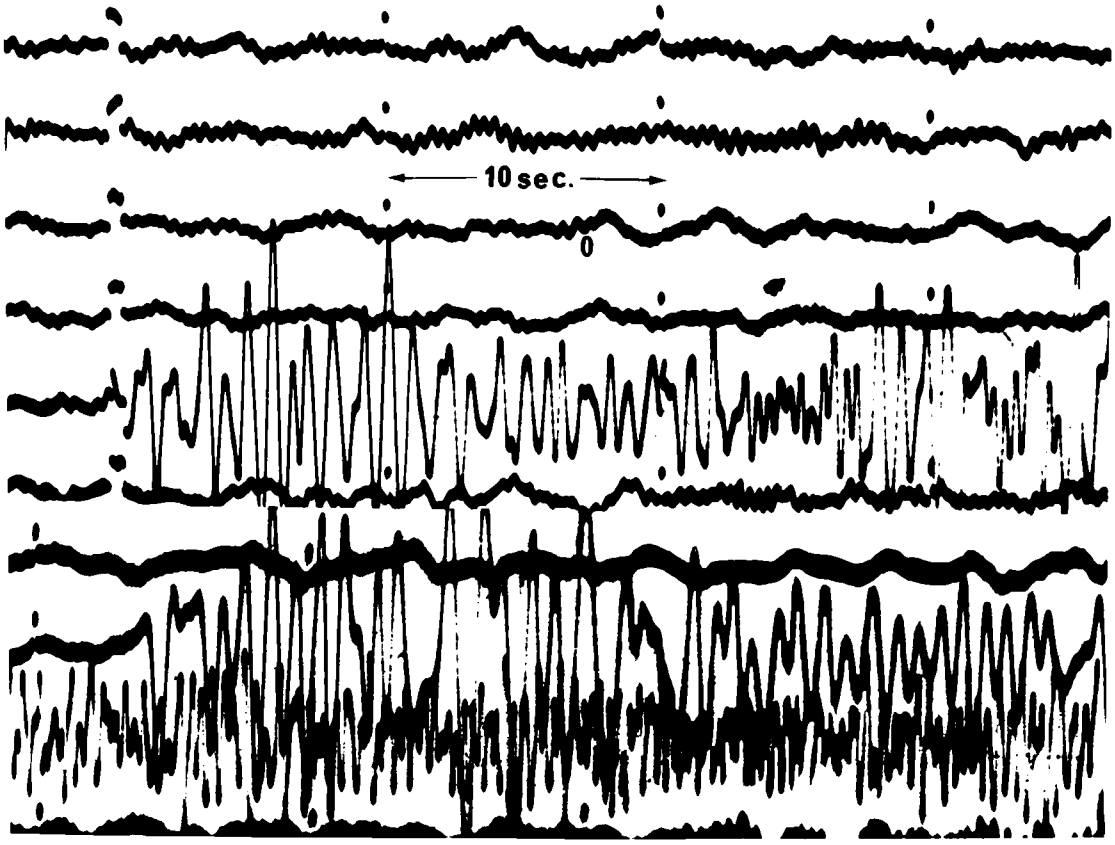

SHORT-PERIOD VERTICAL SEISMOGRAMS RECORDED AT WINNEMUCCA (TOP, 455K) AND MINA (BOTTOM, 593K), NEVADA, FROM THE JANUARY 24, 1963 EARTHQUAKE LOCATED SE OF SEATTLE. DISTANCE AND AZIMUTHS TO STATIONS ARE:

WINNEMUCCA	768KM	151°
MINA	1060KM	167°

Figure 6. Seismograms displaying the apparent absence of the P_n phase.

wave, beginning with the "Post-P_n" wave and continuing for more than six cycles. A subsequent out-of-phase correlation continues for a time thereafter. It is also observed that while the "Post-P_n" waves are nearly identical in form at the two stations, the P_n wave was observed at Winnemucca but appears to be absent at Mina.

(6) On some records there seems to be two arrivals following P_n and on other records a sequence of several arrivals is evident.

(7) On some records the second motion on the short-period seismograms seems to be coincident with the first arrival recorded by the long-period instruments, while on other records the first arrivals on both the short-period and long-period instruments are coincident in time.

LIST OF HYPOTHESES

From the preliminary considerations, it is possible to set down the following list of hypotheses concerning the origin of the second motions observed on seismograms of Pacific Northwest earthquakes as recorded in the P_n epicentral distance range.

(1) Instrumental effects.

(2) Large-angle, sub-Moho relfections.

(3) Signal-generated noise: coupling between surface waves and body waves along with other effects of crustal inhomogenieties near the station.

(4) Wave conversions by crustal discontinuities.

(5) Refracted waves following a slightly different path than P_n.

(6) Second source motion in terms of (a), multiple shocks or (b), the stopping phase or the breakout phase.

(7) Reflected and/or converted head waves in the region of the source or in the region of the station.

Each of the above hypotheses will be discussed separately in an attempt to determine the degree of consistency between the experimental observations and the theoretical consequences of each hypothesis. Each section except the one dealing with instrumental effects will be followed by a summary of the consistency with the observations of the "Post-P_n" wave listed previously.

Some points requiring detailed calculations or discussion will appear in the body of the section, while obvious or minor points may appear only in the summary at the end of the section. In any event, a descriptive term of evaluation along with a possible clarifying statement will appear for each experimental observation as given in the list of the previous section. The terms and meanings used here are as follows:

CONSISTENT: The theoretical predictions agree with the experimental observations.

INCONSISTENT: The opposition of the theoretical predictions and experimental observations tends to rule out the hypothesis.

QUESTIONABLE: Under fortuitous circumstances, the theoretical predictions can be made to be either consistent or inconsistent with the observations.

NO CONCLUSION: Either the observation is not pertinent or there is no method of comparing theoretical predictions with the experimental observations.

INSTRUMENTAL EFFECTS

For the purpose of checking whether the Post-P_n phases are a result of instrumental resonance, the dominant period of the signal must be determined as a function of time. The technique used was to consecutively number the peaks on the record starting with the P_n phase and continuing through the last phase of interest. The arrival time of each peak was plotted as a function of its phase number. Two representative examples of the resulting curves are shown in Figure 7, and the corresponding seismograms are shown in Figure 13. The slope of the curves in Figure 7 at any point is indicative of the dominant period of the corresponding phase and is assumed to represent the frequency component of the signal which determines the instrument magnification. The dashed lines in Figure 7 indicate the slope corresponding to the wave period for which the instrument would produce a maximum amplitude response. The heavy lines correspond to the wave period for which the magnification of the instrument would be 1/10 of its maximum value.

It is seen that in each case the average period of ground motion for the initial low amplitude portion of the seismogram is the same as the average period of the later large amplitude portion. Thus, the change in amplitude is not caused by instrument resonance, and as several cycles of the record have a small amplitude, the cramping

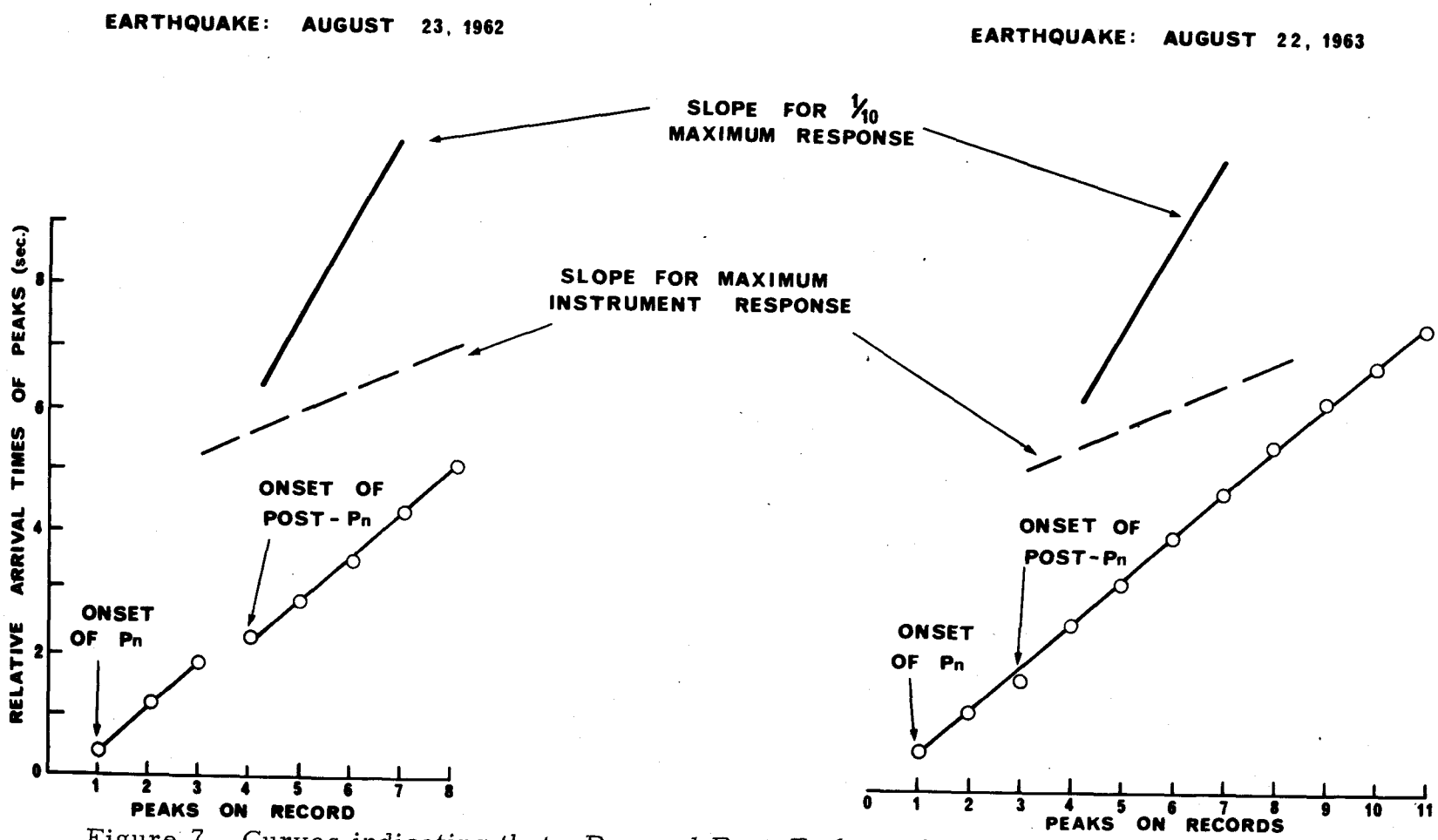

Figure 7. Curves indicating that P_n and Post-P_n have the same period of vibration.

effect on the first half cycle cannot account for the amplitude difference. It is concluded, then, that the later motion must represent a more energetic arrival than the first motion.

The cramping effect on the first half cycle of the signal could become important where large amplitude motion follows very closely behind small amplitude motion (Figure 8). An interpretation of a second arrival is possible, however, if the character of the record is such as to suggest an abrupt change. These cases require a subjective interpretation. Experience with the more obvious cases (Figure 9) has provided credence to the judgments used in this study.

A pendulum with a free period near one second acts as an accelerometer to ground motion having a period of ten seconds or longer. The possibility was investigated that short-period pulses may be recorded by the short-period systems at times corresponding to the passage of the maximum acceleration in the long-period ground motion. These considerations were investigated experimentally by direct comparison of short-period and long-period records of the same earthquake. In the earlier portion of the records, where body waves are present, large amplitude motion on the long-period records was accompanied by large amplitude motion on the short-period records. In the later portions of the records, however, long-period surface waves were not accompanied by comparable motion on the short-period instruments. Thus, the phases recorded on the

STATION: HAILEY (LRSM)

DATE: JANUARY 24, 1963

EPICENTER: SE OF SEATTLE

Δ 735 KM

AZIMUTH: 126°

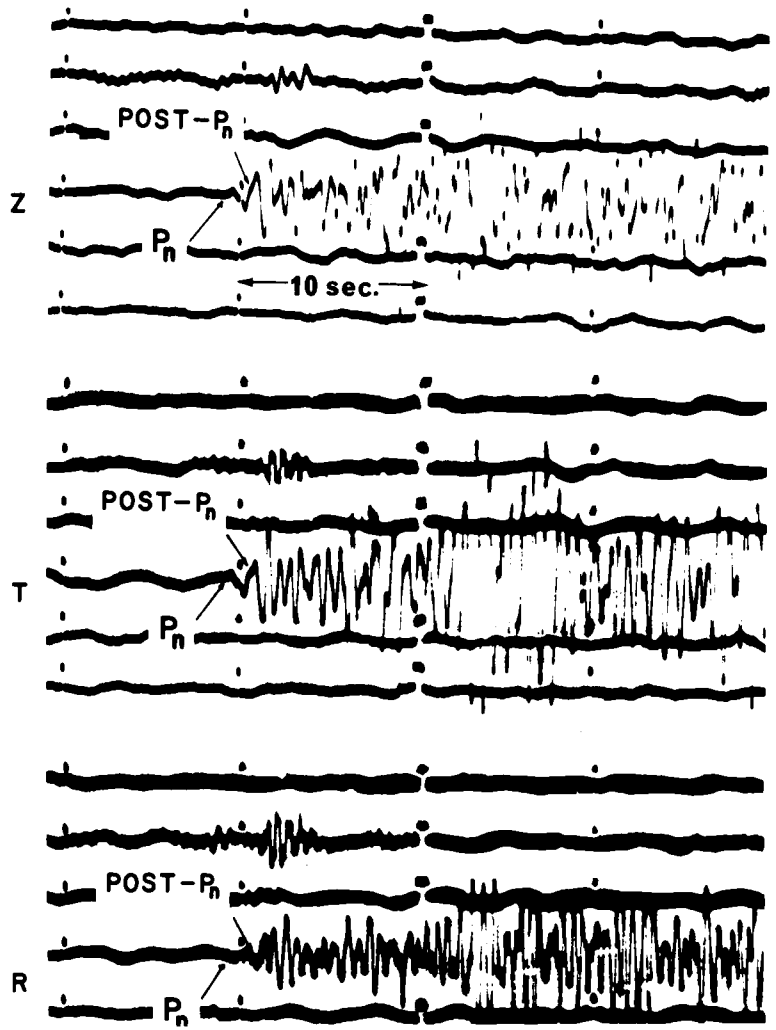

Figure 8. Typical example of the Post-P_n phase. Vertical record, Z, and perpendicular horizontal components, T and R (transverse and radial components with respect to the Nevada Test Site).

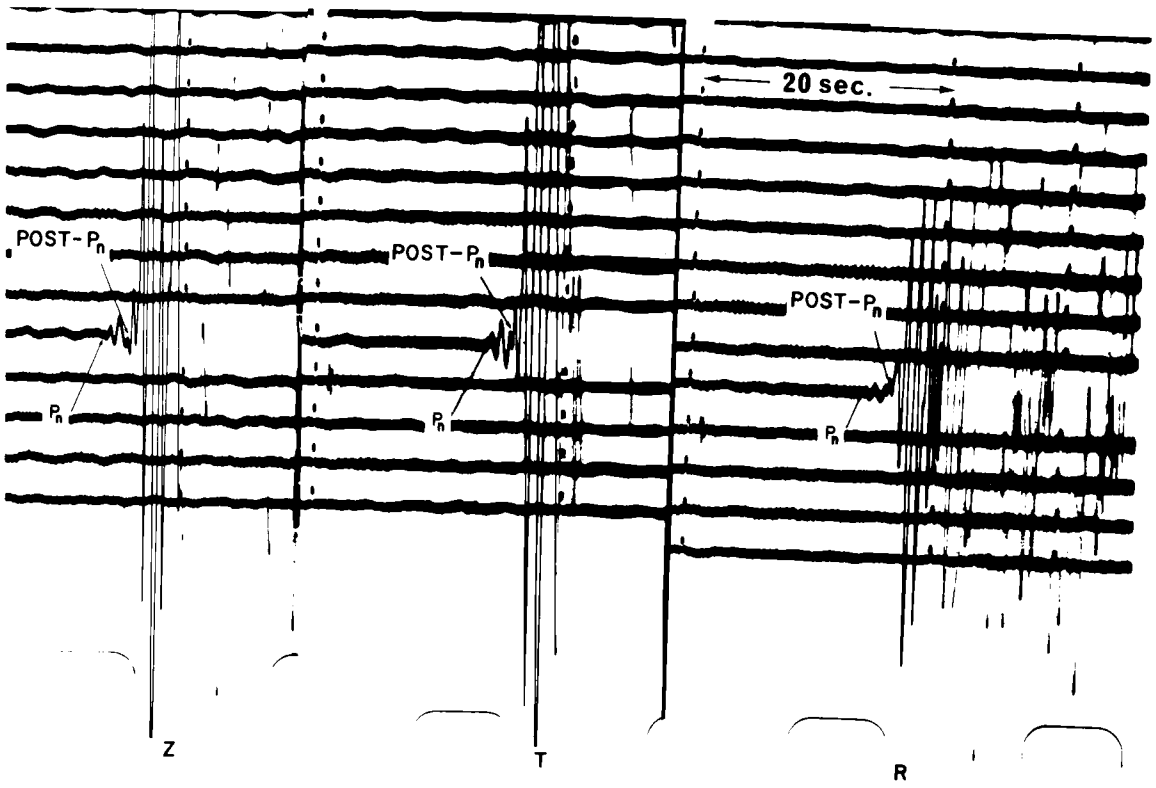

STATION: HAILEY (LRSM)

DATE: AUGUST 23, 1962

EPICENTER: CRESCENT CITY

Δ 835 KM

AZIMUTH: 70°

Figure 9. Example of the Post-P_n phase with a large amplitude relative to P_n.

short-period records represent a portion of the existing signal spectrum and are not the result of a signal-instrument interaction.

LARGE-ANGLE SUB-MOHO REFLECTIONS

As reflections from discontinuities within the crust cannot account for the observed short time delay of the phases following P_n, the main concern in this section will be with reflections from discontinuities in the upper mantle.

The model is that of a hypothetical reflector in the mantle. The mantle is assumed to be overlain by a one-layer crust, and the geometry is as indicated in Figure 10. The seismic parameters are considered to be constant within each layer, all of the segments of the ray paths pictured represent dilitational waves, and d is the distance between the Moho and the hypothetical reflector in the mantle. For convenience, the source is considered to be at the surface of the earth.

Figure 11 shows the time interval between the first arrival, P_n, and the reflected wave as a function of epicentral distance for four values of d. The curves constructed for this model were based on simple geometrical optics, and the values of d were chosen so as to display the effect of this parameter.

The curves of Figure 11 indicate that the range of observations of the "Post-P_n" wave in the Pacific Northwest region (i.e. epicentral distances from 300 to 900 km and time intervals from 1 to 5 seconds--see Table 3) would require reflectors in the depth range of from 40 to

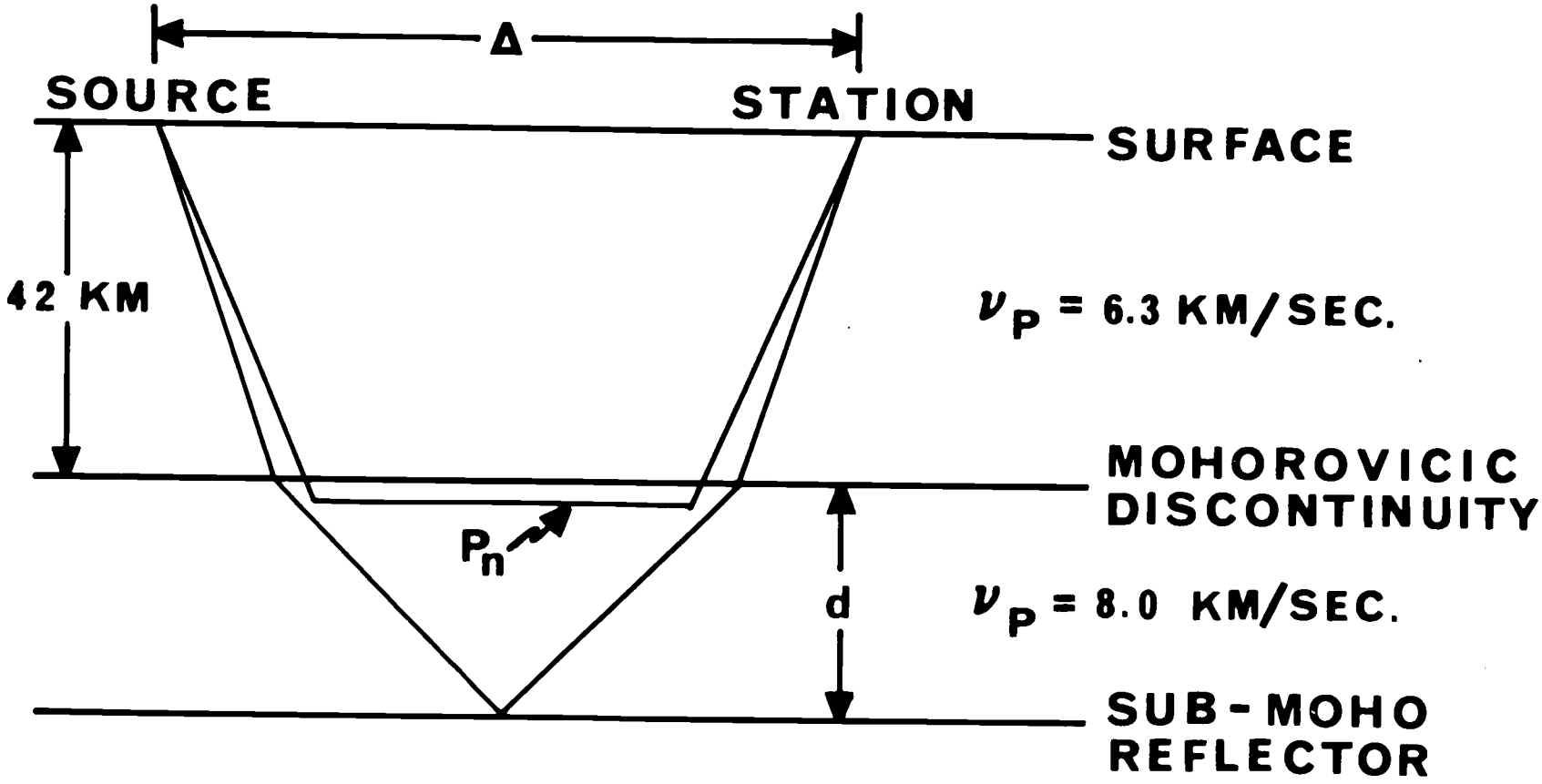

Figure 10. Geometry for sub-Moho reflections.

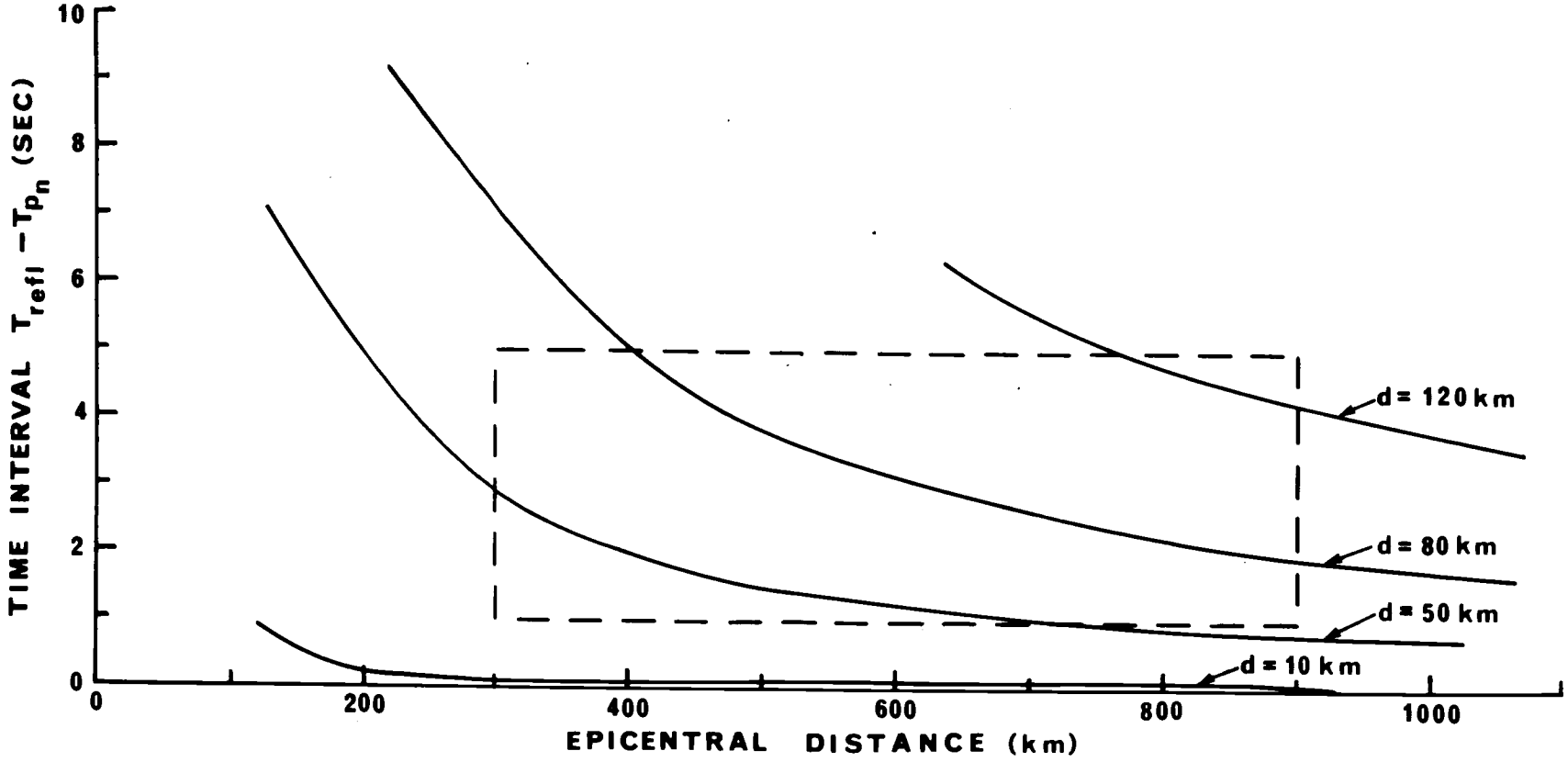

Figure 11. Arrival time interval between the two waves shown in Figure 10 vs epicentral distance. The dashed rectangle represents the scatter in the observational data of Table 3.

100 km beneath the Moho. Before carrying these results any further, the possibility of the existence of a reflecting discontinuity in this depth range must be examined.

It is very unlikely that a discontinuity at a depth of from 40 to 100 km below the Moho could be described in terms of a sudden increase in the seismic velocity with depth. Such a discontinuity has not been described in the literature. In fact, Gutenberg (1959, p. 88) concludes that: "... There is now a sufficient number of different methods which, without exception, support the hypothesis that under continents the velocities of longitudinal as well as of transverse waves decrease beginning at or slightly below the Mohorovicic discontinuity, and reach a minimum at a depth of between 100 and 200 km which differs regionally." On the other hand, there seems to be no evidence which could be used to rule out the possibility of a reflector in this depth range caused by a sudden decrease in velocity or velocity gradients.

For a single plane discontinuity at a depth d below the Moho, it is seen from Figure 11 that the time interval between P_n and the reflected wave decreases noticeably with increasing epicentral distance. The experimental results of Table 3 do not show such a systematic decrease. In addition, the fact that there is a scatter in the observational results at a given epicentral distance is not consistent with a plane discontinuity. This is true even if the depth of the

source in the crust is allowed to vary or if more layers are added to the crustal model, as the crustal segments of the P_n path and reflected path are negligibly different. The above calculations also hold when the upper mantle is assumed to have several plane reflecting discontinuities (such as a stepwise decrease in velocity through the low-velocity channel in the upper mantle), as the uppermost discontinuity would always produce the first large-angle reflection to be observed on seismograms.

The possibility that the Post-P_n phases can be explained by a single sub-Moho reflector with large topographic features poses a more difficult problem. A range of time intervals between P_n and the reflected wave could be found because the point of reflection may be at a different depth below the Moho for different positions of the source and station, even though the epicentral distance may be the same. On the other hand, the relative directions of first motions for P_n and Post-P_n should not change with azimuth if Post-P_n is a reflected wave. That is, if the upper region of the low velocity layer is the "reflector," the Post-P_n first motions should always be opposite to the P_n first motions.

Although the first motion data are considered to be reliable, they will be ignored for the moment in an attempt to determine the type of topographic features which are required to explain the observed time intervals by these reflected phases. Figure 12 was

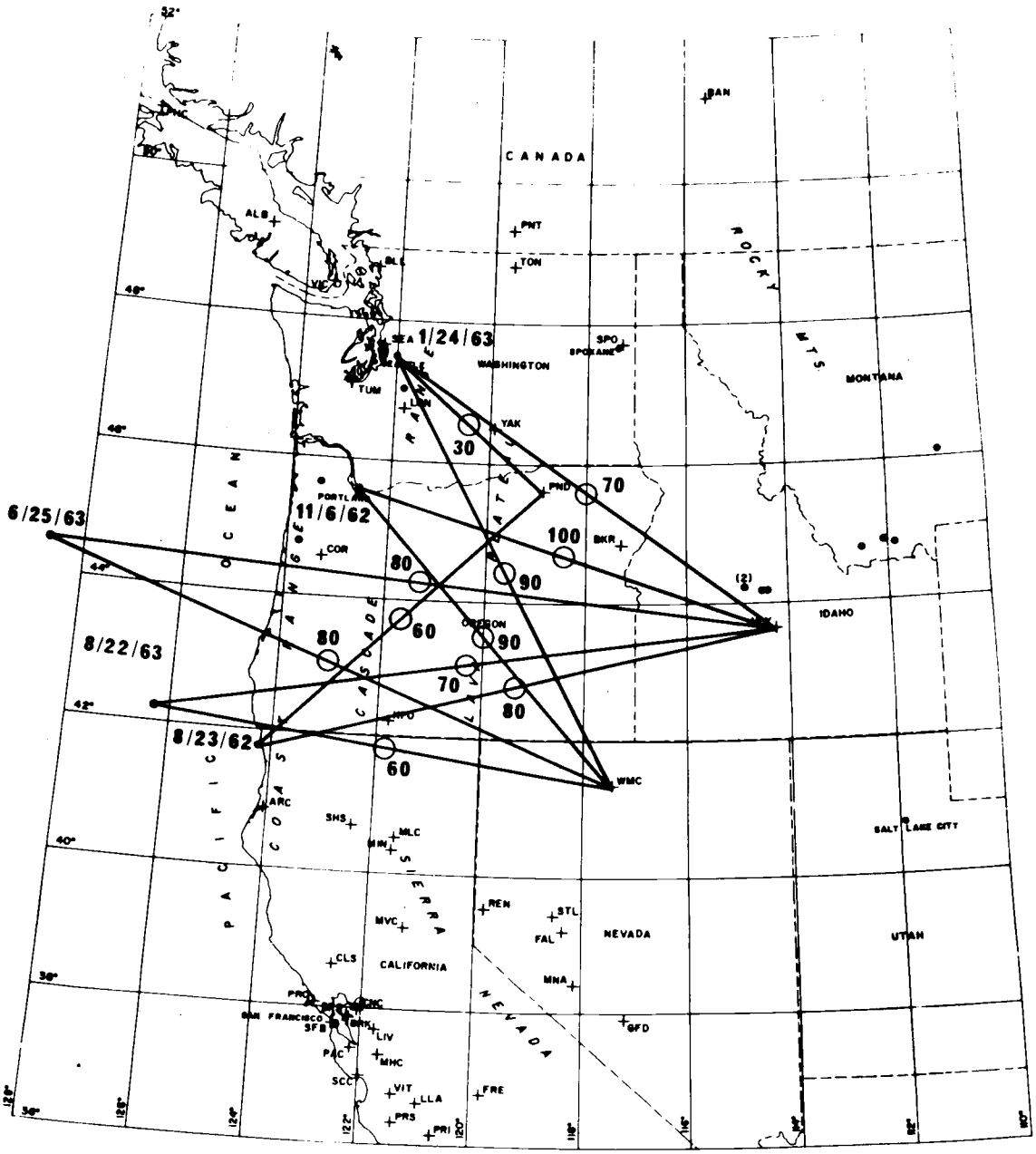

DEPTHS IN KILOMETERS BELOW MOHO

Figure 12. Topography of a sub-Moho reflector which would be required to explain the observed time intervals between Post-P_n and P_n.

constructed using only those earthquakes and stations which, in the authors opinion, most clearly exhibit large amplitude second arrivals. The circles of Figure 12 are the midpoints of the epicentral distance and would approximately represent the reflection points for the waves being considered here. The numbers give the depth beneath the Moho in kilometers to the reflection points, as determined by interpolating Figure 11 using the observed time intervals. The results are not inconsistent, and a discontinuity whose geometry is similar to that indicated in Figure 12 could account for the observed second arrivals. The topographic features indicated in Figure 12 are rather extreme if the low-velocity layer is considered to be a thermal phenomenon.

Summary

1. Consistency with the observed time intervals between P_n and Post-P_n.

   QUESTIONABLE

2. Consistency with the observed amplitude ratios of Post-P_n to P_n.

   NO CONCLUSION

3. Consistency with the observed average periods of Post-P_n and P_n.

   INCONSISTENT: The apparent period of a body wave should always be shorter than the apparent period of the head wave that it

generates for the transient pulses observed on seismograms (head waves have a time dependence which is the integral of that of the body wave).

4. Consistency with the observed relative first motion of Post-P_n to P_n.

   INCONSISTENT

5. Consistency with the observed change in character of seismograms with azimuth.

   INCONSISTENT: As the initial segment of the P_n ray path is nearly identical to that for the reflected ray path, a null direction for P_n energy would also be a null direction for the reflected ray.

6. Consistency with the observation of several second arrivals.

   QUESTIONABLE

7. Consistency with the observed discrepancy of the initial motions of short- and long-period seismograms.

   NO CONCLUSION

WAVE CONVERSIONS BY CRUSTAL DISCONTINUITIES

The predictable characteristics of second arrivals produced by the partitioning of upcoming seismic energy towards the station between the transmitted compressional and shear waves can be compared to the observational data without a lengthy discussion.

Summary

1. Consistency with the observed time intervals between P_n and Post-P_n.

   INCONSISTENT: The time interval between the parent wave and the converted wave would be a constant for a given station for all shocks.

2. Consistency with the observed amplitude ratios of Post-P_n and P_n.

   INCONSISTENT: The amplitude of a converted wave compared to the parent wave would be a property of the station and not of the earthquake. See Figure 13 for an example of changes in the time intervals and the amplitude ratios for P_n and Post-P_n from several shocks recorded at the same station.

3. Consistency with the observed average periods of Post-P_n and P_n.

   CONSISTENT: A converted wave should have the same time

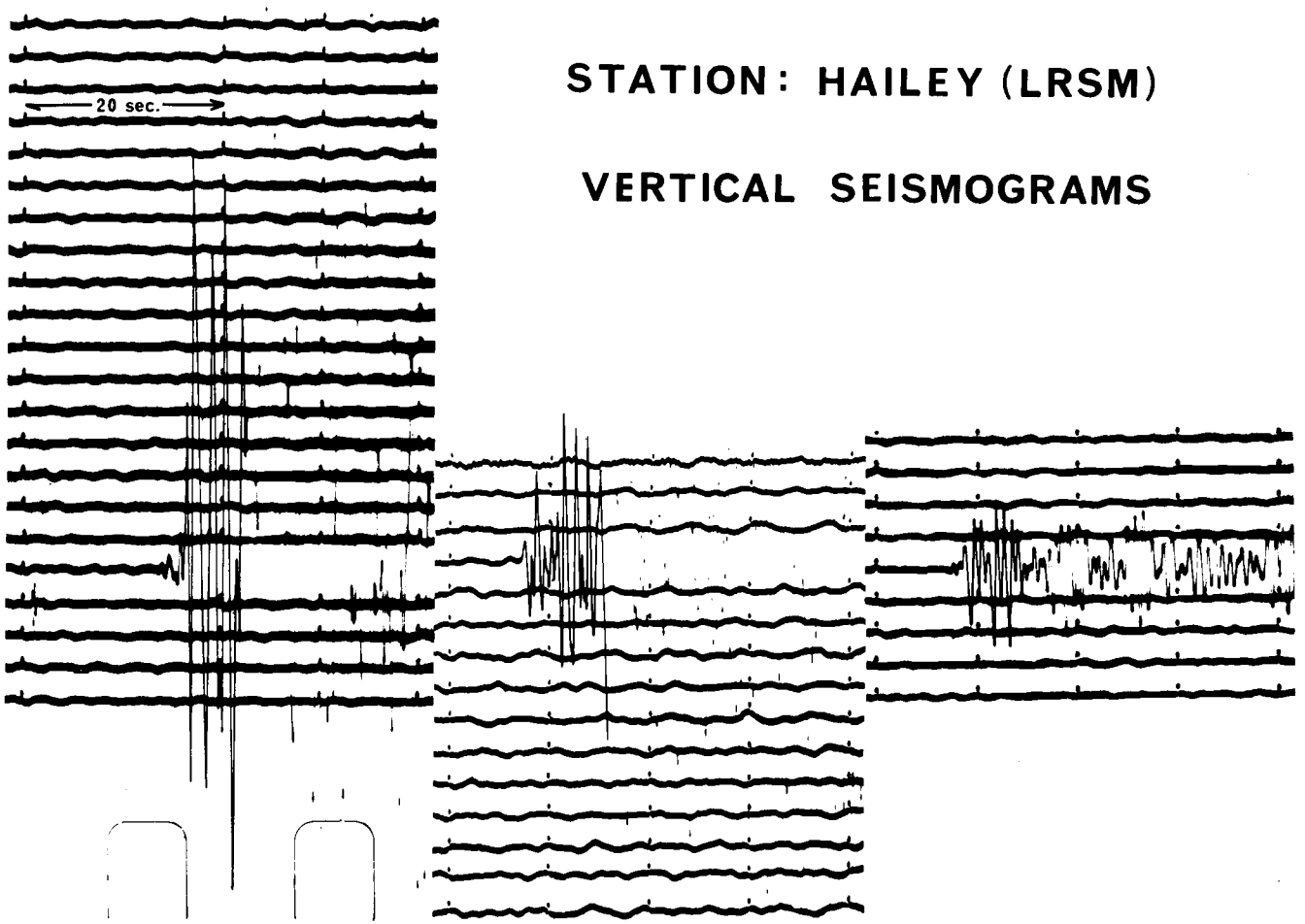

Figure 13. Records showing changes in the time intervals and amplitude ratios for several shocks recorded at the same station.

dependence as the parent wave.

4. Consistency with the observed relative first motion of Post-P_n to P_n.

   INCONSISTENT

5. Consistency with the observed change in character of seismograms with azimuth.

   INCONSISTENT

6. Consistency with the observation of several second arrivals.

   INCONSISTENT: The same sequence of converted waves would be present on all records at a given station.

7. Consistency with the observed discrepancy of the initial motions of short- and long-period seismograms.

   NO CONCLUSION

SIGNAL-GENERATED NOISE

Particle-motion diagrams were constructed for the purpose of determining the character of the ground motion which produced the second phases on the seismograms. Records were selected which had the most favorable signal-to-microseism ratio, and the three components of the earth's vibration were digitized by laying a transparent grid directly over the seismograms. As the seismographs record time fiducials simultaneously on all three components, the grid could be placed on the three different records with sufficient accuracy to insure simultanaiety of the three sets of digitized data. A digitizing interval of 0.05 second was used.

As the microseismic activity is seldom negligible and as the zero-level of the trace on the seismogram is somewhat arbitrary, a simple vector addition of the two horizontal components is not adequate for determining the total horizontal motion. This can be seen by referring to Figure 14(a) where points A and B would represent nearly zero horizontal displacement for the rectilinear vibration resulting from the earthquake signal. The slight departure from rectilinear motion causes the value of $(N^2 + E^2)^{1/2}$ for point B to be much larger than that for point A. This results in a rather erratic diagram when the vertical data are plotted against the total horizontal component calculated in this manner. Therefore, a

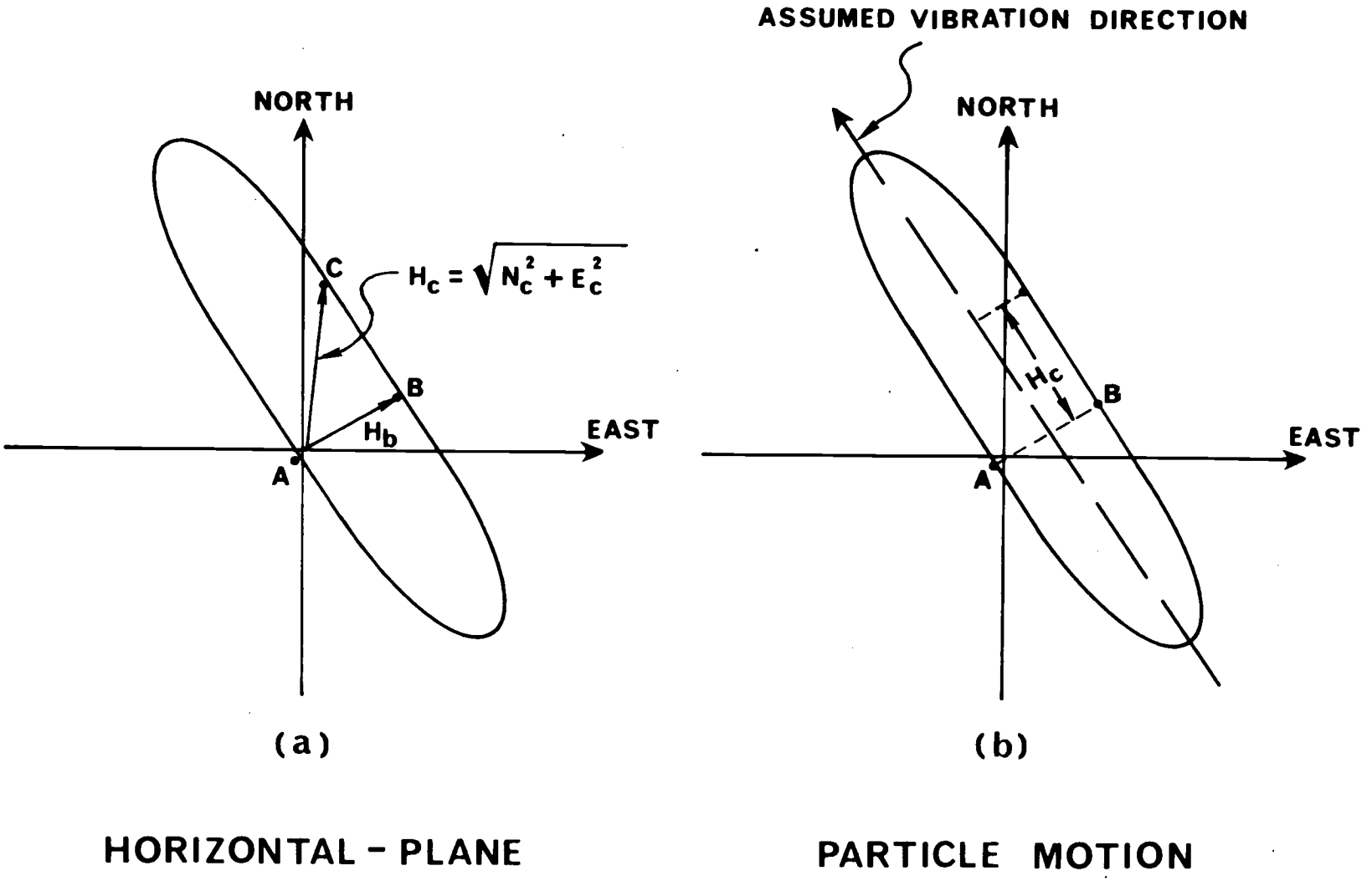

Figure 14. Determination of the total horizontal motion by vector addition and by the assumed-vibration-direction method.

direction of vibration was assumed in the horizontal plane as shown in Figure 14(b), and the component in this direction was used as the total horizontal component. This procedure was carried out manually by first plotting the digitized data from the horizontal instruments and aligning the x-axis of an overlay grid with the assumed vibration direction. The horizontal component of motion was then read as the x component of each point.

Vertical plane particle motion diagrams were constructed by plotting the digitized data from the vertical seismograms against the simultaneous total horizontal component as determined by the assumed-vibration-direction method. Examples of the resulting vertical plane diagrams are shown in Figure 15. The diagrams show that the Post-P_n phase has the same apparent angle of emergence as the P_n phase, and that Post-P_n arrives with the vibration of a compressional wave rather than that of a surface wave or a shear wave. It was characteristic of the diagrams to become very complex a few seconds after the onsets of the arrivals.

A particularly puzzling phenomenon was observed when the particle motion diagrams in the horizontal plane were continued for several seconds. It is expected that the horizontal vibration would be somewhat rectilinear and along the azimuth from the source to the station prior to the time of arrival of the shear waves from the source. This follows from the concept that the ray paths lie in a

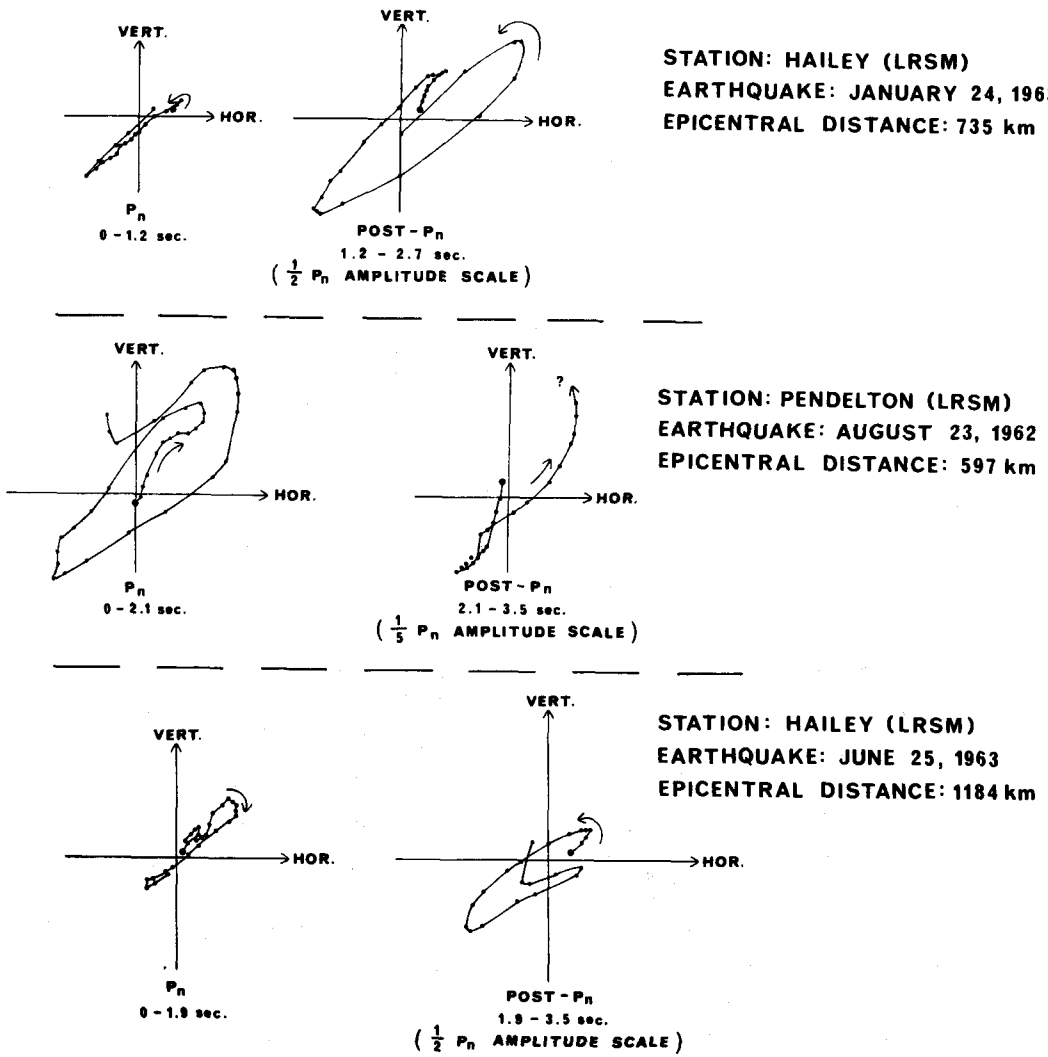

Figure 15. Vertical-plane particle motion diagrams constructed by the assumed-vibration-direction method.

vertical plane passing through the source and the station. The compressional vibrations would lie wholly in this vertical plane, as would any vertically polarized shear waves, SV waves, resulting from P to S conversions by horizontal discontinuities under the station. Of course, P to S conversions from dipping discontinuities could produce horizontally polarized shear waves, SH waves, but the SV component should always be present. Thus, any pulse of pure SH motion would not be expected before the arrival time of the direct S wave from the earthquake.

The horizontal ground motion of the January 24, 1963 earthquake as recorded at WMC (768 km epicentral distance) is shown in Figure 16. It is seen from Figure 16(a) that the initial ground motion is along the direction from the source to the station. The initial motion is rectilinear to the extent that deviations can be accounted for by the existing microseismic noise. In Figure 16(b), the departure from rectilinear vibration is now greater than can be accounted for by microseismic noise, but perhaps it can be explained by some SH contamination produced by dipping interfaces. In Figure 16(c), however, the ground motion becomes nearly rectilinear in a direction transverse to the source-to-station azimuth. The arrival time is much too soon for this motion to be the result of SH waves from the source. The subsequent motion [Figure 16(a)] becomes very complicated. The reasons for these departures from the expected

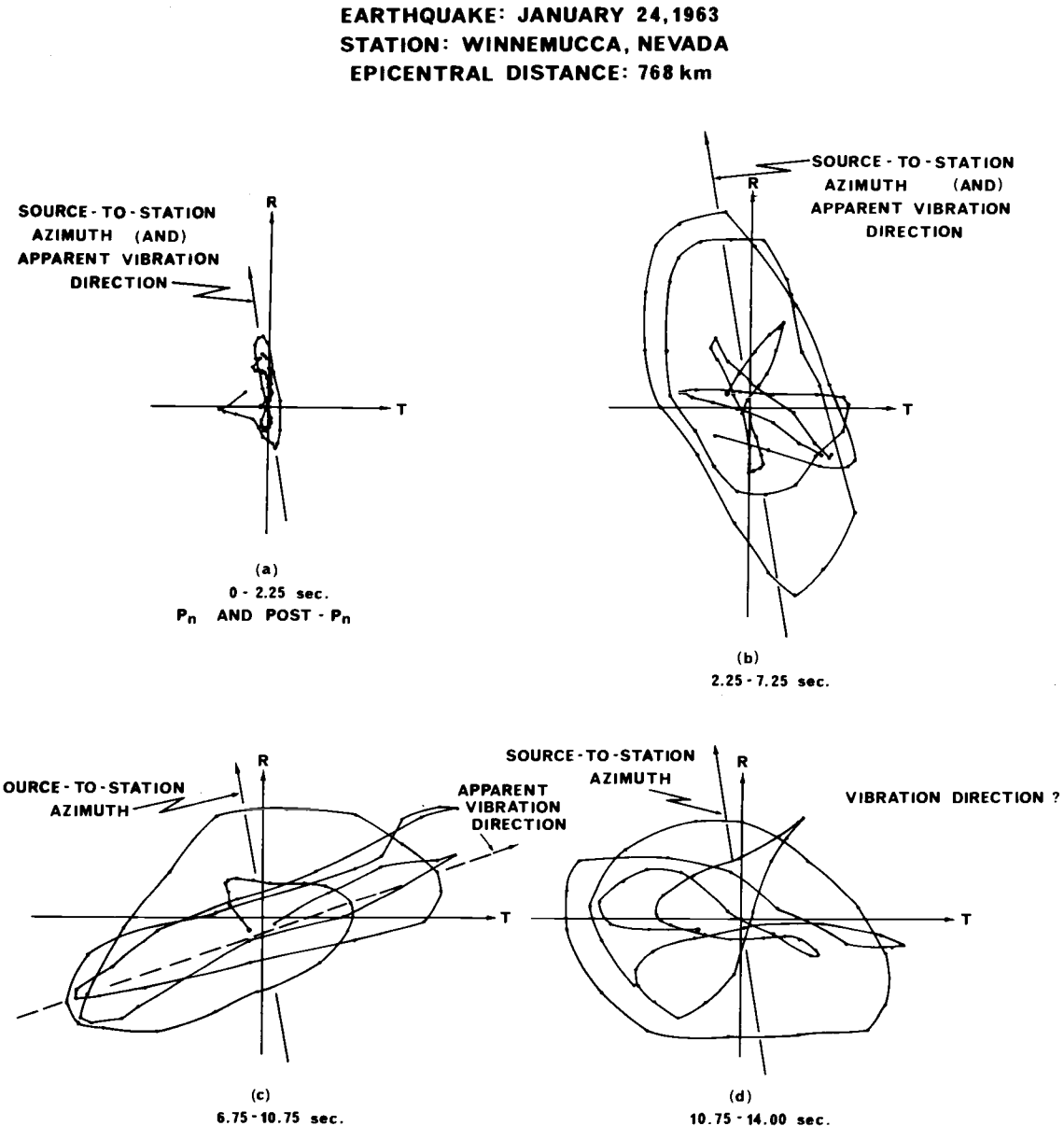

Figure 16. Horizontal-plane particle motion diagrams for 14 seconds following the onset of the earthquake.

vibration direction are unknown. These observations will be mentioned further in the next section and in the discussion section.

Returning to the considerations of signal-generated noise, the particle-motion diagrams show that the first large amplitude second arrival seems to have the same vibration azimuth in the horizontal plane and the same apparent angle of emergence in the vertical plane as the P_n wave. The character of the second arrival is that of a P wave rather than that of a surface wave. These results indicate that the assumption of inhomogenieties under the station producing converted, scattered, or reflected energy is not required to explain the Post-P_n phase. As the particle-motion diagrams quickly become complex, these conclusions cannot be drawn for the third and later phases.

Summary

1. Consistency with the observed time intervals between P_n and Post-P_n.

   INCONSISTENT: This hypothesis would require the time interval to be a property of the station rather than a property of the earthquake.

2. Consistency with the observed amplitude ratios of Post-P_n to P_n.

   NO CONCLUSION

3. Consistency with the observed average periods of Post-P_n and P_n.

NO CONCLUSION

4. Consistency with the observed relative first motion of Post-P_n and P_n.

   INCONSISTENT: This would be a property of the structure under the station and would be the same for all earthquakes.

5. Consistency with the observed change in character of seismograms with azimuth.

   NO CONCLUSION

6. Consistency with the observation of several second arrivals.

   QUESTIONABLE

7. Consistency with the observed discrepancy of the initial motions of short- and long-period seismograms.

   NO CONCLUSION

REFRACTED WAVES TRAVELING MODIFIED PATHS FROM THAT OF P_n

As the P_n wave is considered to travel within the mantle near the crust-mantle interface along the source-to-station azimuth, it is necessary to consider the possibility that seismic energy may travel by slightly different paths in either the vertical or horizontal planes.

Because the observed time interval between P_n and Post-P_n is independent of epicentral distance, Post-P_n cannot be explained as an additional refracted wave in the vertical plane. The possibility of different refraction paths in the horizontal plane were brought into consideration by the horizontal particle-motion diagrams of the preceding section, which indicated rectilinear motion along azimuths other than the source-to-station azimuth. The results of numerous refraction surveys have shown that horizontal gradients exist for both the average crustal velocity and the P_n velocity. These horizontal gradients (whether they are considered to be uniform velocity gradients or differences in velocity between adjacent crustal blocks) could result in different horizontal refraction paths, just as a vertical velocity structure can result in different vertical refraction paths.

Without detailed knowledge of the velocity structure of the

crust and upper mantle, it is difficult to evaluate the significance of horizontal refraction. The data presented by James and Steinhart (1966), however, indicate that horizontal velocity changes in the Pacific Northwest states are not large, and would allow for only very small angle refractions in the horizontal plane. Thus, as first motions should always be the same for refraction paths which differ only slightly, the data indicate that Post-P_n is not produced by horizontal refraction. In addition, the time interval between P_n and Post-P_n does not display the dependence upon epicentral distance which would be expected if different horizontal refraction paths were involved.

Summary

1. Consistency with the observed time intervals between P_n and Post-P_n.

   QUESTIONABLE

2. Consistency with the observed amplitude ratios of Post-P_n to P_n.

   NO CONCLUSION

3. Consistency with the observed average periods of Post-P_n and P_n.

   CONSISTENT

4. Consistency with the observed relative first motion of Post-P_n

to P_n.

INCONSISTENT: The relative first motions should always be the same for paths differing only slightly.

5. Consistency with the observed change in character of seismograms with azimuth.

   QUESTIONABLE

6. Consistency with the observation of several second arrivals.

   QUESTIONABLE

7. Consistency with the observed discrepancy of the initial motions of short- and long-period seismograms.

   NO CONCLUSION

SECOND SOURCE MOTION

The multiple shock concept can be used to explain numerous phases when one is studying a limited portion of an earthquake seismogram. For example, if a definite sequence of arrivals is observed within the first ten seconds on seismograms from the same earthquake along different azimuths, it could be assumed that separate pulses were emitted at the source. Furthermore, if the sequences of arrivals were different on seismograms recorded along different source-to-station azimuths, then the assumption could be made that a second source exists which is displaced in space as well as in time from the initial source.

Under certain fortuitous circumstances, it may be possible to check the above assumptions directly, but in areas such as the Pacific Northwest the requirements on earthquake magnitudes and station magnifications would rarely be met by the few seismic recording installations available. Therefore, for the purpose of predicting realistically observable effects of true second source motion, it is necessary to develop a more specific model of the events occurring in the focal region.

There seem to be no a priori arguments which can be used to predict the time intervals between the initial disturbance at an earthquake focus and subsequent emission of seismic energy from the

focal region--whether this second motion is considered to be the result of varying frictional effects on the fault surface, triggering of neighboring points of stress concentration by stress changes resulting from the initial disturbance, the passage of a newly forming fault surface through regions of differential structural characteristics, interference effects of continuous radiation from all points on a fault surface with finite slippage duration, or any other failure mechanism which could produce acoustic radiation shortly after the initial disturbance.

It does not seem unrealistic to assume that any second emissions (with amplitude comparable to the initial disturbance) would have radiation patterns similar to that of the initial disturbance. This assumption is based upon the concept that the radiation patterns are governed by a combination of the regional stress pattern and local tectonics which could not differ significantly for associated disturbances occurring within a few seconds of each other. Indeed, focal mechanism studies for localized areas display a similarity in the radiation patterns of shocks of comparable magnitude separated in time by hours, days and even months (see, for example, Udias, 1965 or McEvilly, 1966). Thus, as multiple source motions would have similar radiation patterns, this explanation of Post-P_n would not account for the observed azimuthal changes in the amplitude ratio of Post-P_n to P_n or the observed azimuthal changes in the relative

directions of first motion of Post-P_n to P_n. In addition, a second source motion of energy comparable to the initial disturbance would produce a duplication of all phases on the seismograms. This duplication of all phases did not appear to be the case for the records studied.

Summary

1. Consistency with the observed time intervals between P_n and Post-P_n.

   CONSISTENT

2. Consistency with the observed amplitude ratios of Post-P_n to P_n.

   CONSISTENT

3. Consistency with the observed average periods of Post-P_n and P_n.

   NO CONCLUSION

4. Consistency with the observed relative first motion of Post-P_n to P_n.

   INCONSISTENT: The directions of first motion would be the same at all azimuths for true second source motion and for the breakout phase, and opposite for the stopping phase.

5. Consistency with the observed change in character of seismograms with azimuth.

INCONSISTENT: The amplitude ratios of the first and second arrivals should be the same for all azimuths as the radiation patterns for the sources are assumed to be the same under this hypothesis.

6. Consistency with the observation of several second arrivals.

   CONSISTENT in part: The stopping phase and breakout phase could account for only one second arrival, but any number of true second sources could be hypothesized.

7. Consistency with the observed discrepancy of the initial motions of short- and long-period seismograms.

   NO CONCLUSION

REFLECTED AND/OR CONVERTED HEAD WAVES

The provisional identification by Dehlinger and French (1965) of the sP_n wave leads to a consideration of all waves which travel from source to receiver as dilitational head waves associated with the Moho. A simple model of a single-layer crust overlying a uniform mantle is used here to predict the gross effects caused by the more detailed velocity-depth structure of the real earth.

Ray paths for the waves to be investigated are shown in Figure 17. The symbols P_1 and S_1 represent compressional and shear waves, respectively, in the crustal layer. P_2 represents the head wave associated with the Moho. The symbols $\uparrow$ and $\downarrow$ indicate respectively whether the initial segment of the ray path is towards the surface or the Moho. The actual directions of the segments $\uparrow P_1$, $\downarrow P_1$, $\uparrow S_1$, and $\downarrow S_1$ depend upon the seismic velocities.

The first wave to arrive at a station will be the $\downarrow P_1P_2P_1$ wave, the conventional P_n wave. The other waves shown in Figure 17 arrive after P_n at time intervals which are independent of the epicentral distance and depend only upon the focal depth for a given crustal model. Using geometrical optics, the time intervals between P_n and the other waves can be calculated as a function of focal depth. Figures 18 to 23 display calculated delay times after P_n for one-layer crustal approximations applicable in each of the three provinces in

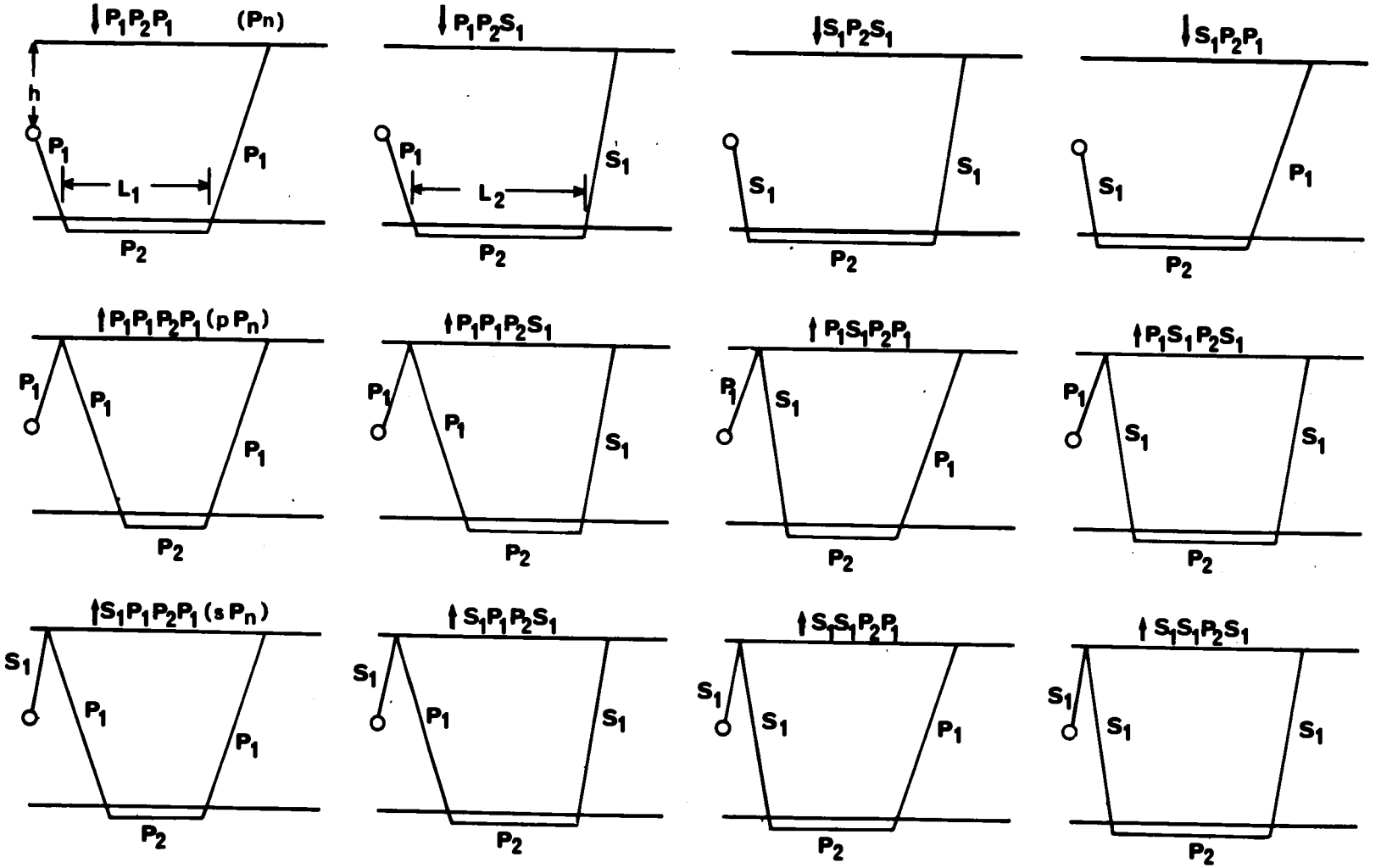

Figure 17. Ray paths for those waves which travel most of the distance from the source to the station as a dilitational head wave associated with the Mohorovicic discontinuity.

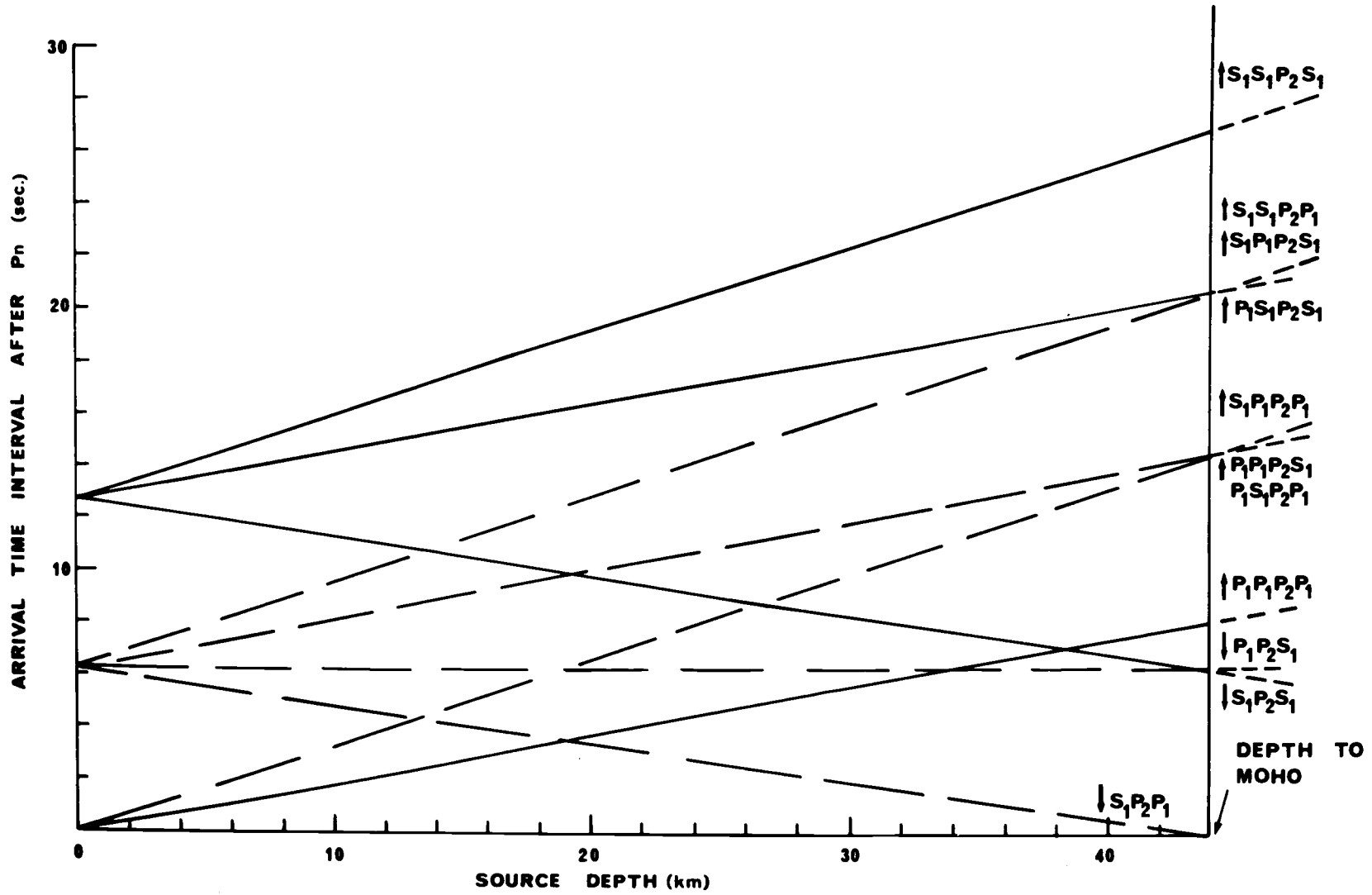

Figure 18. Time delay after P_n vs focal depth for source and station in the continental province east of the Cascade Range (see text).

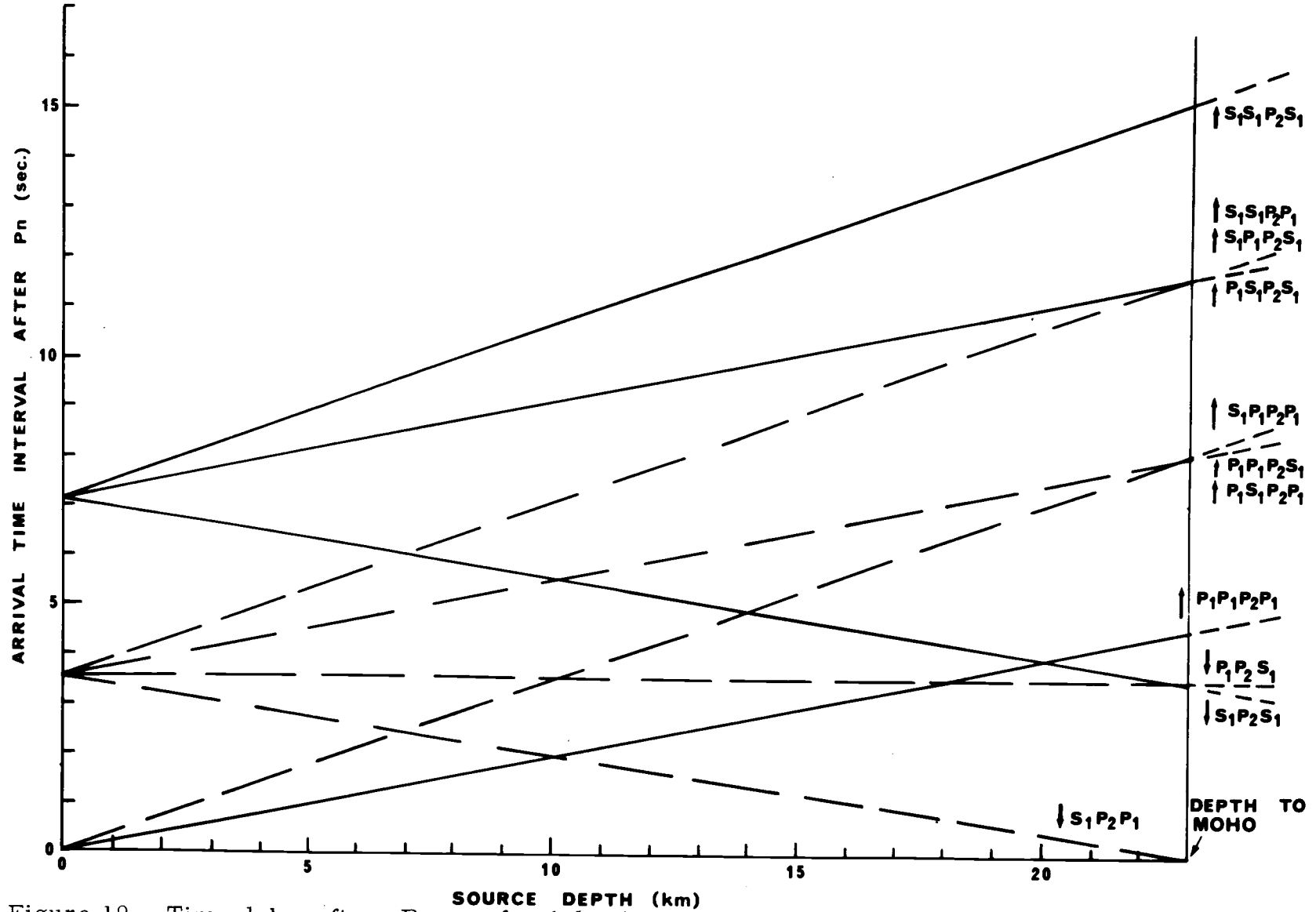

Figure 19. Time delay after P_n vs focal depth for source and station in the continental province west of the Cascade Range.

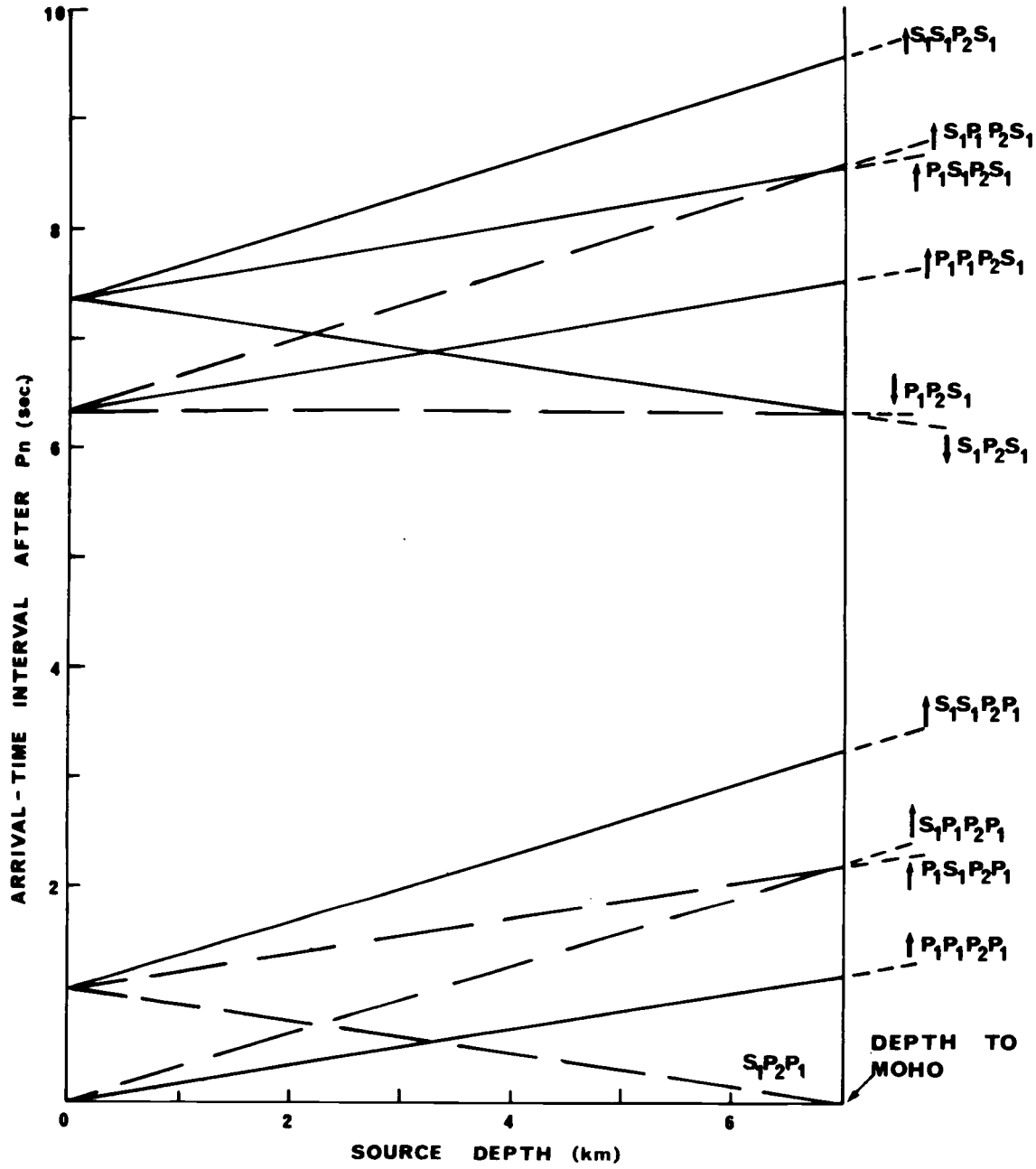

Figure 20. Time delay after P_n vs focal depth for a source in the oceanic province and a station in the continental province east of the Cascade Range.

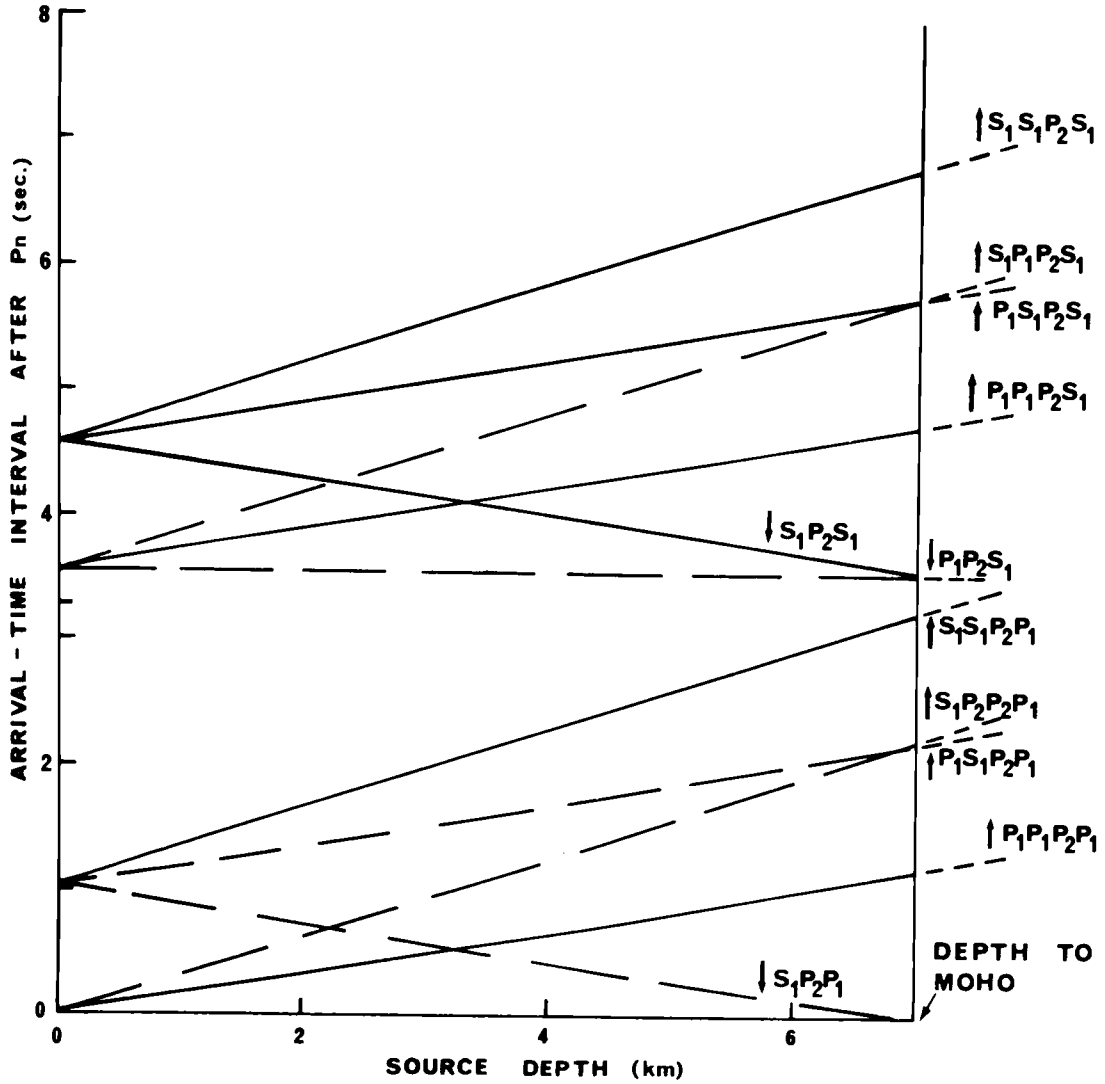

Figure 21. Time delay after P_n vs focal depth for a source in the oceanic province and a station in the continental province west of the Cascade Range.

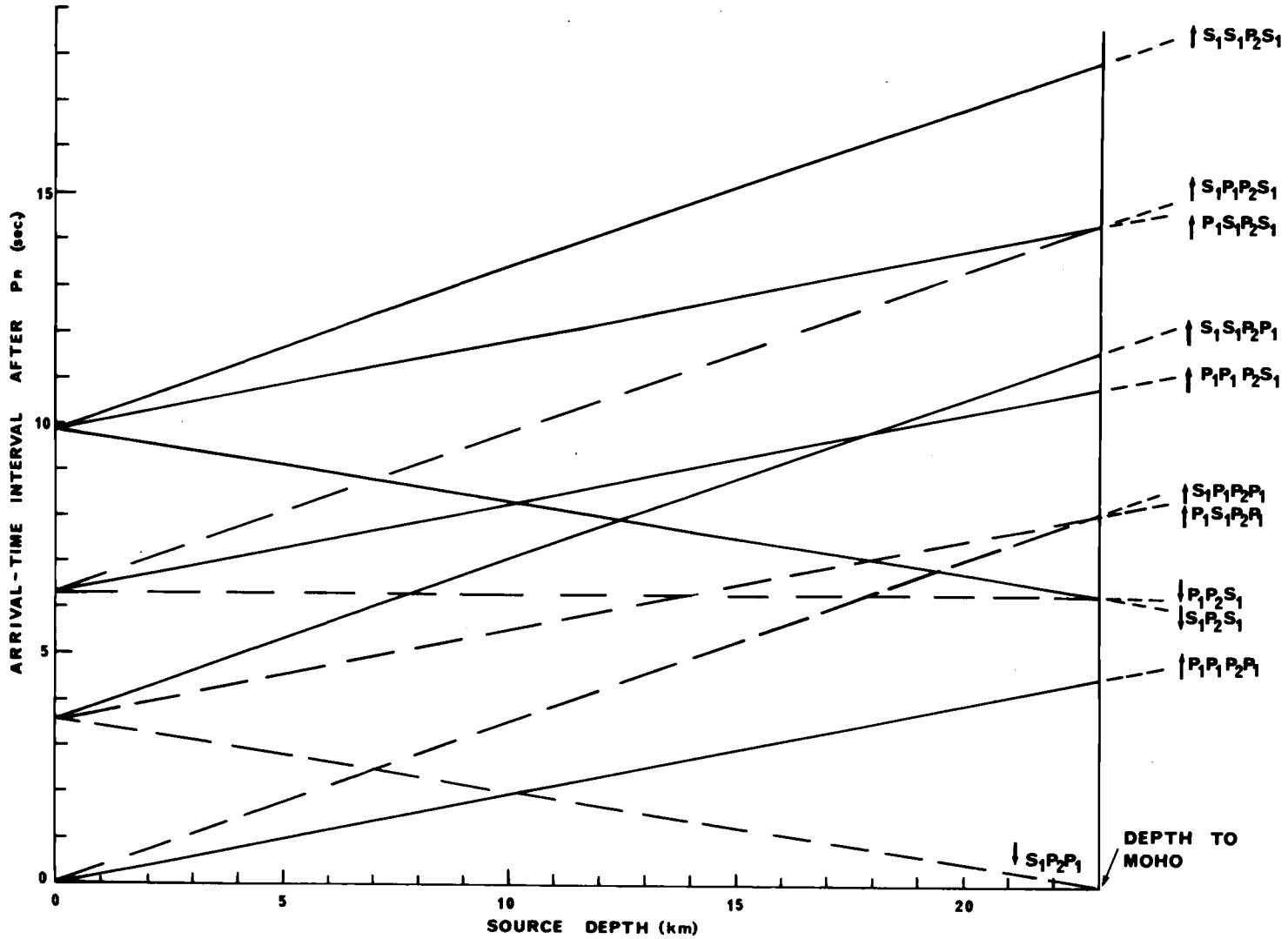

Figure 22. Time delay after P_n vs focal depth for a source in the continental province west of the Cascade Range and a station in the continental province east of the Cascade Range.

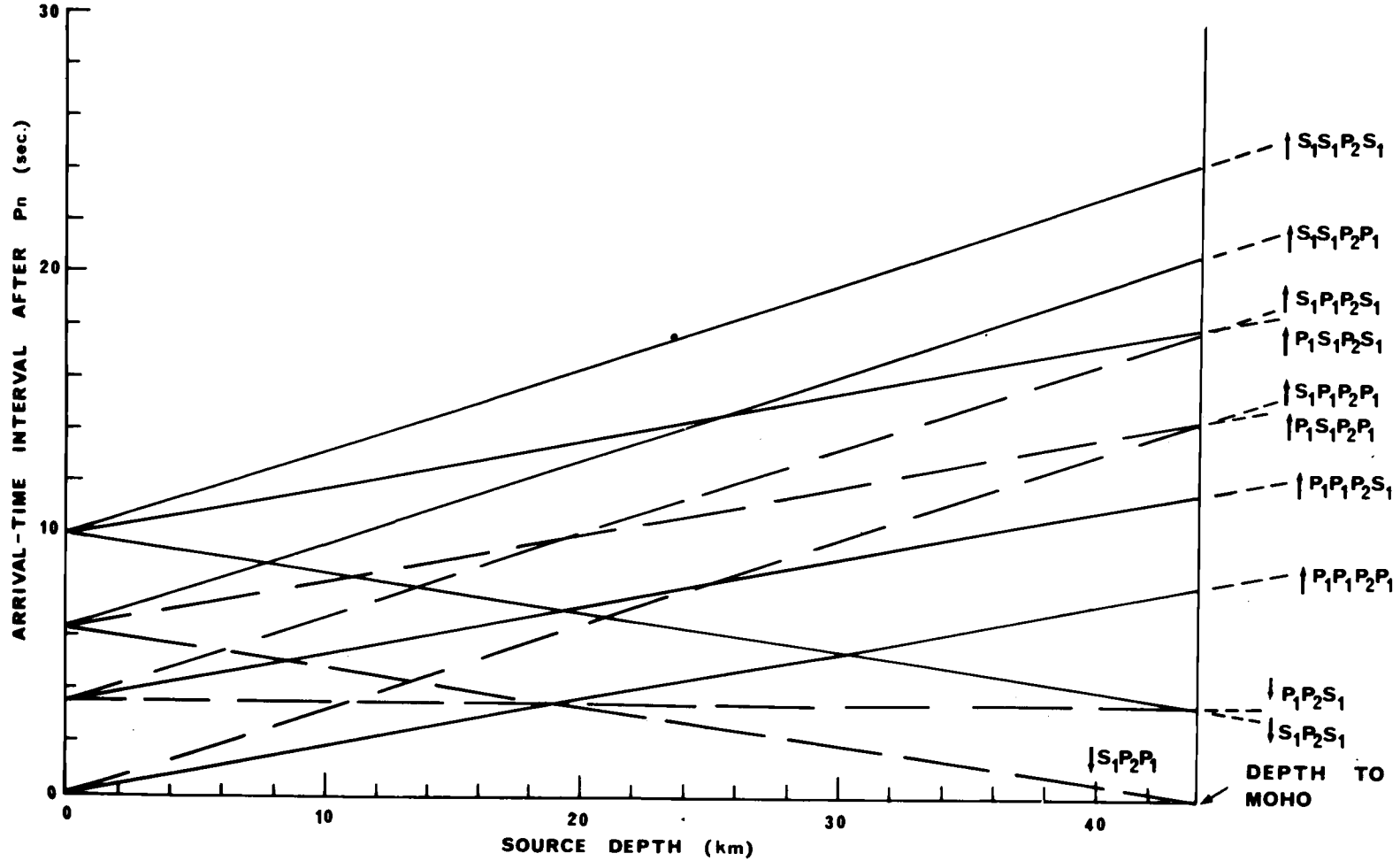

Figure 23. Time delay after P_n vs focal depth for a source in the continental province east of the Cascade Range and a station in the continental province west of the Cascade Range.

the Pacific Northwest states and for combinations of a source in one province and a station in another. The dashed curves correspond to waves which should be recorded on the seismograms. The solid lines represent waves which will be shown later to have insufficient energy to be recorded. Table 4 was constructed from Figure 22 for a source west of the Cascade Range and a station east of the Cascades. The table gives the sequence of arrivals and time intervals corresponding to four focal depths.

Some of the waves listed in Table 4 arrive within the time interval of the observations of the Post-P_n wave. Furthermore, a sequence of arrivals is indicated and the order of the arrivals depends upon focal depth.

The question arises whether any of these waves carries sufficient energy to be registered on a seismogram. It is therefore necessary to investigate the amplitude considerations of these head waves.

The problem of solving the wave equation subject to the conditions of a time dependent source imbedded in an acoustic layer overlying a half-space is quite formidable. Fortunately, the results of published theoretical analyses of head wave propagation (Newlands, 1952; Heelan, 1953; Brekhovskikh, 1960) can be applied here. Most theoretical treatments deal with the acoustic fields within two half-spaces in welded contact. The seismograph, on the other hand, registers the motion of the earth's surface so that the effects of the interaction of

Table 4. Sequence of head wave arrivals for a source located in the crust west of the Cascade Range and a station located east of the Cascades. Crustal parameters given in Figure 5. (h is the focal depth of the earthquake in kilometers. T is the time interval in seconds that the listed wave arrives after P_n ($\downarrow P_1P_2P_1$)

h = 5		h = 10		h = 15		h = 20	
Wave	T	Wave	T	Wave	T	Wave	T
$\uparrow P_1P_1P_2P_1$	1.0	$\uparrow P_1P_1P_2P_1$	1.9	$\downarrow S_1P_2P_1$	1.3	$\downarrow S_1P_2P_1$	0.5
$\uparrow S_1P_1P_2P_1$	1.8	$\downarrow S_1P_2P_1$	2.0	$\uparrow P_1P_1P_2P_1$	2.9	$\uparrow P_1P_1P_2P_1$	3.9
$\downarrow S_1P_2P_1$	2.8	$\uparrow S_1P_1P_2P_1$	3.5	$\uparrow S_1P_1P_2P_1$	5.3	$\downarrow P_1P_2S_1$	6.3
$\uparrow P_1S_1P_2P_1$	4.5	$\uparrow P_1S_1P_2P_1$	5.5	$\downarrow P_1P_2S_1$	6.3	$\downarrow S_1P_2S_1$	6.8
$\uparrow S_1S_1P_2P_1$	5.3	$\downarrow P_1P_2S_1$	6.3	$\uparrow P_1S_1P_2P_1$	6.5	$\uparrow S_1P_1P_2P_1$	7.1
$\downarrow P_1P_2S_1$	6.3	$\uparrow S_1S_1P_2P_1$	7.1	$\downarrow S_1P_2S_1$	7.6	$\uparrow P_1S_1P_2P_1$	7.5
$\uparrow P_1P_1P_2S_1$	7.3	$\uparrow P_1P_1P_2S_1$	8.3	$\uparrow S_1S_1P_2P_1$	8.8	$\uparrow P_1P_1P_2S_1$	10.3
$\uparrow S_1P_1P_2S_1$	8.1	$\downarrow S_1P_2S_1$	8.4	$\uparrow P_1P_1P_2S_1$	9.3	$\uparrow S_1S_1P_2P_1$	10.6
$\downarrow S_1P_2S_1$	9.1	$\uparrow S_1P_1P_2S_1$	9.8	$\uparrow S_1P_1P_2S_1$	11.6	$\uparrow S_1P_1P_2S_1$	13.4
$\uparrow P_1S_1P_2S_1$	10.9	$\uparrow P_1S_1P_2S_1$	11.8	$\uparrow P_1S_1P_2S_1$	12.8	$\uparrow P_1S_1P_2S_1$	13.8
$\uparrow S_1S_1P_2S_1$	11.6	$\uparrow S_1S_1P_2S_1$	13.4	$\uparrow S_1S_1P_2S_1$	15.2	$\uparrow S_1S_1P_2S_1$	17.0

the free surface with the incident waves must be taken into account.

The point source problem has not been caried to the extent of providing a theoretical description of all the individual waves shown in Figure 17. Newlands (1952), however, has carried the solution of the line source problem to this end. In the following, Newlands' calculations will be briefly reviewed and extended to obtain numerical values for the relative amplitudes of the waves in Figure 17. The applicability of these results to earthquake seismograms will be discussed later.

Newlands' Theory for a Line Source

Newlands' model (Figure 24) consists of a line source S and receiver R within a solid layer of thickness H, having a free upper surface and a lower surface in welded contact with a solid half-space. The compressionsal and shear wave velocities in the layer are α_1 and β_1 respectively. The corresponding velocities in the half-space are α_2 and β_2. Using the coordinate system shown, the source is at (O, h), the receiver at (x, z), the welded interface at $z = H$, and the free surface at $z = 0$. The figure extends to infinity in the y-direction, perpendicular to the paper.

In the case of a line source, the wave equations to be solved for the two displacement potentials in each layer can be written as follows:

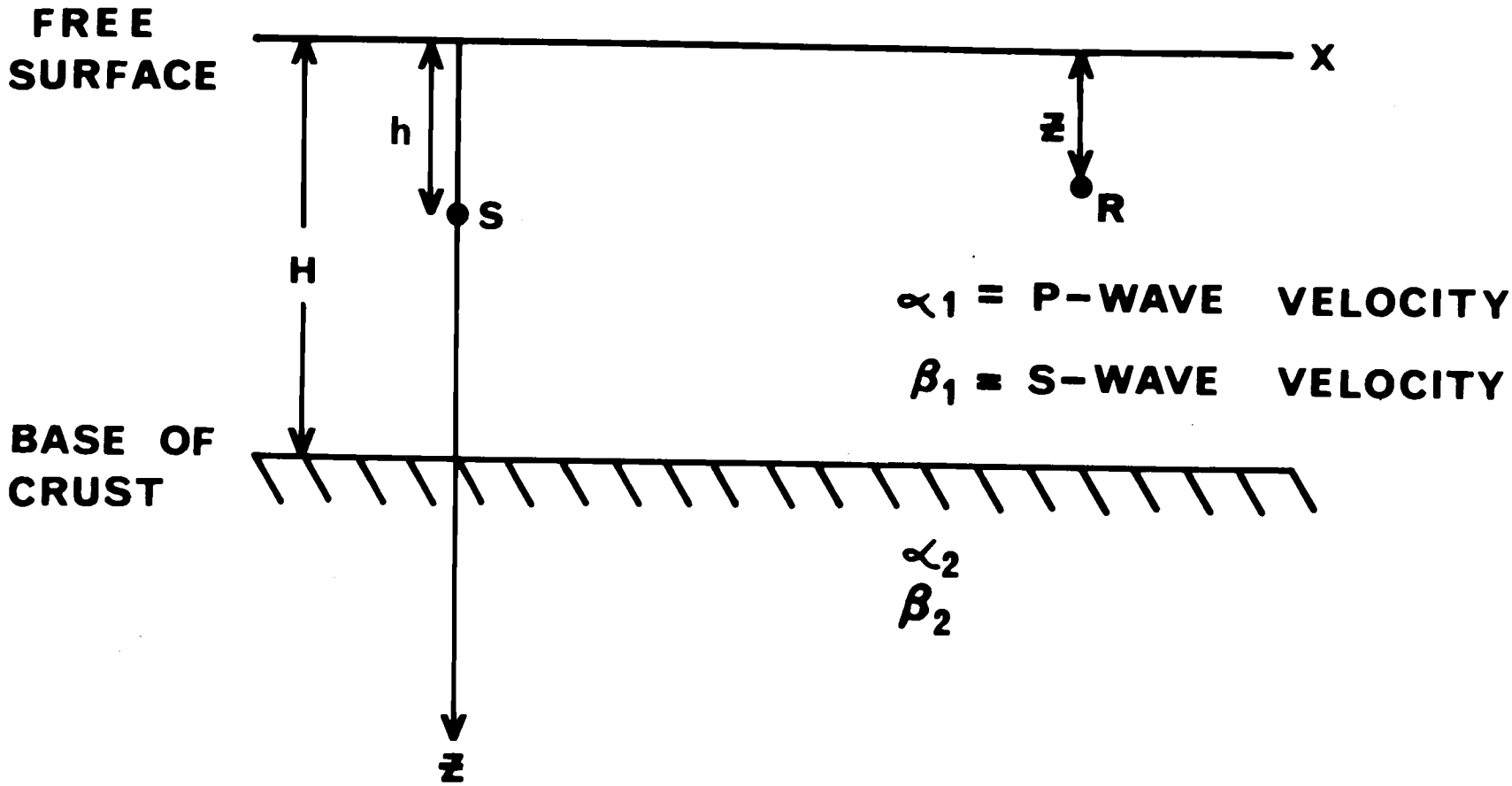

Figure 24. Newlands' model of a line source in a one-layer crust.

$$\nabla^2\phi_q = \frac{1}{\alpha_q^2}\frac{\partial^2\phi_q}{\partial t^2}, \quad \nabla^2\psi_q = \frac{1}{\beta_q^2}\frac{\partial^2\psi_q}{\partial t^2} \tag{1}$$

where $q=1, 2$ for the layer and half-space respectively. The particle displacements U and W in the x and z directions are given by:

$$\begin{aligned} U_q &= \frac{\partial\phi_q}{\partial x} + \frac{\partial\psi_q}{\partial z} \\ W_q &= \frac{\partial\phi_q}{\partial z} - \frac{\partial\psi_q}{\partial x} \end{aligned} \tag{2}$$

If the x, y and z axes are indicated by 1, 2, and 3, the general expression for the stress P_{ij} in the j^{th} direction acting on a plane perpendicular to the i^{th} axis is given by

$$P_{ij} = \lambda_q \theta_q \delta_{ij} + 2\mu_q \epsilon_{ij}, \quad \delta_{ij} = \begin{cases} 0, & i \neq j \\ 1, & i = j \end{cases} \tag{3}$$

where λ_q and μ_q are Lame's constants for the layer or half-space $(q=1, 2)$, $\theta_q = \nabla^2\phi_q$, $\epsilon_{ij} = \frac{1}{2}\left(\frac{\partial u_i}{\partial x^j} + \frac{\partial u_j}{\partial x^i}\right)$, $U_1 = U$, $U_2 = V$, $U_3 = W$, $x^1 = x$, $x^2 = y$, and $x^3 = z$.

The solutions of Equations (1) are subject to the six boundary conditions that the normal and tangential components of stress vanish at $z = 0$ and that both the normal and tangential components of displacement and of stress are continuous across the interface $z = H$.

Newlands represented the source of compressional waves as a uniform radial expansion of the line source and the source of shear

waves as a counterclockwise twist of the line source (pure SV radiation), with the time dependence of both being a Heavyside step function.

By placing an image source at the point (0, -h) and requiring that the potentials decrease with depth in the half-space (no sources at infinity), Newlands solved equations (1) in cylindrical coordinates for the steady state time dependence $e^{i\omega t}$ and expressed the solution in cartesian coordinates by using in integral relation of Lapwood (1949). Newlands' solutions for the potentials in the two media for an initial **P** pulse are:

$$\phi_1 = -4e^{i\omega t} \int_0^\infty [\, F(\zeta) - Ae^{-(z-H)\lambda \alpha_1} - Be^{(z-H)\lambda \alpha_1}] \cos x\,\zeta\, d\zeta$$

$$F(\zeta) = \begin{cases} \dfrac{1}{\lambda \alpha_1} e^{-\lambda \alpha_1 z \sinh h\lambda \alpha_1}, & h \leq z \leq H \\ \dfrac{1}{\lambda \alpha_1} e^{-\lambda \alpha_1 h \sinh z\lambda \alpha_1}, & 0 \leq z \leq h \end{cases} \qquad (4)$$

$$\psi_1 = 4e^{i\omega t} \int_0^\infty [\, Ce^{-(z-H)\lambda \beta_1} + De^{(z-H)\lambda \beta_1}] \sin x\zeta\, d\zeta$$

$$\phi_2 = 4e^{i\omega t} \int_0^\infty Re^{-(z-H)\lambda \alpha_2} \cos x\zeta\, d\zeta$$

$$\psi_2 = 4e^{i\omega t}\int_0^\infty Qe^{-(z-H)\lambda_{\beta_2}} \sin x\zeta \, d\zeta$$

where $\lambda_{\alpha_1} = (\zeta^2 - R_{\alpha_1}^2)^{\frac{1}{2}}$, $\lambda_{\beta_1} = (\zeta^2 - R_{\beta_1}^2)^{\frac{1}{2}}$, $\lambda_{\alpha_2} = (\zeta^2 - R_{\alpha_2}^2)^{\frac{1}{2}}$, $\lambda_{\beta_2} = (\zeta^2 - R_{\beta_2}^2)^{\frac{1}{2}}$, $R_{\alpha_1} = \omega/\alpha_1$, $R_{\beta_1} = \omega/\beta_1$, $R_{\alpha_2} = \omega/\alpha_2$, $R_{\beta_2} = \omega/\beta_2$, and ζ is the integration variable required for Lapwood's integral representation of a cylindrical wave in cartesian coordinates. For mathematical definiteness, the λ's were chosen so that $R(\lambda) > 0$.

Substitution of these potentials into the six boundary conditions leads to a set of linear equations which can be solved to express each of the six coefficients A, B, C, etc. as the quotient of two 6x6 determinants. Newlands denoted the system determinant by Δ_p and the other determinants by Δ_A, Δ_B, Δ_C, etc. such that $A = \Delta_A/\Delta_p$, $B = \Delta_B/\Delta_p$, etc. . Then, by partial expansion of the 6x6 determinants, the values of Δ_p, Δ_A, Δ_B, etc. can be expressed as functions of the following 4x4 determinants.

$$s = \begin{vmatrix} -\zeta & \lambda_{\beta_1} & -\zeta & -\lambda_{\beta_2} \\ \lambda_{\alpha_1} & -\zeta & -\lambda_{\alpha_2} & -\zeta \\ -2\zeta\lambda_{\alpha_1} & (2\zeta^2 - R_{\beta_1}^2) & 2\zeta\lambda_{\alpha_2}\frac{\mu_2}{\mu_1} & (2\zeta^2 - R_{\beta_2}^2)\frac{\mu_2}{\mu_1} \\ (2\zeta^2 - R_{\beta_1}^2) & -2\zeta\lambda_{\beta_1} & (2\zeta^2 - R_{\beta_2}^2)\frac{\mu_2}{\mu_1} & 2\zeta\lambda_{\beta_2}\frac{\mu_2}{\mu_1} \end{vmatrix}$$

$$T = \begin{vmatrix} -\zeta & -\lambda_{\beta_1} & \cdots \\ \lambda_{\alpha_1} & -\zeta & \cdots \\ -2\zeta\lambda_{\alpha_1} & (2\zeta^2 - R^2_{\beta_1}) & \cdots \\ (2\zeta^2 - R^2_{\beta_1}) & 2\zeta\lambda_{\beta_1} & \cdots \end{vmatrix}, \quad V = \begin{vmatrix} -\lambda_{\beta_1} & \lambda_{\beta_1} & \cdots \\ -\zeta & -\zeta & \cdots \\ (2\zeta^2 - R^2_{\beta_1}) & (2\zeta^2 - R^2_{\beta_1}) & \cdots \\ 2\zeta\lambda_{\beta_1} & -2\zeta\lambda_{\beta_1} & \cdots \end{vmatrix} \tag{5}$$

$$U = \begin{vmatrix} -\zeta & -\lambda_{\beta_1} & \cdots \\ -\lambda_{\alpha_1} & -\zeta & \cdots \\ 2\zeta\lambda_{\alpha_1} & (2\zeta^2 - R^2_{\beta_1}) & \cdots \\ (2\zeta^2 - R^2_{\beta_1}) & 2\zeta\lambda_{\beta_1} & \cdots \end{vmatrix}$$

$$Y = \begin{vmatrix} -\zeta & -\zeta & \cdots \\ -\lambda_{\alpha_1} & \lambda_{\alpha_1} & \cdots \\ 2\zeta\lambda_{\alpha_1} & -2\zeta\lambda_{\alpha_2} & \cdots \\ (2\zeta^2 - R^2_{\beta_1}) & (2\zeta^2 - R^2_{\beta_1}) & \cdots \end{vmatrix} \quad W = \begin{vmatrix} -\zeta & \lambda_{\beta_1} & \cdots \\ -\lambda_{\alpha_1} & -\zeta & \cdots \\ 2\zeta\lambda_{\alpha_1} & (2\zeta^2 - R^2_{\beta_1}) & \cdots \\ (2\zeta^2 - R^2_{\beta_1}) & -2\zeta\lambda_{\beta_1} & \cdots \end{vmatrix}$$

The last two colums are identical for all the determinations.

In particular Δ_p can be expressed as

$$\Delta_p = e^{\{H(\lambda_{\alpha_1} + \lambda_{\beta_1})\}} \left(1 + \frac{T'}{S'} e^{\{-2H\lambda_{\beta_1}\}} + \frac{V' + Y'}{S'} e^{\{-H(\lambda_{\alpha_1} + \lambda_{\beta_1})\}} \right.$$

$$+ \frac{W'}{S'} e^{\{-2H\lambda_{\alpha_1}\}} + \frac{U'}{S'} e^{\{-2H(\lambda_{\alpha_1} + \lambda_{\beta_1})\}} \Bigg) \tag{6}$$

where

$S' = FS \quad T' = -\bar{F}T \quad V' = 4\zeta\lambda_{\alpha_1}(2\zeta^2 - R^2_{\beta_1})V, \quad Y' = -4\zeta\lambda_{\beta_1}(2\zeta^2 - R^2_{\beta_1})Y,$
$W' = -\bar{F}W, \quad U' = FU, \quad F(\zeta) = (2\zeta^2 - R^2_{\beta_1})^2 - 4\zeta^2\lambda_{\alpha_1}\lambda_{\beta_1}, \quad \bar{F}(\zeta) =$
$(2\zeta^2 - R^2_{\beta_1})^2 + 4\zeta^2\lambda_{\alpha_1}\lambda_{\beta_1}$. The remaining quantities $\Delta_A, \Delta_B, \ldots, \Delta_Q$ have similar forms and consist of a sum of terms, each of which is a function of the determinants T, V, ... , S times an exponential term which is some linear form of h, z, and H. Using relation (6), $1/\Delta_p$ can be expanded in an infinite series of exponentials, provided that the sum of the second and later terms in the parenthesis of (6) is less than unity. Subsequent multiplication of this series for $1/\Delta_p$ by Δ_A leads to a representation of the coefficient A as in infinite series of exponentials multiplied by a function of T, V, etc. . Similar series representations can be found for each of the other coefficients. This proceedure is known as the Bromwich expansion method; it yields the result that each term in the series for the potentials can be interpreted as a different kind of seismic pulse.

Newlands used the following form for the Heavyside step function.

$$H(t) = \frac{1}{2\pi i} \int_{\Omega} \frac{1}{\omega} e^{i\omega t} d\omega = \begin{cases} 0, & t < 0 \\ 1, & t > 0 \end{cases} \tag{7}$$

where Ω is the line parallel to the real axis in the complex ω-plane, from $-\infty$-ic to $+\infty$-ic, or any equivalent contour. Since the differential equations for the potentials are linear, the above steady-state solutions for ϕ and ψ can be used to construct solutions for the time dependent source given by Equation (7). Thus, Newlands obtained

$$\Phi(x, z, t) = \frac{1}{2\pi i} \int_{\Omega} \frac{1}{\omega} \phi(x, z, \omega)\, e^{i\omega t}\, d\omega$$

$$\Psi(x, z, t) = \frac{1}{2\pi i} \int_{\Omega} \frac{1}{\omega} \psi(x, z, \omega)\, e^{i\omega t}\, d\omega \qquad (8)$$

where Φ and Ψ are the solutions of Equations (1) for the time dependence given by (7). Equations (2) with ϕ and ψ replaced by Φ and Ψ respectively, along with Equations (8) constitute the complete formal solution to the problem for an initial P source with a step-function time dependence. The formal solution for the case of an initial S source can be carried out in a parallel manner.

As the interest here is in numerical values of head wave amplitudes, it is necessary to continue with Newlands' approximations to the integrals in the ζ - and ω- planes and to carry out the expansions which she indicates symbolically. Also, the mathematical approximations used in the evaluation of the integrals must be interpreted in physical terms so that the applicability to earthquake seismograms can be determined.

Newlands carried out the ω-integrations without particular

difficulty, but the ζ-integrations of Equations (4) require attention to detail. The integrations shown in Equations (4) are along the real axis of the ζ-plane, but the contour was distorted in evaluating the integrals. Since each term in the series expressions for the potentials is a function of λ_{α_1}, λ_{β_1}, λ_{α_2}, and λ_{β_2}, branch cuts must be made in the ζ-plane to insure single valuedness of the integrands (recall that $\lambda_{\alpha_1} = (\zeta^2 - R_{\alpha_1}^2)^{\frac{1}{2}}$, etc.). There are also poles in the integrands, but Newlands demonstrated that the contributions from the poles represent Rayleigh and Stoneley waves, which are surface waves that are not of interest here. For a given value of ω there are four branch points to consider: R_{α_1}, R_{β_1}, R_{α_2}, and R_{β_2}. Newlands used the Sommerfeld contour distortion for the integrations with the result that the integration along the real axis can be expressed as the sum of branch line integrals plus the contributions from the poles. The resultant integration paths for a given ω are shown below.

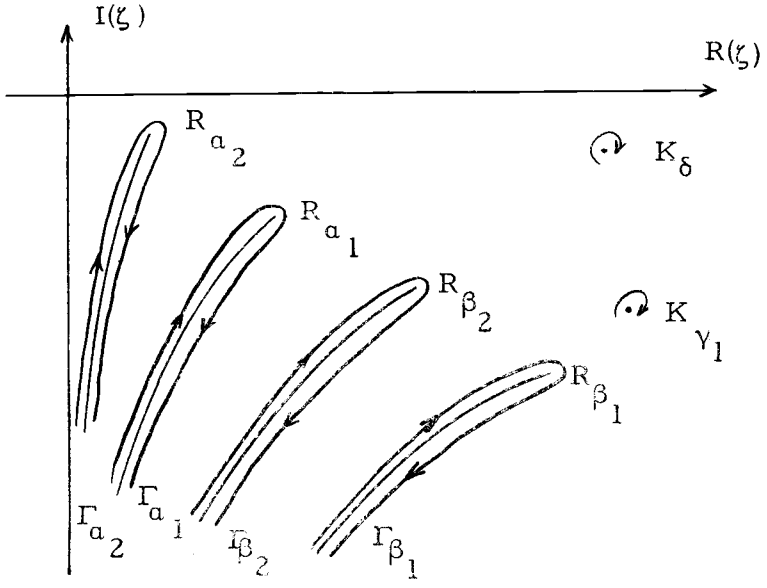

The restriction has been made that $R(\lambda) > 0$ so the branch lines were chosen to be the lines corresponding to $R(\lambda) = 0$.

Upon substituting the infinite series representation of the coefficients into Equations (4), it is seen that a general term for the ϕ series corresponding to the contribution from Γ_{α_1} is

$$\phi_p = \int_{\Gamma_{\alpha_1}} G(\zeta)\, e^{\{-i\zeta x - h_1\lambda_{\alpha_1} - h_2\lambda_{\beta_1}\}}\, d\zeta \qquad (9)$$

where the subscript p indicates that the solution is for an initial compressional source; h_1 and h_2 are linear forms in h, z, and H; and $G(\zeta)$ is some algebraic combination of T, Y, S, W, F and $\overline{F}$. Newlands has shown that by manipulation of the ω-plane contour of Equation (7), the exponential factor of Equation (9) can be made to vary much faster than $G(\zeta)$. Then, as the imaginary part of ζ becomes more negative upon receeding from R_{α_1} on Γ_{α_1} and as x can be chosen large compared to h_1 or h_2, the main contribution to the integral (9) comes from the neighborhood of $\zeta = R_{\alpha_1}$. Upon inserting the time factor $e^{i\omega t}$, the exponent in (9) becomes approximately $\exp(i\omega t - iR_{\alpha_1} x)$, which is seen to represent a wave traveling most of the distance from source to receiver with velocity α_1. Parallel arguments can be made for Γ_{α_1}, Γ_{β_1}, and Γ_{β_2}, and it is concluded that the paths shown in Figure 17 (for which most of the distance from source to receiver is traversed with velocity α_2) are

contained in the contribution from Γ_{a_2}.

Newlands introduces a new variable, u, measured along Γ_{a_2} such that $\lambda_{a_1} = +iu$ on the left side of the branch line, $\lambda_{a_2} = -iu$ on the right side of the branch line and $u = 0$ is the branch point R_{a_2}. The functions composing $G(\zeta)$ in Equation (9) are then expanded in terms of u. For example,

$$T_{(on\Gamma_{a_2})} = (T_O \pm iuT_1)_{(on\Gamma_{a_2})} \qquad \begin{pmatrix} +, \text{ left side of cut} \\ -, \text{ right side of cut} \end{pmatrix}$$

where higher order terms in u are neglected and T_0 and T_1 are independent of u. Similar definitions of zero and first order terms in u are made for S, V, Y, W and U. Using these approximations, Newlands was able to carry out the ζ - integrations on Γ_{a_2} (expressed in terms of the new variable, u).

For the purpose of numerical calculation, it is necessary to determine the explicit expressions for the quantities which Newlands denoted by T_0, T_1, S_0, S_1, etc. . To this end, the factors in the determinants S, T, V, Y, W and U must be expressed as expansions in terms of the variable u. From the definitions given in Equation (4) and from the definition of u, it is seen that

$$\lambda_{a_2} = iu$$

$$\zeta = (\lambda_{a_2}^2 + R_{a_1}^2)^{\frac{1}{2}} \doteq R_{a_2} - u^2/2R_{a_2}$$

$$\lambda_{\alpha_1} = (\zeta^2 - R_{\alpha_1}^2)^{\frac{1}{2}} \doteq i(R_{\widehat{\alpha_1\alpha_2}} + u^2/2R_{\widehat{\alpha_1\alpha_2}})$$

$$\lambda_{\beta_1} = (\zeta^2 - R_{\beta_1}^2)^{\frac{1}{2}} \doteq i(R_{\widehat{\beta_1\alpha_2}} + u^2/2R_{\widehat{\beta_1\alpha_2}})$$

where $R_{\widehat{\alpha_1\alpha_2}} = (R_{\alpha_1}^2 - R_{\alpha_2}^2)^{\frac{1}{2}}$ and $R_{\widehat{\beta_1\alpha_2}} = (R_{\beta_1}^2 - R_{\alpha_2}^2)^{\frac{1}{2}}$.

The simplifying observation can be made that there will be no quotients of differences of the above terms in the Laplace expansion of the determinants in Equations (5) (i. e. quadratic and higher order terms in u will not be reduced), so that the u^2 terms can be immediately dropped and ζ, λ_{α_1} and λ_{β_1} can be considered as independent of u in the first approximation. Furthermore, Equation (5) show that λ_{α_2} appears only linearly and only in the third colum of each determinant. Thus, a simple Laplace expansion on the third column along with the substitution $\lambda_{\alpha_2} = \pm iu$ gives the desired zero and first order terms directly. In order to carry out the ω integrations, Newlands redefined S_0, S_1, T_0, ... , U_1 to make them independent of ω and dependent only upon the properties of the two media. This was done by factoring $R_{\alpha_2}^n = \omega^n/a_2$ out of each determinant where n is equal to the power of ω appearing in the original determinant. As only the frequency independent quantities were used from this point on, Newlands retained the same notation for the frequency independent terms without resulting confusion. The above outline

was used to find the explicit expressions for the normalized determinants and the results are as follows.

$$S_0 = \begin{vmatrix} \dfrac{ia_2}{\widehat{a_1 a_1}} & -1 & -1 \\ \dfrac{-2ia_2}{\widehat{a_1 a_2}} & 2-a_2^2/\beta_1^2 & (2-a_2^2/\beta_2^2)\mu_2/\mu_1 \\ 2-a_2^2/\beta_1^2 & \dfrac{-2ia_2}{\widehat{\beta_1 a_2}} & \dfrac{2ia_2}{\widehat{\beta_2 a_2}}\ \mu_2/\mu_1 \end{vmatrix}$$

$$-(2-\frac{a_2^2}{\beta_2^2})\frac{\mu_2}{\mu_1} \begin{vmatrix} -1 & \dfrac{ia_2}{\widehat{\beta_1 a_2}} & \dfrac{-ia_2}{\widehat{\beta_1 a_2}} \\ \dfrac{ia_2}{\widehat{a_1 a_2}} & -1 & -1 \\ \dfrac{-ia_2}{\widehat{a_1 a_2}} & 2-\dfrac{a_2^2}{\beta_1^2} & (2-\dfrac{a_2^2}{\beta_2^2})\mu_2/\mu_1 \end{vmatrix}$$

$$S_1 = \begin{vmatrix} -1 & \dfrac{i\alpha_2}{\widehat{\beta_1\alpha_2}} & \dfrac{-i\alpha_2}{\widehat{\beta_2\alpha_2}} \\ \dfrac{-2i\alpha_2}{\widehat{\alpha_1\alpha_2}} & 2-\dfrac{\alpha_2^2}{\beta_1^2} & \left(2-\dfrac{\alpha_2^2}{\beta_2^2}\right)\dfrac{\mu_2}{\mu_1} \\ 2-\dfrac{\alpha_2^2}{\beta_1^2} & \dfrac{-2i\alpha_2}{\widehat{\beta_1\alpha_2}} & \dfrac{2i\alpha_2}{\widehat{\beta_2\alpha_2}}\dfrac{\mu_2}{\mu_1} \end{vmatrix}$$

$$+ 2\frac{\mu_2}{\mu_1}\begin{vmatrix} -1 & \dfrac{i\alpha_2}{\widehat{\beta_1\alpha_2}} & \dfrac{-i\alpha_2}{\widehat{\beta_2\alpha_2}} \\ \dfrac{i\alpha_2}{\widehat{\alpha_1\alpha_2}} & -1 & -1 \\ 2-\dfrac{\alpha_2^2}{\beta_1^2} & \dfrac{-2i\alpha_2}{\widehat{\beta_1\alpha_2}} & \dfrac{2i\alpha_2}{\widehat{\beta_2\alpha_2}}\dfrac{\mu_2}{\mu_1} \end{vmatrix}$$

where

$$\widehat{\alpha_1\alpha_2} = (1/\alpha_1^2 - 1/\alpha_2^2)^{-\frac{1}{2}}$$

$$\widehat{\beta_1\alpha_2} = (1/\beta_1^2 - 1/\alpha_2^2)^{-\frac{1}{2}}$$

$$\widehat{\beta_2\alpha_2} = (1/\beta_2^2 - 1/\alpha_2^2)^{-\frac{1}{2}}$$

Now, if $S_{0,1}$, $S_{0,2}$, $S_{1,1}$ and $S_{1,2}$ are defined to be the four determinants respectively in the above expression, and if the notation is adopted that given a determinant A, the expression $[a_{ij}, a_{kl}, \text{etc.}]A$ means to change the algebraic signs of the factors a_{ij}, a_{kl}, etc.

in the determinant A, then

$$S_0 = -S_{0,1} - (2 - \alpha_2^2/\beta_2^2)(\mu_2/\mu_1) S_{0,2}$$

$$S_1 = S_{1,1} + 2(\mu_2/\mu_1) S_{1,2}$$

$$W_0 = -[a_{11}, a_{21}] S_{0,1} - (2 - \alpha_2^2/\beta_2^2)(\mu_2/\mu_1)[a_{21}, a_{31}] S_{0,2}$$

$$W_1 = [a_{21}] S_{1,1} + 2(\mu_2/\mu_1)[a_{21}] S_{1,2}$$

$$T_0 = -[a_{32}] S_{0,1} - (2 - \alpha_2^2/\beta_2^2)(\mu_2/\mu_1)[a_{12}] S_{0,2}$$

$$T_1 = [a_{12}, a_{32}] S_{1,1} + 2(\mu_2/\mu_1)[a_{12}, a_{32}] S_{1,2}$$

$$U_0 = -[a_{11}, a_{21}, a_{32}] S_{0,1} - (2 - \alpha_2^2/\beta_2^2)(\mu_2/\mu_1)[a_{21}, a_{31}, a_{12}] S_{0,2}$$

$$U_1 = [a_{21}, a_{12}, a_{32}] S_{1,1} + 2(\mu_2/\mu_1)[a_{21}, a_{12}, a_{32}] S_{1,2}$$

and

$$Y_0 = -\begin{vmatrix} \dfrac{-i\alpha_2}{\widehat{\alpha_1\alpha_2}} & \dfrac{i\alpha_2}{\widehat{\alpha_1\alpha_2}} & -1 \\ \dfrac{2i\alpha_2}{\widehat{\alpha_1\alpha_2}} & \dfrac{-2i\alpha_2}{\widehat{\alpha_1\alpha_2}} & (2 - \dfrac{\alpha_2^2}{\beta_2^2})\dfrac{\mu_2}{\mu_1} \\ (2 - \dfrac{\alpha_2^2}{\beta_1^2}) & (2 - \dfrac{\alpha_2^2}{\beta_1^2}) & \dfrac{2i\alpha_2}{\widehat{\beta_2\alpha_2}}\dfrac{\mu_2}{\mu_1} \end{vmatrix} \qquad (10)$$

$$+ \left(2 - \frac{a_2^2}{\beta_2^2}\right)\frac{\mu_2}{\mu_1}\begin{vmatrix} -1 & -1 & \dfrac{-ia_2}{\widehat{\beta_2 a_2}} \\ \dfrac{-ia_2}{\widehat{a_1 a_2}} & \dfrac{ia_2}{\widehat{a_1 a_2}} & -1 \\ \dfrac{2ia_2}{\widehat{a_1 a_2}} & \dfrac{-2ia_2}{\widehat{a_1 a_2}} & \left(2 - \dfrac{a_2^2}{\beta_2^2}\right)\dfrac{\mu_2}{\mu_1} \end{vmatrix}$$

$$Y_1 = -\begin{vmatrix} -1 & -1 & \dfrac{-ia_2}{\widehat{\beta_2 a_2}} \\ \dfrac{2ia_2}{\widehat{a_1 a_2}} & \dfrac{-2ia_2}{\widehat{a_1 a_2}} & \left(2 - \dfrac{a_2^2}{\beta_2^2}\right)\dfrac{\mu_2}{\mu_1} \\ \left(2 - \dfrac{a_2^2}{\beta_1^2}\right) & \left(2 - \dfrac{a_2^2}{\beta_1^2}\right) & \dfrac{2ia_2}{\widehat{\beta_2 a_2}}\dfrac{\mu_2}{\mu_1} \end{vmatrix}$$

$$+ 2\frac{\mu_2}{\mu_1}\begin{vmatrix} -1 & -1 & \dfrac{-ia_2}{\widehat{\beta_2 a_2}} \\ \dfrac{-ia_2}{\widehat{a_1 a_2}} & \dfrac{ia_2}{\widehat{a_1 a_2}} & -1 \\ \left(2 - \dfrac{a_2^2}{\beta_1^2}\right) & \left(2 - \dfrac{a_2^2}{\beta_1^2}\right) & \dfrac{2ia_2}{\widehat{\beta_2 a_2}}\dfrac{\mu_2}{\mu_1} \end{vmatrix}$$

Newlands provided a table giving the expressions for the potentials and corresponding displacements which resulted from carrying out the ω- and ζ- integrations for 40 of the terms in the infinite

series representation of Equations (4). The explicit expressions for the various determinants derived in Equations (10), along with Newlands' displacement equations (see Appendix I for those of interest here) provide a basis for the numerical evaluation of head wave amplitudes. Before doing so, however, ray paths must be associated with each term in the series representation of the potentials. Newlands' method of labeling the terms will be followed here. A preceding subscript p or s represents respectively a compressional or shear wave source; the following subscript α_2 indicates that the terms considered here are contributions from the branch line Γ_{α_2}; the potential from which the term was taken is represented by ϕ or ψ and indicates whether the station arrival is a P or an S wave, respectively; a following superscript was used by Newlands simply to represent the numerical order of appearence of the term in her series expansion for the potentials. Thus $_p\phi^{(6)}_{\alpha_2}$ represents the contribution from the Γ_{α_2} integration of the sixth term in her series for the ϕ potential from a compressional source. This label, along with the apparent travel time of the pulse as seen directly from the time dependence of the displacement equation (Appendix I), identifies the ray path.

Consider the three terms pictured below.

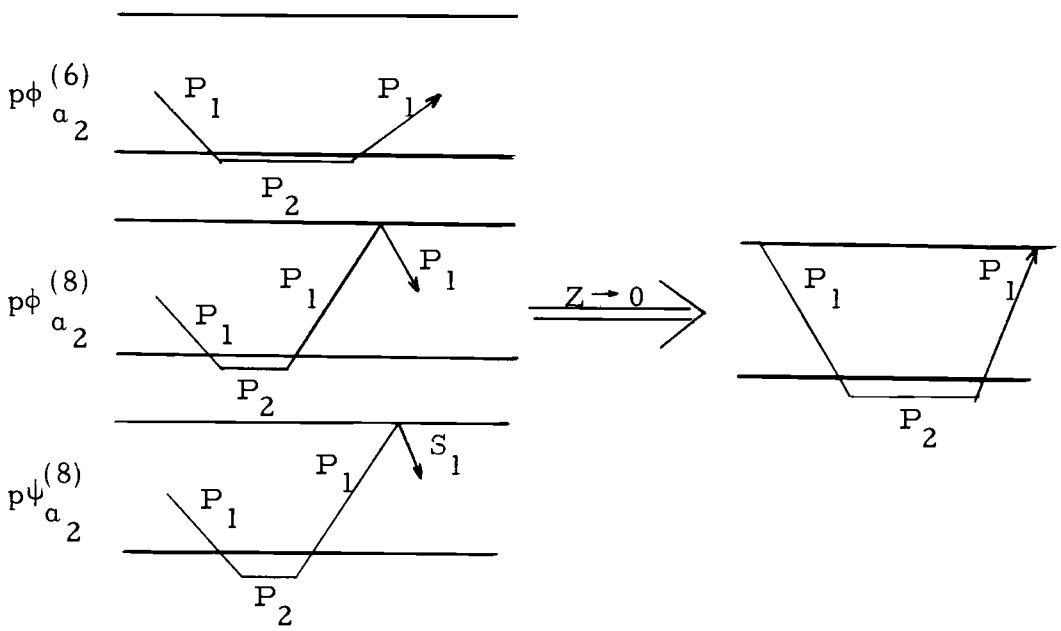

As $z \rightarrow 0$ (which is allowed in Newlands' theory), the travel-times for the three terms shown approach the same value. All three terms correspond to parts of the P_n wave as observed on the surface of the earth. $p\phi_{a_2}^{(6)}$ represents the incident wave, while $p\phi_{a_2}^{(8)}$ and $p\psi_{a_2}^{(8)}$ represent the reflected compressional and shear waves, respectively. The surface displacement recorded by a seismograph will be the vector sum of the displacements from these three terms. Similarily, each of the 12 ray paths shown in Figure 17 will be the result of combining three of Newlands' potentials. Construction of Table 5 was therefore necessary, and the table gives the terms which must be combined to describe each ray.

The Bromwich expansion method applied to a one-layer crust combines waves with the same travel-times due to the fact that their

Table 5. Combination of potentials required for the total displacement when the receiver is at the free surface.

Ray	Incident (P, S)	Reflected P	Reflected S
$\downarrow P_1P_2P_1$ (P_n)	$p\phi^{(6)}_{a_2}$	$p\phi^{(8)}_{a_2}$	$p\psi^{(8)}_{a_2}$
$\downarrow P_1P_2P_1$	$p\psi^{(4)}_{a_2}$	$p\phi^{(4)}_{a_2}$	$p\psi^{(5)}_{a_2}$
$\downarrow S_1P_2S_1$	$s\psi^{(6)}_{a_2}$	$s\phi^{(2)}_{a_2}$	$s\psi^{(8)}_{a_2}$
$\downarrow S_1P_2P_1$	$s\phi^{(4)}_{a_2}$	$s\phi^{(6)}_{a_2}$	$s\psi^{(4)}_{a_2}$
$\uparrow P_1P_1P_2P_1$ (pP_n)	$p\phi^{(7)}_{a_2}$	$p\phi^{(9)}_{a_2}$	$p\psi^{(9)}_{a_2}$
$\uparrow P_1P_1P_2S_1$	$p\psi^{(6)}_{a_2}$	$\frac{1}{2}p\phi^{(5)}_{a_2}$	$p\psi^{(7)}_{a_2}$ {first term}
$\uparrow P_1S_1P_2P_1$	$p\phi^{(3)}_{a_2}$	$\frac{1}{2}p\phi^{(5)}_{a_2}$	$p\psi^{(7)}_{a_2}$ {first term}
$\uparrow P_1S_1P_2S_1$	$p\psi^{(2)}_{a_2}$	$p\phi^{(2)}_{a_2}$	$p\psi^{(3)}_{a_2}$
$\uparrow S_1P_1P_2P_1$ (sP_n)	$s\phi^{(8)}_{a_2}$	$s\phi^{(9)}_{a_2}$	$s\psi^{(2)}_{a_2}$
$\uparrow S_1P_1P_2S_1$	$s\psi^{(3)}_{a_2}$	$s\phi^{(7)}_{a_2}$ {second term}	$\frac{1}{2}s\psi^{(5)}_{a_2}$
$\uparrow S_1S_1P_2P_1$	$s\phi^{(5)}_{a_2}$	$s\phi^{(7)}_{a_2}$ {first term}	$\frac{1}{2}s\psi^{(5)}_{a_2}$
$\uparrow S_1S_1P_2S_1$	$s\psi^{(7)}_{a_2}$	$s\phi^{(3)}_{a_2}$	$s\psi^{(9)}_{a_2}$

exponential terms are identical. These combined waves have been separated in Table 5. For example, when the crust in the region of the source is identical to the crust in the region of the station the waves $\uparrow P_1P_1P_2S_1$ and $\uparrow P_1S_1P_2P_1$ will arrive simultaneously. In realistic cases, however, the crustal sections at source and receiver will not be identical, and the waves will be separated in time.

Numerical Application of Newlands' Theory

Numerical values for the amplitudes of the phases shown in Figure 17 were obtained using: (1) Newlands' displacement equations (Appendix I), (2) the explicit forms of the zero and first order terms of the determinental expansions [Equations (10)], (3) the combinations of incident and reflected waves as indicated in Table 5. As relative amplitudes on a given seismogram are to be investigated, the results were normalized by making the vertical and horizontal components of the P_n amplitude unity. The expressions involved were programmed for calculation on a CDC 3300 computer (Appendix II).

Figure 25 is an example of the results of the calculation for the horizontal component of displacement produced by a uniformly radiating source of equal shear and compressional wave amplitudes. Waves whose amplitudes are less than one-tenth that of P_n are not considered significant and are not shown in the figure. Figure 25 represents the results for a source at a depth of 10 km in a one-layer

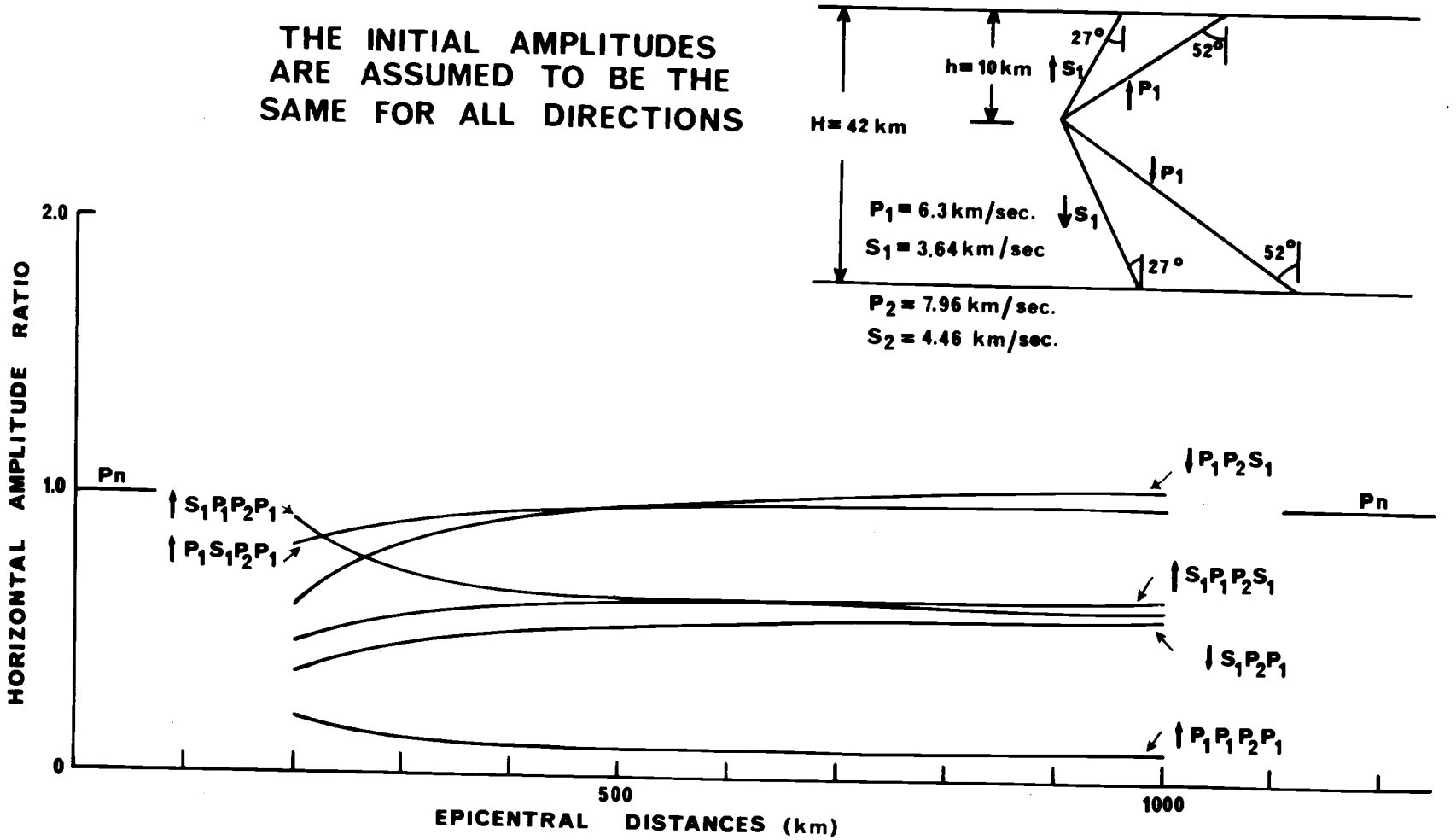

Figure 25. Results of Post-P_n to P_n amplitude-ratio calculations. Waves with ratios less than 0.1 are not shown.

crust whose physical parameters are appropriate to the province east of the Cascade Range. The arrow and first symbol in the ray path label along with the insert in Figure 25 give the direction and wave type of the initial energy leaving the source. Numerical values for the vertical displacements are similar and will be given later.

The displacement equations for each of the waves contain the geometrical factor $1/L_i^{3/2}$ (see Appendix I) where L_i is the interface distance of a given wave as indicated in Figure 17. As each of the wave amplitudes are normalized by that of the P_n wave ($i = 1$), the expressions represented by Figure 25 each contain the geometrical factor $(L_1/L_i)^{3/2}$. The change in amplitude ratio with epicentral distance displayed to about 350 km is due to the fact that the interface distances, L_i ($i \neq 1$), are significantly different from L_1 for distances less than 350 km. Beyond about 350 km, all the interface distances become approximately equal and the geometrical term becomes unity, with the result that the amplitude ratios cease to display any dependence upon epicentral distance.

Figure 26 displays the effect of changing source depth on amplitude ratios of significant phases. The large changes in the curves at 200 and 300 kilometers are due to the source-depth dependence of the factor $(L_1/L_i)^{3/2}$. It is seen that beyond about 350 km, the amplitude ratios are nearly independent of the source depth. It should be pointed out that the crustal thickness H appears only in

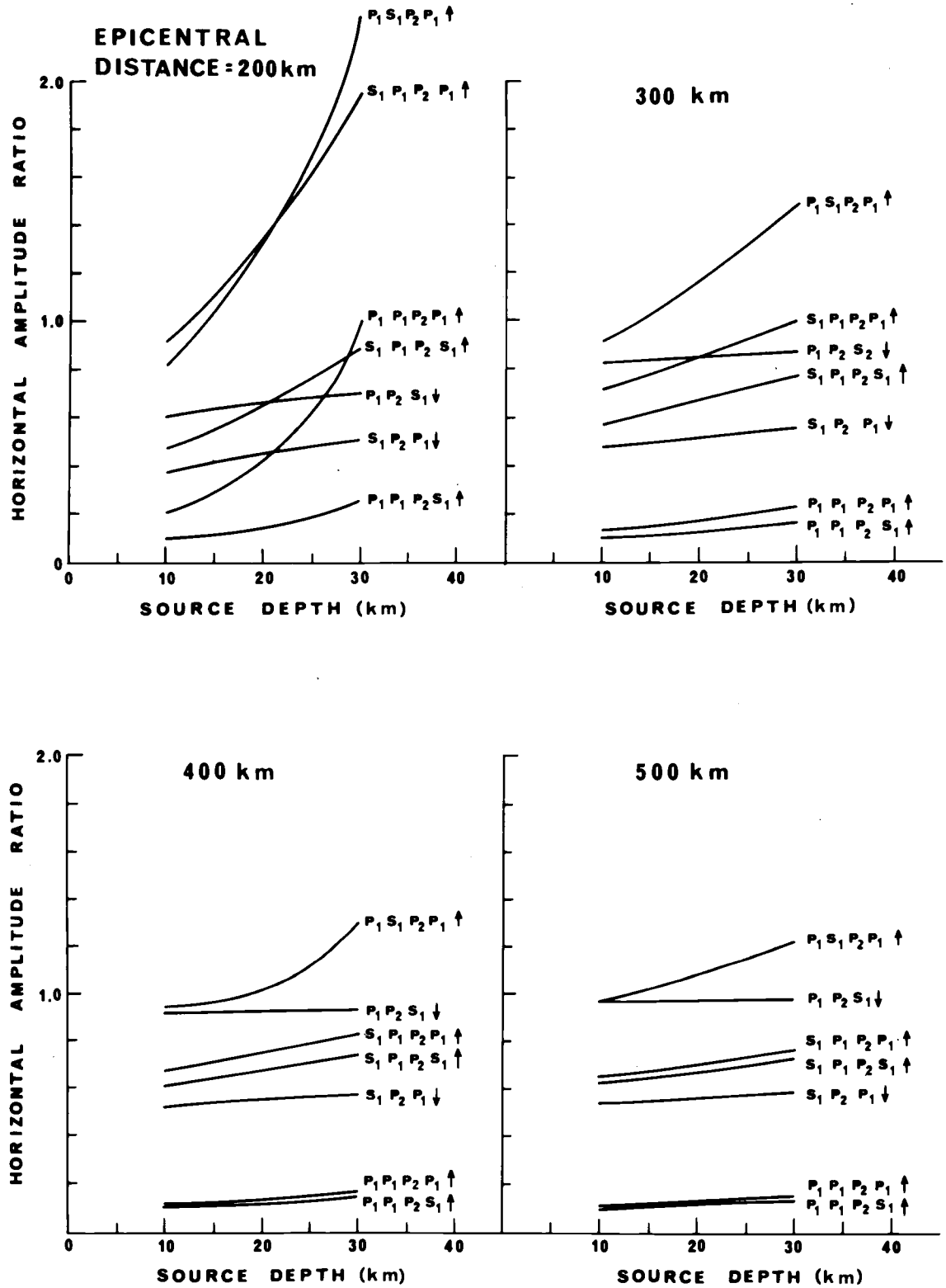

Figure 26. Effect of source depth on the curves in Figure 25.

the geometrical factor, L_i, (see displacement equations in Appendix II) and does not affect amplitude ratios at the larger epicentral distances. Furthermore, as H diminishes, the epicentral distance at which the approximation $L_i = L_1$ becomes valid likewise diminishes.

Figure 27 displays the effect on the amplitude ratios of changing the velocity contrast of compressional waves at the interface. The curves are relatively insensitive to changes in Poisson's ratio of either medium up to about 20% and to changes in the density contrast at the interface of more than 20%. Dehlinger, et al. (1965) found Poisson's ration, σ, to have essentially the same value of .26 in the upper mantle for the two continental provinces (east and west of the Cascade Range) in the Pacific Northwest states, and Gutenberg (1959, p. 181) reports that determinations of Poissin's ratio for the crystalline layers of the earth's crust fall in the range from .22 to .27. The values assumed in this thesis are $\sigma_2 = .26$ for the upper mantle and $\sigma_1 = .25$ for the crustal material. Thus, any realistic differences between the values of Poisson's ratio in the model used here and those of the real earth will not effect the results displayed in Figure 27.

The velocity contrasts at the Moho for the one-layer crust approximations in the three provinces in the Pacific Northwest states are as follows: Oceanic, $\alpha_1/\alpha_2 = .835$; West of Cascades, $\alpha_1/\alpha_2 =$

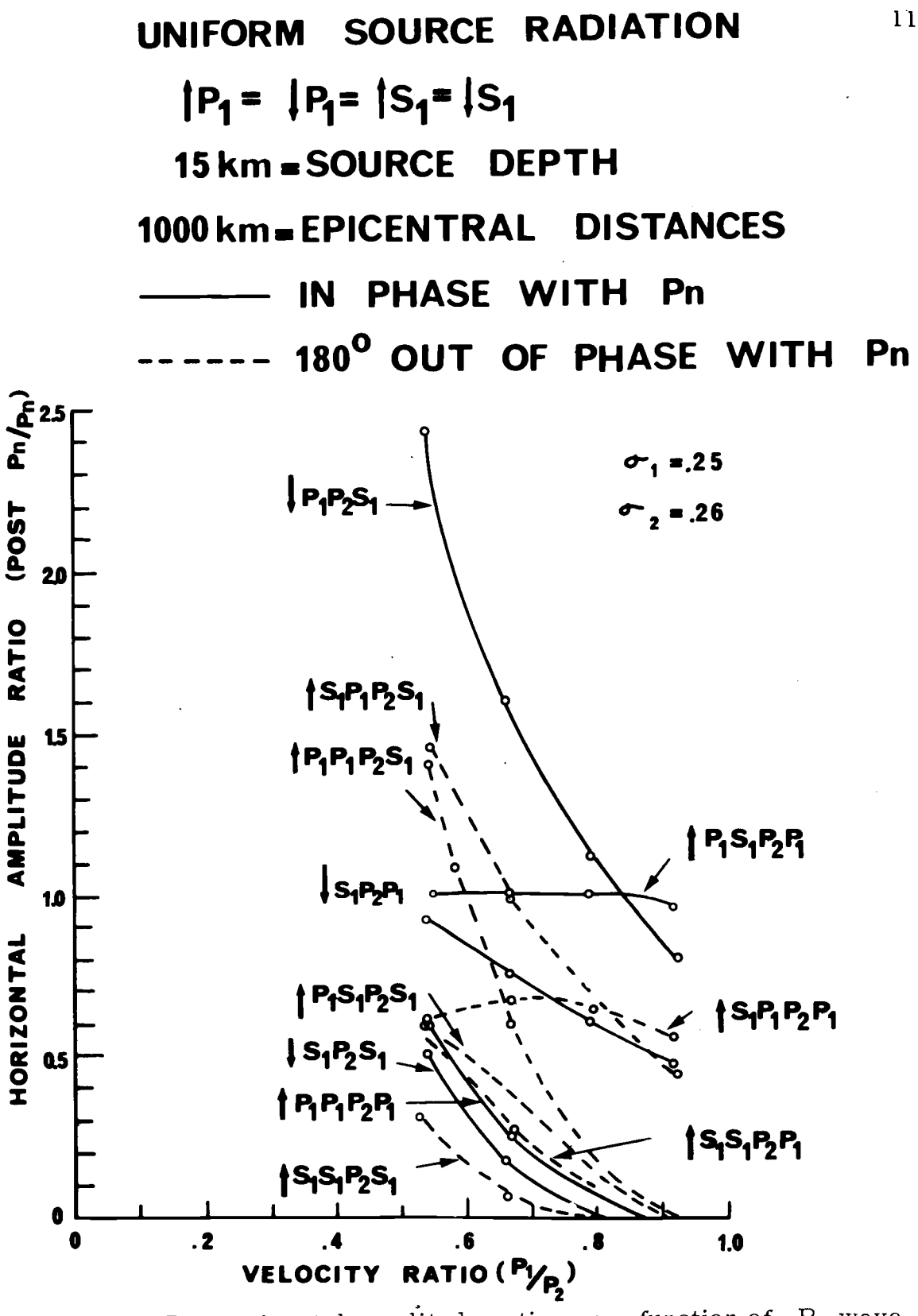

Figure 27. Horizontal amplitude ratios as a function of P wave velocity contrast at the Moho.

.797; East of Cascades, $a_1/a_2 = .790$. Figure 27 shows that within this small range of values for a_1/a_2 there are no significant changes in the amplitude ratios of any of the waves under consideration. Furthermore, Figure 27 shows that in the relatively broad range of $a_1/a_2 = .7$ to $a_1/a_2 = .92$ (e.g., $a_1 = 5.6$ km/sec, $a_2 = 8.0$ km/sec to $a_1 = 7.36$ km/sec, $a_2 = 8.0$ km/sec) the values of theoretical amplitude ratios for significant waves do not change appreciably from the corresponding values at the midpoint of the range. The above range of a_1/a_2 allows realistic changes in velocities determined by seismic refraction experiments, and adds confidence to the application of theoretical results from constant velocity models to observations made on records of the real earth.

In addition to changes in the head wave coefficients, the effect of crustal layering on the body wave portions of the rays of Figure 17 must be examined. Crustal layering will produce departures from spherical spreading of the body wave portions of the rays of Figure 17 along with changes in the reflection coefficients for those waves reflected from the free surface.

Figure 28 shows ray paths and incidence angles for a multi-layered crust, which was found to be consistent with the Rayleigh wave dispersion data of Chiburis (1965). The incidence angles displayed in Figure 28 can be compared with those for the one layer crust shown in the insert of Figure 25. Gutenberg's curves illustrating

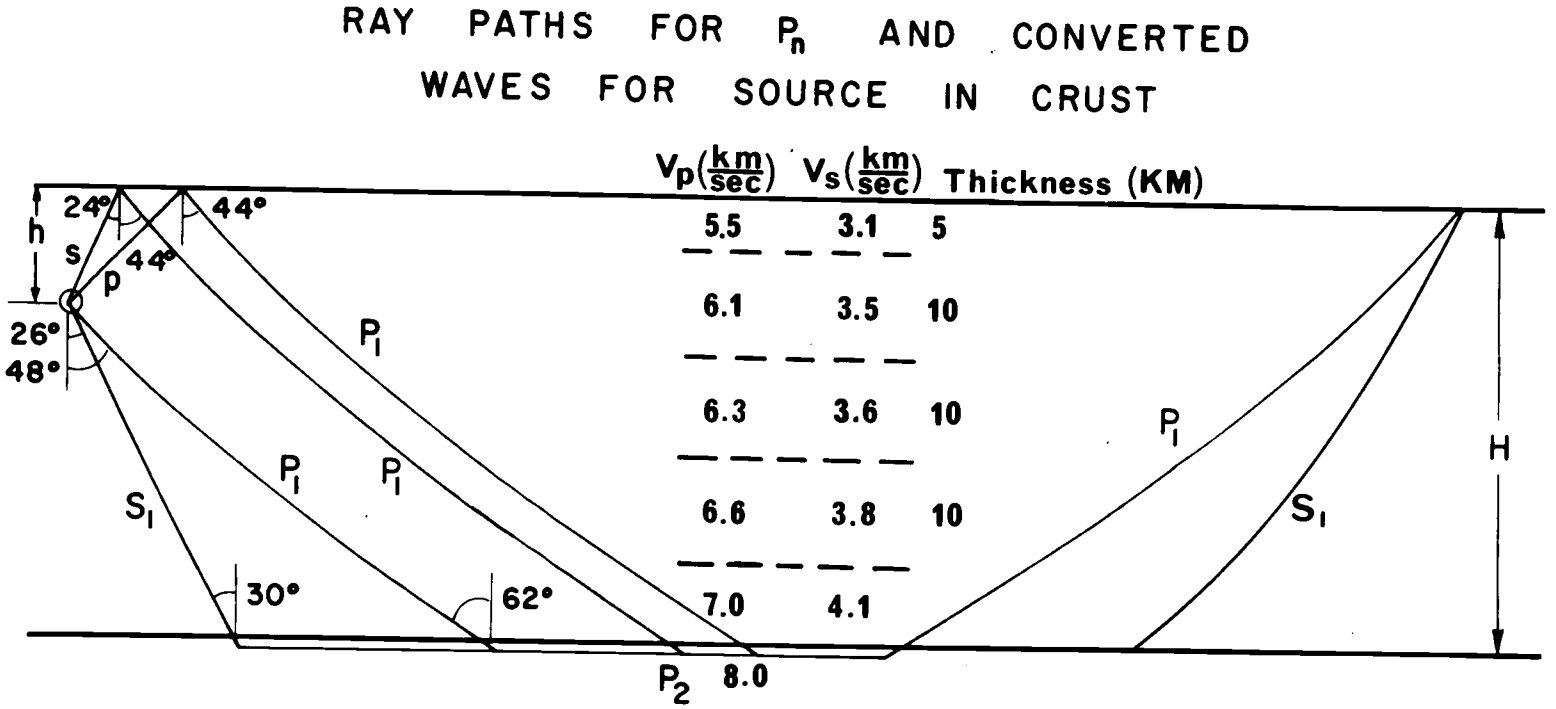

Figure 28. Ray paths for a layered crustal section. The section shown is identical to that given by Chiburis (1965) except for the addition of a 7.0 km/sec layer of variable thickness at the base of the crust.

reflection coefficients at a free surface (see, for instance, Ewing, et al., 1957, p. 30-31) show that the reflection coefficient for a P-to-SV reflection is very nearly unity over the range of incidence angle from 44° to 62°, and that the coefficients for a P-to-P reflection remains small over this range of angles. The coefficients for the P and S reflections of an incident S wave change little for incidence angles of 24° to 30°. In addition, as the refraction angles at the intercrustal discontinuities are far from critical, the geometrical attenuation for the crustal rays of Figure 28 should not differ significantly from the case of a single layer crust. Therefore, although the complete solution for head wave displacements from a source in a crust of variable velocity would be desirable, the calculations based on a one-layer crust should provide a good approximation to the more detailed problem.

Table 6 provides a comparison of the amplitude calculations for the three provinces. The values listed in the table represent the theoretical ratios of the amplitudes of the reflected and/or converted head waves to that of the P_n wave as observed on the same seismogram. That is, the horizontal displacement components of the Post-P_n waves have been divided by the horizontal component of the P_n wave, and the vertical components have been divided by the vertical component of the P_n wave. The values in Table 6 were calculated for an epicentral distance of 1000 km, although these same values apply at epicentral distances greater than about 350 km for the eastern province, 250 km for the western province, and 150 km for

Table 6. Theoretical head-wave amplitude ratios for the three provinces in the Pacific Northwest for an epicentral distance of 1000 km. ($\uparrow S_1$, $\downarrow S_1$, $\uparrow P_1$, $\downarrow P_1$ are equal in amplitude).

$$\left(\frac{\text{Wave Displacement}}{P_n \text{ displacement at the same distance}} \right)$$

	Provinces							
	Oceanic		West of Cascades		East of Cascades		Averages	
Wave	Hor. Disp.	Vert. Disp.	Hor. Disp.	Vert. Disp.	Hor. Disp.	Vert. Disp.	Hor. Disp.	Vert. Disp.
$\downarrow P_1P_2S_1$	1.057	-0.995	1.140	-0.891	1.117	-0.867	1.1	-0.9
$\downarrow S_1P_2S_1$	0.018	-0.017	0.041	-0.032	0.034	-0.027	0.03	-0.02
$\downarrow S_1P_2P_1$	0.606	0.606	0.634	0.634	0.643	0.643	0.6	0.6
$\uparrow P_1P_1P_2P_1$ (pP_n)	-0.051	-0.051	-0.124	-0.124	-0.143	-0.143	-0.1	-0.1
$\uparrow P_1P_1P_2S_1$	-0.054	0.049	-0.141	0.110	-0.159	0.124	-0.1	0.1
$\uparrow P_1S_1P_2P_1$	1.013	1.013	1.010	1.010	1.104	1.104	1.0	1.0
$\uparrow P_1S_1P_2S_1$	0.031	-0.028	0.065	-0.051	0.059	-0.045	0.04	-0.04
$\uparrow S_1P_1P_2P_1$ (sP_n)	-0.605	-0.605	-0.627	-0.627	-0.683	-0.683	-0.6	-0.6
$\uparrow S_1P_1P_2S_1$	-0.639	0.578	-0.715	0.559	-0.760	0.590	-0.7	0.6
$\uparrow S_1S_1P_2P_1$	-0.031	-0.031	-0.078	-0.078	-0.085	-0.085	-0.05	-0.05
$\uparrow S_1S_1P_2S_1$	-0.001	0.001	-0.005	0.004	-0.005	0.004	-0.003	0.002

the oceanic province.

In view of the small differences in the theoretical values from province to province, the single set of values given in the last two columns of Table 6 will be used for all three provinces. It is further assumed that these values are applicable when the source and receiver are located in different provinces.

Applicability of the Theoretical Results

Lapwood (1949) has shown that the part of the solution of Equations (1), corresponding to the direct wave, could be found exactly. Therefore, by comparing Newlands' approximate solution with the exact solution, a measure of validity can be obtained. Newlands made this comparison and found that the solutions agree, provided that the observation time after the onset of the arrival is small compared to the total travel time. As the same approximations were made for the solutions on Γ_{a_2} (in which the terms corresponding to the ray paths of Figure 17 appear) as were made on Γ_{a_1} (in which the approximation to the direct wave is found), it is concluded that the above restriction on the observation time applies also to the head waves. This restriction is automatically satisfied when short-period seismograms are used.

The solutions are also subject to the condition that the main contributions to the branch line integrals come from the immediate

vicinity of the branch points. This restriction can be interpreted physically as meaning that the epicentral distances are much greater than the dominant wavelengths under consideration, and that the distance is such that all wavefronts are well developed (i. e, (1) the epicentral distance is well past the critical reflection point where the head wave travel-time curve branches off from the reflection parabola of the parent body wave, and (2) the receiver is not near the boundary). Restriction (1) is automatically satisfied by actual earthquake seismograms as the observed small amplitude of P_n requires that it be the first arrival on the record in order to be seen. In addition, (2) is satisfied as the seismographs are separated from the boundary by a distance equal to the crustal thickness.

The question arises whether amplitude ratios from the line source model are applicable to the case of a finite source, such as a fault plane, where some spreading in the y-direction must be allowed.

Heelan (1953) has considered the particle displacement at the interface between two half-spaces, resulting from head waves produced by a small vertically oriented cylindrical source in the upper medium. His calculations included the spreading in the y-direction, and he found that the particle displacement in irrotational head waves is in a vertical plane passing through the source. Although the particle displacement is irrotational, it is not parallel to the apparent

direction of propagation, as is the case for irrotational body waves. This vibration direction couples the particle motion at the interface with the particle motion of deeper points along the refracted wave in the same vertical plane and establishes a mechanism for the vertical flux of energy required for explaining the finite energy of the head waves. It does not, however, allow for a lateral flux of energy. Thus, the energy leaving the point source between two vertical planes is conserved, and the concept of cylindrical spreading through an expanding cylinder whose axis coincides with the z-axis can be applied to these head waves even though geometrical arguments can not be used in the vertical planes themselves. This heuristic argument indicates that displacement equations for head waves from a line source and a finite source differ only by a geometrical spreading factor.

As the additional factor for the case of spreading in the y-direction will be the same for all of the waves shown in Figure 17, the amplitude results for the line source will be applicable to the finite source case when amplitude ratios are used. A further result from Heelan is that the amplitude ratios will be independent of the actual time function of the source.

Extension to Nonuniform Source Radiation

Figure 25 shows amplitude ratios which would be observed if the amplitudes radiated from the source in the directions $\uparrow S_1$, $\uparrow P_1$, $\downarrow S_1$ and $\downarrow P_1$ were all equal. To account for a nonuniform radiation pattern, the values of Figure 25 must be multiplied by the radiation amplitude in the desired direction normalized by the amplitude in the direction of the P_n wave ($\downarrow P_1$). This follows from Heelan's result that the amplitude of the head wave is directly proportional to the amplitude of the incident critical ray. For example, if the shear wave amplitude radiated in the direction $\uparrow S_1$ were two times the compressional wave amplitude in the direction $\downarrow P_1$, then the amplitude ratio of $\uparrow S_1P_1P_2P_1/P_n = .6$ (at $\Delta > 400$ km) from Figure 25 would be multiplied by $\uparrow S_1/\downarrow P_1 = 2$ with the result that the observed $\uparrow S_1P_1P_2P_1$ amplitude would be 1.2 times that of the P_n wave on the same short-period horizontal seismogram.

The foregoing numerical amplitude results lead to the important conclusion that some of the arrivals predicted in Table 4 should have sufficient amplitudes to be registered on seismograms. Furthermore, the radiation pattern at the source determines which of the waves will be recorded at a given source-to-station azimuth.

Synthetic Seismograms

The results of the preceeding sections were used to construct the head wave portions of synthetic seismograms which should be observed at various azimuths from a given earthquake source model. The source model used was a simple fault of various orientations and motions as represented by a simple couple. The equations used to calculate the radiation amplitude ratios $\uparrow S_1/\downarrow P_1$, $\uparrow P_1/\downarrow P_1$ and $\downarrow S_1/\downarrow P_1$ for this model were Mikumo's (1962) equations for a simple couple. The above ratios were then multiplied by the appropriate value from Table 6, resulting in the theoretical amplitude of the head waves. The wave shape for each pulse was assumed to be one cycle of a sinusoid with a period of .8 second. The time interval vs. source depth curves of Figure 22 were used to find the sequence of arrivals. More complicated radiation patterns and wave forms could be used, but the above simple model will display the essential features of the theoretical predictions.

The theoretical seismograms are shown in Figures 29 to 36. It is noted that although the seismograms were constructed for an epicentral distance of 1000 km, the character of a record at a given azimuth (i. e., the relative amplitudes of the phases on the record) will be maintained for epicentral distances as short as 350 km.

The synthetic seismograms show that the phases $\downarrow S_1 P_2 S_1$,

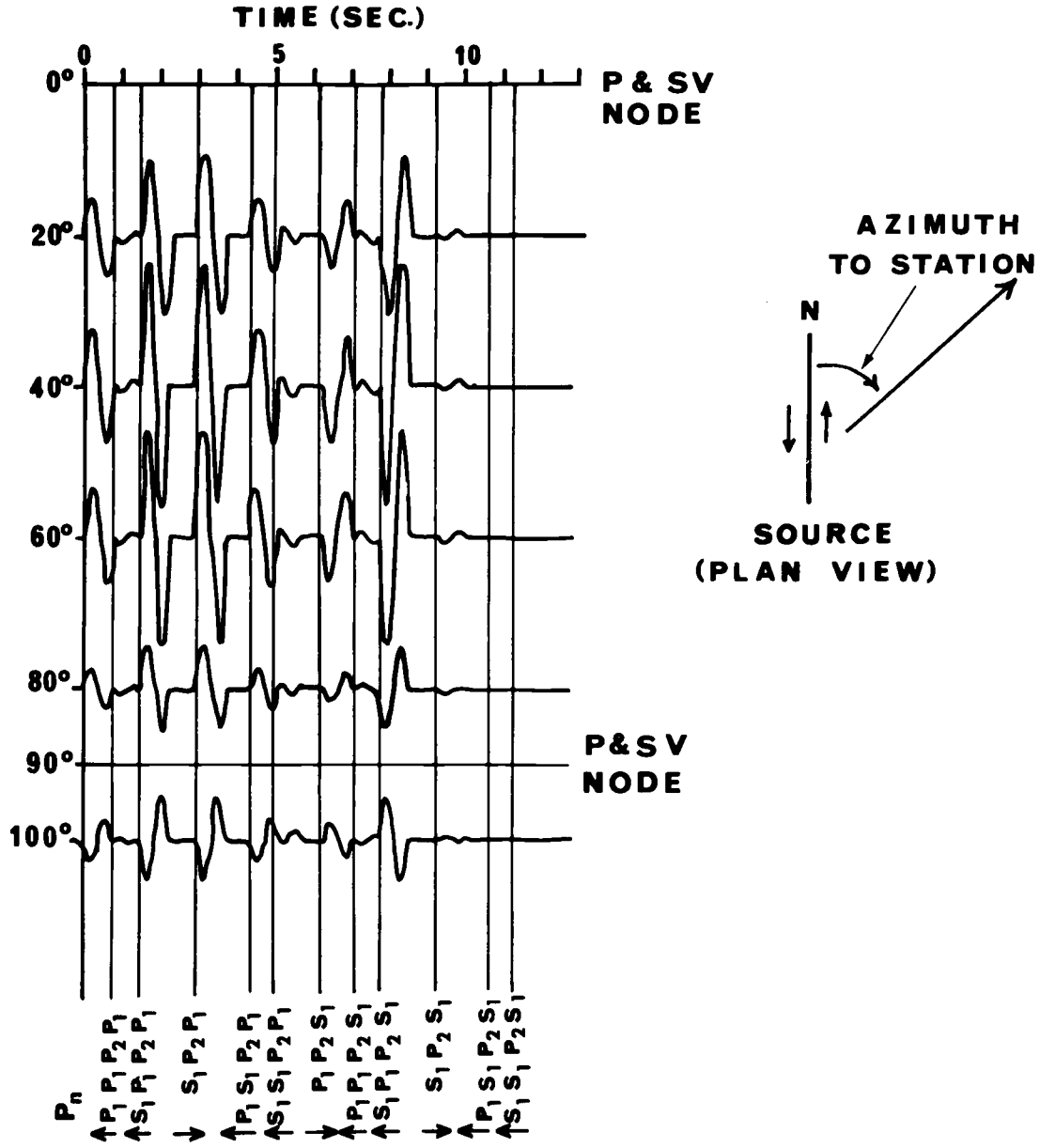

Figure 29. Synthetic vertical seismograms for vertical fault, striking N-S. Left lateral motion (see text for description).

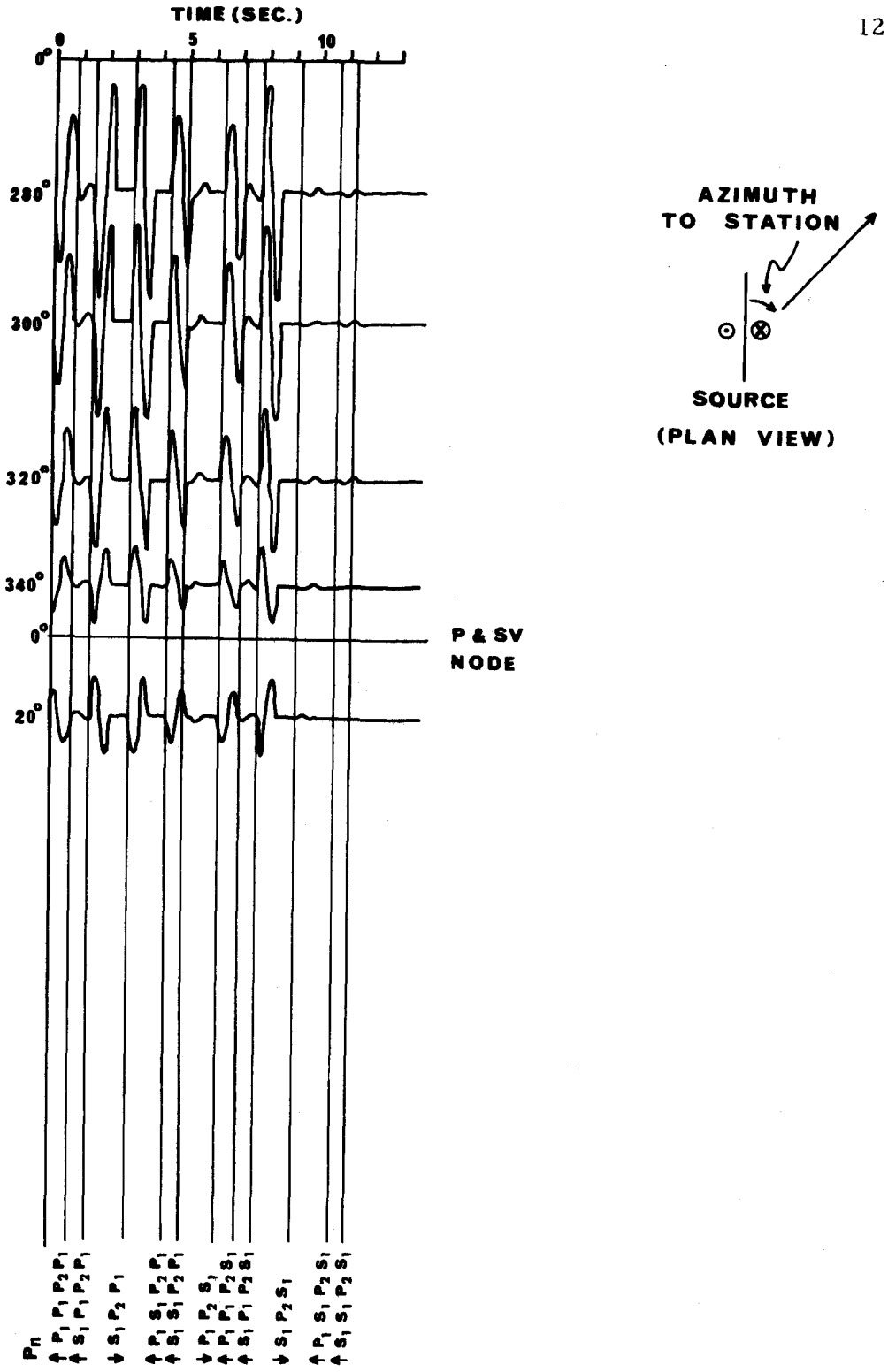

Figure 30. Synthetic vertical seismograms for vertical fault, striking N-S. East block down-dropped, west block uplifted an equal amount (see text for description).

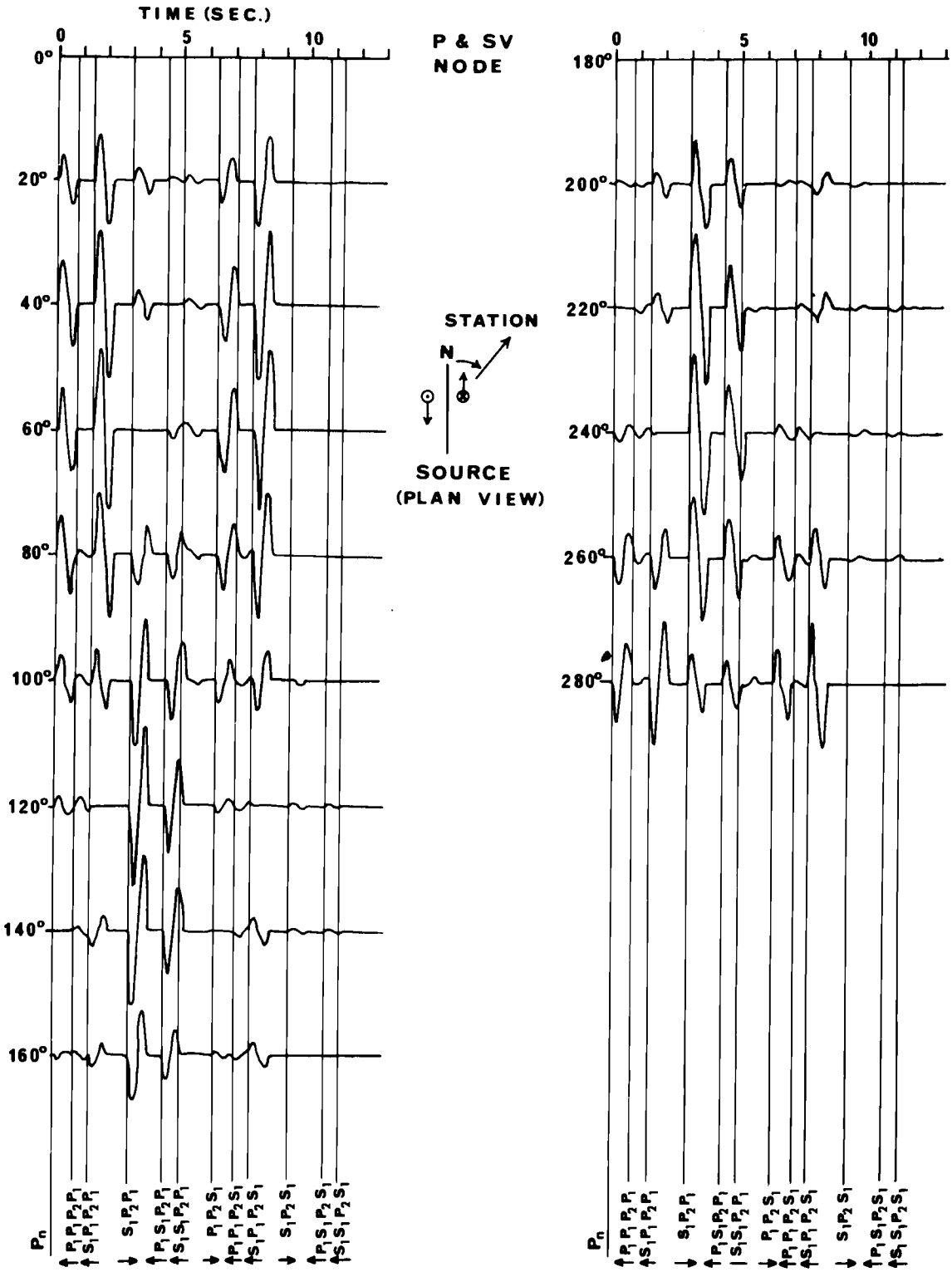

Figure 31. Synthetic vertical seismograms for vertical fault, striking N-S. Equal strike-slip and dip-slip motion (see text for description).

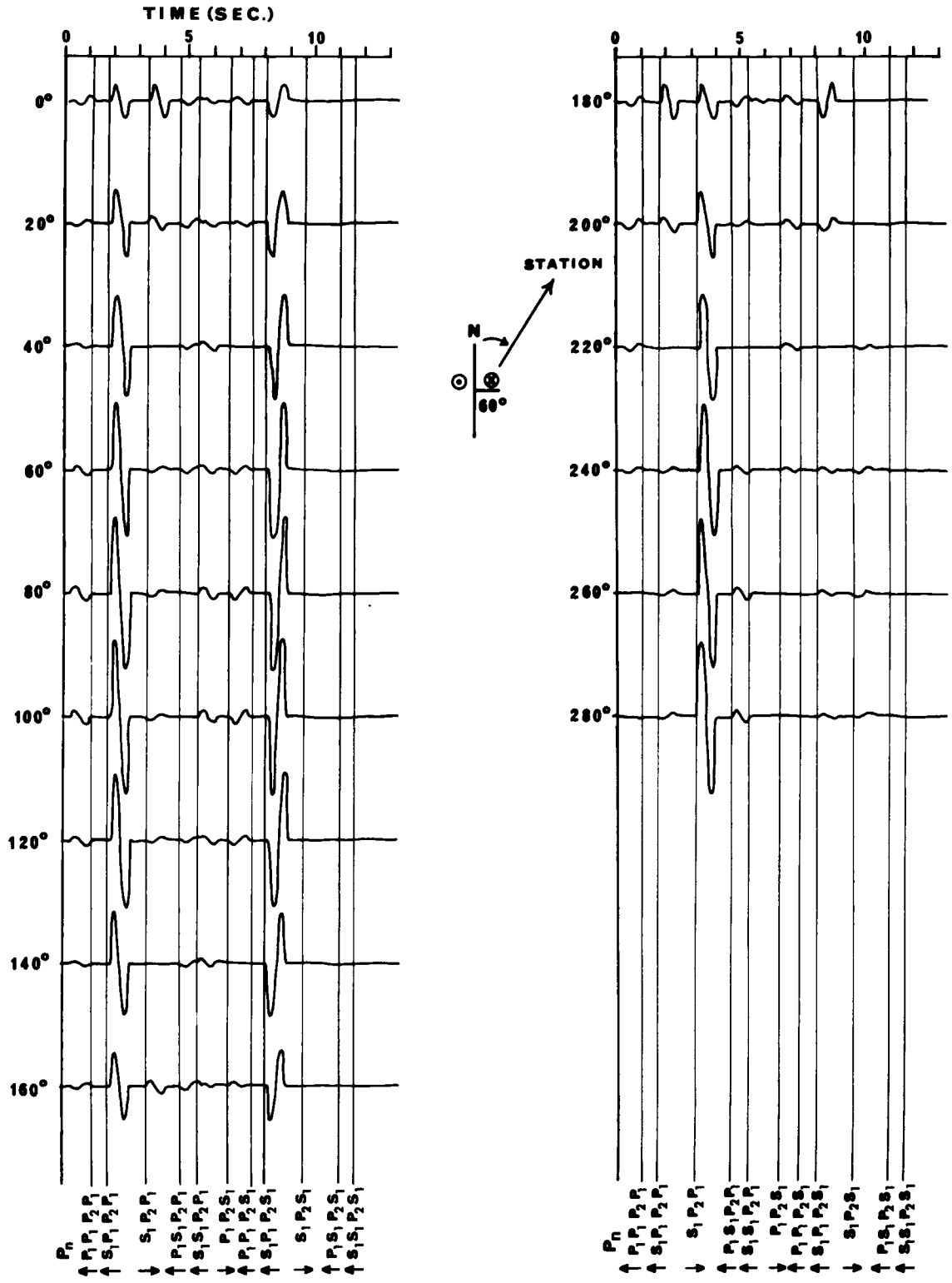

Figure 32. Synthetic vertical seismograms for normal fault, striking N-S, dipping 60 E.

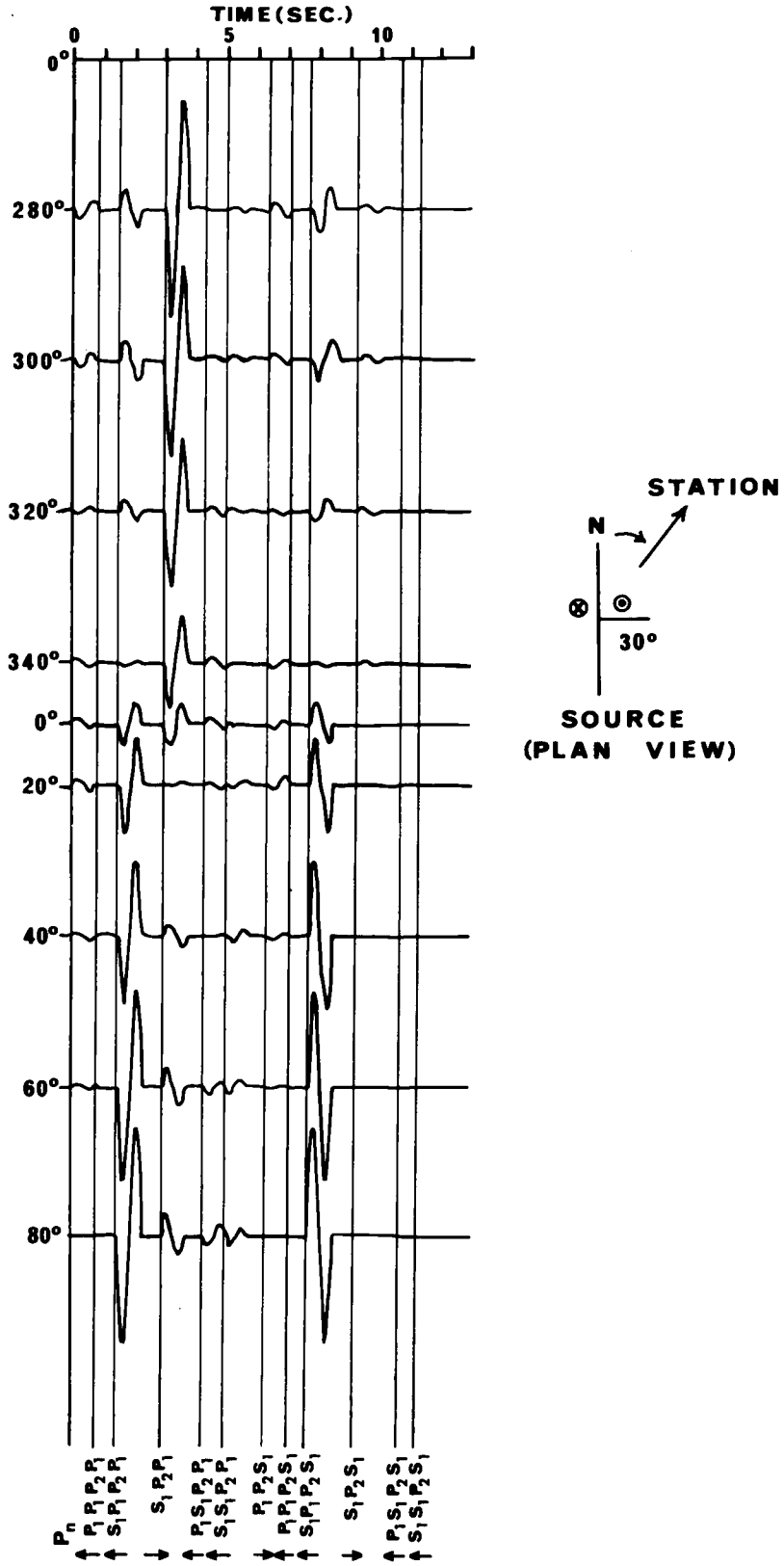

Figure 33. Synthetic vertical seismograms for thrust fault, striking N-S, dipping 30 E.

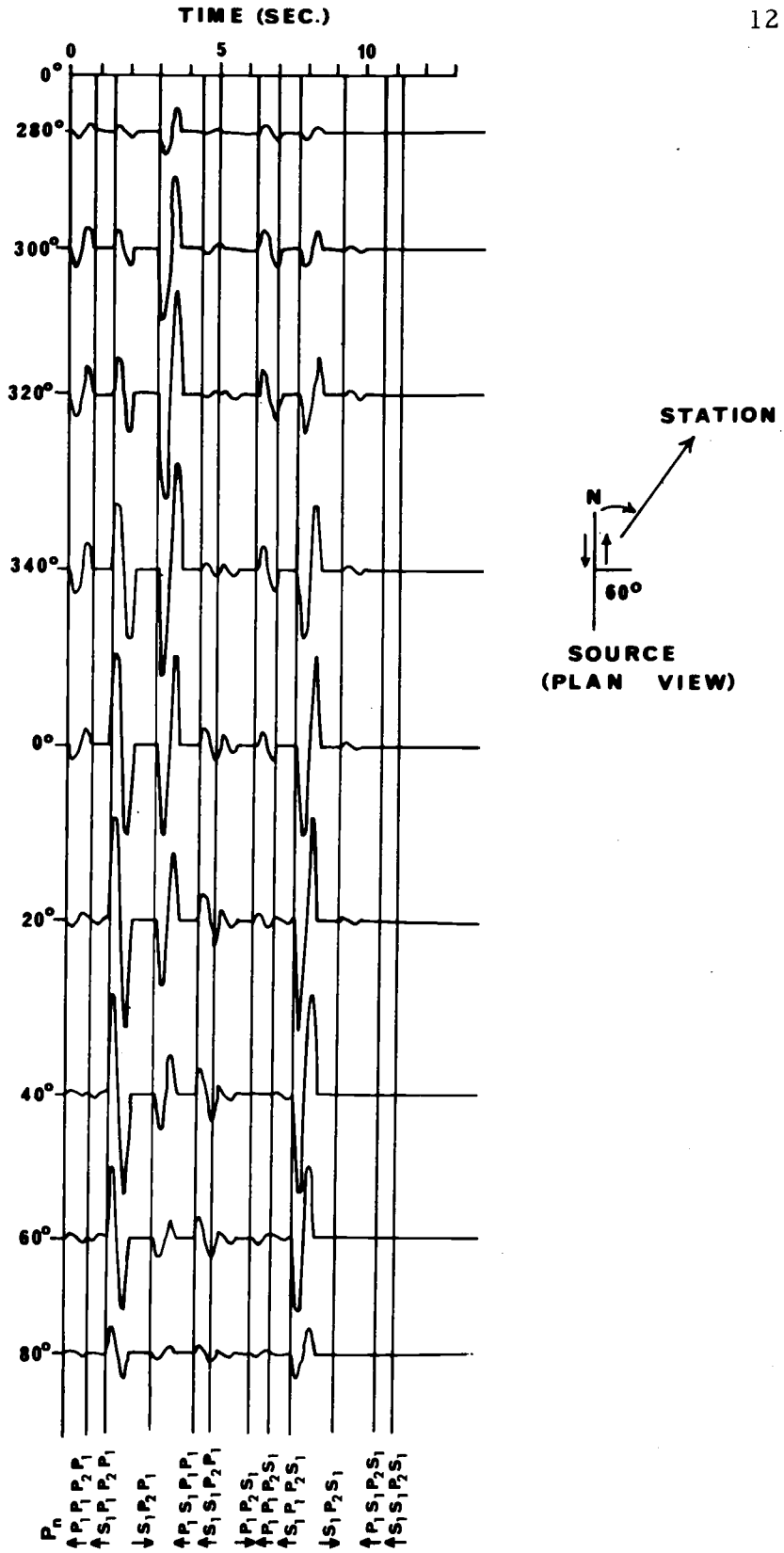

Figure 34. Synthetic vertical seismograms for faul striking N-S and dipping 60 E. Left lateral motion only.

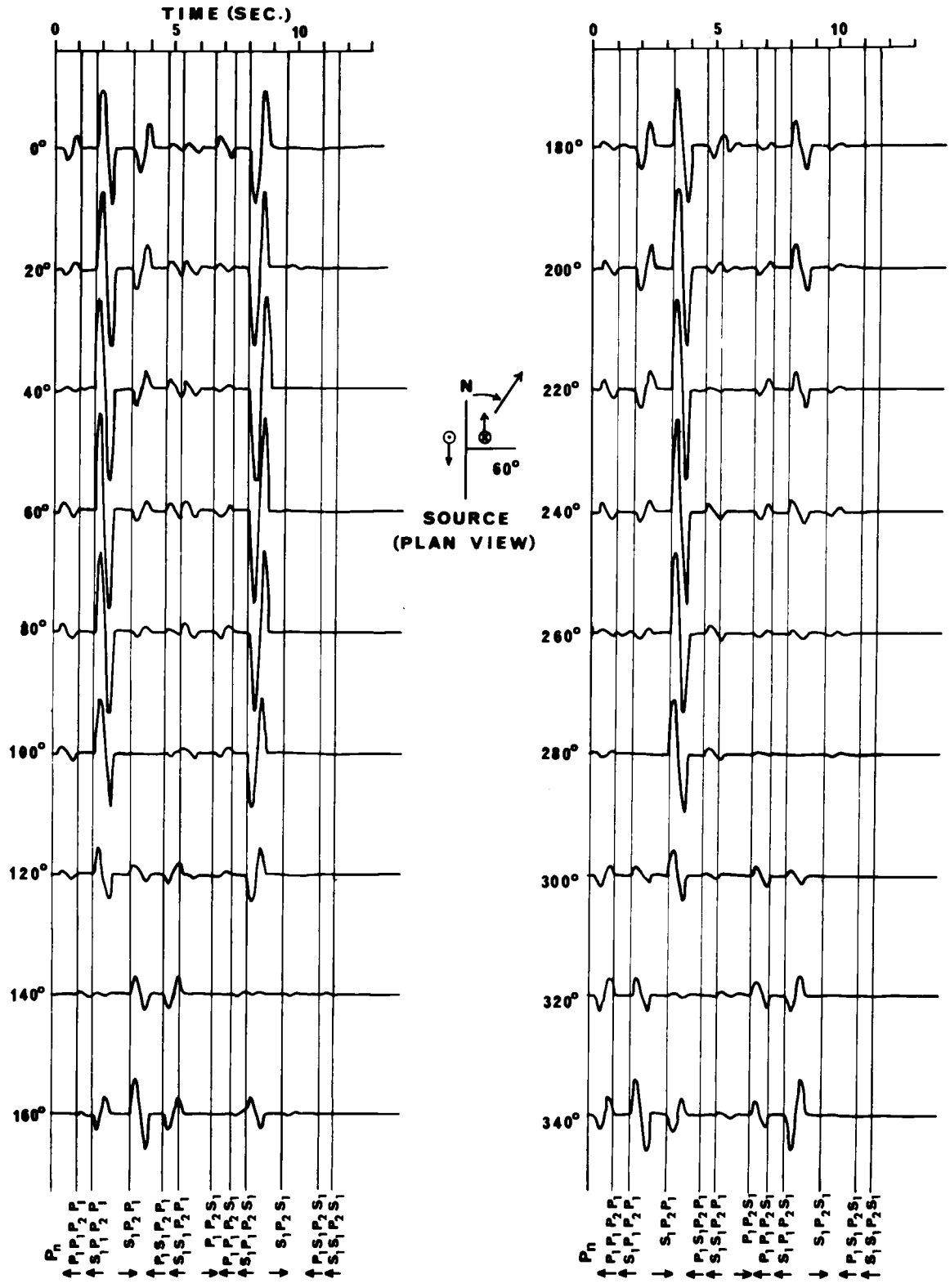

Figure 35. Synthetic vertical seismograms for fault striking N-S and dipping 60 E. Equal left lateral and normal fault motion.

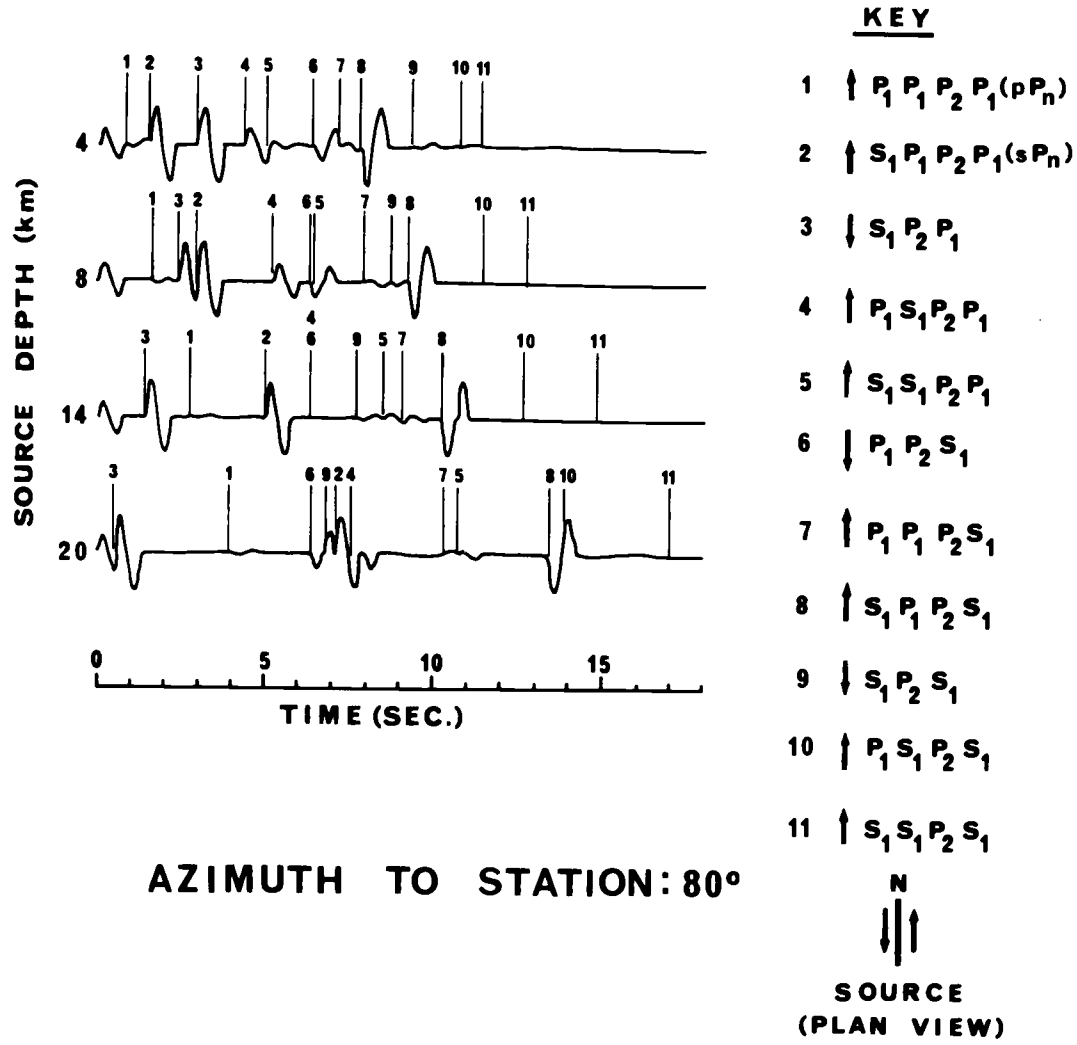

Figure 36. Effect on preceeding seismograms of different source depths.

$\uparrow P_1P_1P_2S_1$, $\uparrow P_1S_1P_2S_1$, $\uparrow S_1S_1P_2P_1$ and $\uparrow S_1S_1P_2S_1$ are always insignificant and would not be useful for the purpose of interpretation. In the event that $\uparrow P_1$ is much larger than $\downarrow P_1$, the wave $\uparrow P_1P_1P_2P_1$ may register as it would arrive at an undisturbed time on the record. The phases P_n, $\downarrow P_1P_2S_1$, $\downarrow S_1P_2P_1$, $\uparrow P_1S_1P_2P_1$, $\uparrow S_1P_1P_2P_1$ and $\uparrow S_1P_1P_2S_1$ are large in certain instances and offer interpretational possibilities.

Figures 29 and 30 show that the character of the head wave portion of the vertical seismograms for a vertical fault source with only strike-slip motion or only dip-slip motion is nearly independent of azimuth, with only a reversal of all phases from one quadrant to the next. The six significant phases should be recorded for all azimuths although some of the phases may coalesce for certain source depths, as shown in Figure 36.

Figure 31 shows a considerable change in the record character with azimuth when the source is a vertical fault with both strike-slip and dip-slip components of motion. This figure also tends to promote caution in the practice of labeling the first observable arrival as P_n, and, furthermore, suggests that the first large amplitude arrival after P_n may not be the same phase for stations at different azimuths.

Figures 32 and 33 show that the records for the normal fault dipping 60^o and the thrust fault dipping 30^o also display a large change in character with azimuth.

These records show fewer large amplitude pulses than those for the vertical fault due to the dominance of the energy radiated in the directions $\uparrow S_1$ and $\downarrow S_1$ except for azimuths nearly parallel to the strike of the fault.

Figures 34 and 35 correspond to Figures 29 and 30 with the fault plane inclined to the vertical.

Finally, Figure 36 shows that the appearance of the head wave portion of the records is altered considerably by a change in the depth of the source even though the amplitude ratios remain the same.

Summary

1. Consistency with the observed time intervals between P_n and Post-P_n.

   CONSISTENT: The time interval between P_n and the second arrival is determined principally by the depth of the shock. This model allows for scatter in the data from a single shock by virtue of changes in the dominant phases with changes in source-to-station azimuth.

2. Consistency with the observed amplitude ratios of Post-P_n to P_n.

   CONSISTENT: The synthetic seismograms display large amplitude second arrivals with the observed ampliutde ratio, and they also account for the cases of rather large and rather small amplitude ratios. In reviewing the synthetic seismograms, it must be

kept in mind that for certain radiation patterns and for certain azimuths, the first arrival which observationally would be labeled P_n may actually be one of the later phases. Also, there is no predicted amplitude variation with epicentral distance, but the scatter in the data from a single shock can be accounted for by the azimuthal variations.

3. Consistency with the observed average periods of Post-P_n and P_n.

   CONSISTENT in part: As these phases are all head waves, the observational periods of all the phases should be the same - provided that the time dependence of the P and S radiation at the source are the same. Different observational periods can occur, however, in the case of phase coalescence (e.g., the apparent first arrival on the seismogram at 140° azimuth of Figure 31).

4. Consistency with the observed relative first motion of Post-P_n to P_n.

   CONSISTENT: Changes in the relative directions of first motion for the first two phases can be accounted for in two ways: (1) The first two observed phases for different azimuths may not be the same two phases (e.g., compare the 20° and the 140° records of Figure 31). (2) For certain radiation patterns, first motion directions may change with azimuth for the same two phases (e.g., compare the first two phases on the 20° and 60° seismograms of

Figure 32).

5. Consistency with the observed change in character of seismograms with azimuth.

   CONSISTENT: The dominant phases change with azimuth causing a change in the character of the records (e.g., compare the 80° and 120° seismograms of Figure 31). Also, P_n can disappear over a small azimuth range with very little change in the later large amplitude phases (e.g., compare the 100° seismogram with the 120° or 140° seismogram of Figure 31). This example would be even more striking for a greater source depth as the large amplitude phase $\downarrow S_1P_2P_1$ would be shifted nearer the P_n arrival according to Figure 36.

6. Consistency with the observation of several second arrivals.

   CONSISTENT: This model not only allows but requires two or more arrivals subsequent to P_n, and, of course, the dominant arrivals may be different for different source-to-station azimuths.

7. Consistency with the observed discrepancy of the initial motions of short- and long-period seismograms.

   QUESTIONABLE: This model does not suggest the observed long period phenomenon unless the spectrum of the S source extends further into the longer period range than does the spectrum of the P source. In that case, the waves derived from the S source

(all of which arrive after P_n) could be accompanied by an arrival on the long-period instruments.

DISCUSSION

The preceding sections were concerned with examining various hypotheses about the origin of the Post-P_n phases. The considerations of some of the hypotheses seem quite incomplete as far as establishing positively the significance of a given mechanism. This was due to several causes. In some cases, the theory required for the calculations has not yet been developed (e.g., the source-time function of failure mechanisms in earth materials), and in some instances the theoretical calculations would require a detailed knowledge of earth structure far exceeding that which is presently available (e.g., amplitude calculations for horizontally refracted waves or waves reflected from discontinuities in the upper mantle). It has been possible, however, to discuss in both descriptive and quantitative terms some aspects of each hypothesis giving an indication of its significance. Of the various hypotheses, only two seem plausible.

Reflections from an irregular discontinuity in the mantle can result in arrivals with the observed time delays after P_n, but the observed variations as a function of azimuth in the direction of first motion of Post-P_n compared to P_n are not consistent with this explanation.

The calculations presented suggest that the waves following P_n are the result of head-wave effects. The synthetic seismograms for

head waves illustrated for several earthquake source motions show that this single explanation can account for the highly complex nature of about the first ten seconds of seismograms recorded at epicentral distances of 150 km to 1000 km. There are a few problems remaining, however, before a definite interpretation of the second arrivals can be given.

First, there is still a considerable amount of discussion as to whether P_n is a head wave or rather a wave refracted in the upper mantle by a velocity-depth structure whose corresponding travel-time curve is indistinguishable from that of a head wave when experimental errors are considered. If P_n is not a head wave the surface reflected waves pP_n and sP_n, which nearly duplicate the P_n travel path, should still have the relative importance as indicated in the synthetic seismograms. The importance of the waves converted at the Moho, however, would have to be re-evaluated on the basis of transmission coefficients or coefficients related to conversions by velocity gradients--depending upon the new velocity structure assumed for the upper mantle. From the equality of the periods of P_n and Post-P_n (as displayed in Table 3) it can be concluded that if P_n is a head wave then the second wave is also a head wave. Conversely, if P_n is a body wave then the second arrival is also a body wave. This conclusion results from considerations of direct-wave and head-wave periods (see, e.g., Berg and Long, 1966).

Gutenberg (1959, pp. 75-89) presents evidence which indicates that velocity decreases with depth in the upper mantle. Under such a condition P_n would be a head wave and, therefore, also the second arrival.

Secondly, the cause of the erratic horizontal-plane particle motion diagrams is as yet unresolved. The existence of large variations in the azimuth of approach for the phases of the first few seconds on earthquake seismograms is not consistent with the present models of the velocity structure of the earth. To maintain consistency, it is necessary to resort to conjecture. It is assumed that the energy registered on the seismograms has propagated along the source-to-station azimuth. The large departures in the apparent azimuth of approach displayed by the particle motion diagrams result from one or more of the following: a slight mismatching of the recording instruments, the possible presence of significant cross-coupling terms which are ignored in the application of horizontal seismograms, or secondary dynamic effects which may result in a more complicated motion of the surface of the earth when additional realistic boundary conditions are taken into consideration. For example, the addition of boundary conditions such as non-zero stress on the planes perpendicular to the free surface coupled with departures from perfect elasticity may give rise to surface vibrations which are not in the same direction as the incident disturbance.

With the above assumptions taken into account, it is concluded that the mechanism of reflected and converted head waves affords the best explanation of the second arrivals, and the remaining discussion will be based upon this model.

The synthetic seismograms show that the first large amplitude wave following P_n will be either $\uparrow S_1P_1P_2P_1$ (sP_n) or $\downarrow S_1P_2P_1$ depending upon focal depth, source radiation pattern, and location of the station relative to the source. Identification of these waves, along with their arrival-time intervals after P_n, can result in a focal-depth determination. These focal-depth determinations will be in error only by a percent comparable to the uncertainties in the average crustal velocities. Hence, the results of this analysis should produce more accurate focal-depth determinations than can be achieved by the methods presently in use, which require rather precise origin-time determinations and unsatisfactory assumptions regarding ray paths.

To apply the Post-P_n method for focal-depth determination, it is necessary that the first arrival on the record be P_n. The synthetic seismograms shown indicate that the practice of labeling the first arrival as P_n is not a sound practice. Over large azimuthal ranges, each of the fault models illustrated (except for vertical faults with only strike-slip or only dip-slip motions) display P_n amplitudes which are very small compared to other head wave phases.

This is illustrated by the seismograms of Figure 31, for which the source is a vertical fault with both strike-slip and dip-slip motion. If the epicenter of this hypothetical earthquake was located in the usual manner by considering the first arrivals to be P_n, then it would be located north of the true epicenter. This results from the fact that the times assumed to represent P_n arrivals for stations in the azimuthal range of 120° to 240° would actually be those of later phases. This effect may explain, in part, why some instrumental epicenters lie to one side or even outside of the meizoseismal area. In this same illustration, a focal depth obtained from the time interval between the first two observable phases would be in error if only stations in the azimuthal range of 120° to 240° recorded the shock and the first wave was considered to be P_n. It is common for seismologists to correlate the first phases on records at such different azimuths as 20° and 140° with complete confidence, while actually the arrivals may be different phases (see Figure 31).

In many cases, additional information is available so that the above difficulties can be avoided. If a preliminary fault-plane solution is available for an earthquake (based upon body or surface waves, but not head waves) then this method can be applied to records for azimuths corresponding to maximum P_n radiation. If fault-plane information is not available, then general considerations of other earthquakes in the region can be used to determine the

azimuths at which P_n should exhibit the largest amplitudes. This follows from the results of Udias (1965) and McEvilly (1966), which show that there is a consistency to the radiation patterns of earthquakes in a given region.

With the seismograms of an earthquake selected to insure that P_n is the first recorded arrival, it should be possible to identify the second arrival as either $\uparrow S_1P_1P_2P_1$ or $\downarrow S_1P_2P_1$ by considering the relative directions of Post-P_n to P_n motions at several azimuths. In practice, the requirement of positive identification of vibration directions for several phases at different azimuths is too stringent. The best method of interpreting arrivals in terms of reflected and converted head waves consists of using all recorded phases in the first 10 to 15 seconds following the first motion. The arrival times of all observable phases are marked on a slip of paper in accord with the time scale of the appropriate master curve (e.g., Figures 18 to 23). The slip is moved across the appropriate time-interval vs. source-depth curve to the depth which gives the most consistent alignment between the observed and theoretical time intervals. It must be kept in mind, however, that some of the phases may not be recorded along certain azimuths.

One further point can be made concerning interpretations based upon this model of reflected and/or converted head waves. The last two columns of Table 6 show that the amplitude ratios of Post-P_n to

P_n are nearly the same on the horizontal as on the vertical seismograms. Thus, all three records from a given station should be checked for consistency.

The head wave model here presented would seem to account for some of the difficulties which Gutenberg encountered in his study of second arrivals. In particular, Gutenberg's P_x phase can be interpreted as a combined effect of several of the head waves described above. For shorter epicentral distances (less than about 400 km), it is seen in Figure 26 that the relative significance of the various phases of Figure 17 may change with epicentral distance. When this is taken into consideration along with the changes in arrival-time intervals with azimuth and source depth, Gutenberg's observation that the P_x-P_n time interval seemed to increase with epicentral distance to about 300 km does not represent an inconsistency. This interpretation requires only that Gutenberg's assumption of a constant focal depth be relaxed. In addition, Figures 25 and 26 indicate that the reflected and converted head waves are best studied at epicentral distances greater than about 350 km.

APPLICATION TO SPECIFIC EARTHQUAKES

It will now be accepted that the second arrivals are the result of reflected and/or converted head waves. This theory, as developed from the composite observations of several earthquakes, will now be applied to focal-depth determinations for specific earthquakes. The curves given in previous sections will be used in the application. All of the earthquakes listed below are considered to have occurred within the crust (Dehlinger et al., 1965) so that the proposed theory appears applicable. Locations and origin times of the earthquakes are listed in Table 2.

August 23, 1962: The epicenter of this earthquake was near Crescent City, California, in the continental province west of the Cascade Range.

This earthquake was larger than a recent average for the area, and the station magnifications were sufficiently high that P_n was registered at all stations. The data from all the stations listed in Table 3 for this earthquake are consistent with a second arrival following P_n by 2.0 seconds. From Figures 19 and 22, then, the focal depth can be determined. Two interpretations are possible. If the second wave is $\uparrow S_1P_1P_2P_1$, then $h = 5\frac{1}{2}$ km and the following sequence of arrivals should be registered for stations east

of the Cascades (see Figure 22).

P_n	
$\uparrow S_1P_1P_2P_1$	2.0 seconds after P_n
$\downarrow S_1P_2P_1$	2.7 seconds after P_n
$\uparrow P_1S_1P_2P_1$	4.6 seconds after P_n
$\downarrow P_1P_2S_1$	6.3 seconds after P_n
$\uparrow S_1P_1P_2S_1$	8.3 seconds after P_n

If the second wave is $\downarrow S_1P_2P_1$, then h = 10 km and the following sequence of arrivals should be registered for stations east of the Cascades (see Figure 22).

P_n	
$\downarrow S_1P_2P_1$	2.0 seconds after P_n
$\uparrow S_1P_1P_2S_1$	3.5 seconds after P_n
$\uparrow P_1S_1P_2P_1$	5.5 seconds after P_n
$\downarrow P_1P_2S_1$	6.3 seconds after P_n
$\uparrow S_1P_1P_2S_1$	9.8 seconds after P_n

A similar set of arrivals could be constructed for stations west of the Cascades using Figure 19. Most of the later arrivals were lost due to excessive record amplitude. However, the records from the station HLY (see Figure 9) clearly show a third arrival with a very large amplitude at 2.6 seconds after P_n (0.6 seconds after Post-P_n). By comparing the arrival time of the third phase with the two possible sequences given above, it is concluded that the first of the above

interpretations is correct, with $h = 5\frac{1}{2}$ km.

In passing, it is pointed out that had the station magnification at HLY been lower, the P_n wave from this shock would probably not have been recorded (see Figure 9).

November 6, 1962: The epicenter of this earthquake was on the north side of Portland, Oregon, in the continental province west of the Cascade Range.

The recorded amplitudes for this earthquake were large, and it can be assumed that P_n was recorded at all stations (listed in Table 3). P_n consisted of several cycles of motion with no obvious second arrival until 3.5 seconds after the onset of P_n. The data from all the stations in Table 3 are consistent with this value, and the focal depth will be interpreted on this basis. If the second arrival is $\uparrow S_1 P_1 P_2 P_1$, then $h = 10$ km and a null direction is required for $\downarrow S_1 P_2 P_1$. If the second arrival is $\downarrow S_1 P_2 P_1$, then $H = 0.3$ km and a null direction is required for $\uparrow S_1 P_1 P_2 P_1$. Actually, a complete null for the waves is not required (i.e., it is only necessary that the recorded amplitudes be comparable to, or less than, the P_n amplitude so that a definite arrival is not apparent on the record). As the stations BKR, WMC, and HLY all lie within a small azimuthal angle with respect to the epicenter, it is not an excessively strict requirement that the second wave be small at all

three stations.

If the interpretation of the second arrival as $\uparrow S_1P_2P_1$ is considered with $h = 0.3$ km, then Figure 22 indicates that there should be a relatively quiet segment of the record from about 1 to 3.5 seconds after the arrival of P_n (assuming that the source is characterized by a pulse of short duration). However, as the ground motion persists with constant amplitude from the onset of P_n to the time of arrival of the large amplitude second wave at 3.5 seconds, it is assumed that some energy arrived around 2 seconds after P_n. Thus, the large amplitude wave is interpreted to be $\uparrow S_1P_1P_2P_1$ with $h = 10$ km, and the wave $\downarrow S_1P_2P_1$ represents energy between P_n and $\uparrow S_1P_1P_2P_1$.

January 24, 1963: The epicenter of this earthquake is near Seattle, Washington, in the continental province west of the Cascade Range.

This earthquake provided the most complete set of seismograms available for this study. The earthquake magnitude and station magnifications were such that good quality records were obtained along various source-to-station azimuths. Accordingly, it was possible to explain nearly all phases in the first 10 seconds of the records on the basis of the head wave model.

Figure 8 shows the seismograms of this earthquake as recorded

at the station HLY. The epicenter was such that the horizontal record T (at HLY) was oriented approximately along the epicenter-to-station azimuth. Therefore, on the basis of the vertical record, Z, and the in-line horizontal record, T, the arrival times of every displacement on the records which could be considered as a distinct pulse were read. The sequence of arrival times measured from the onset of P_n was found to be as follows: 0.83, 1.7, 3.7, 5.3, 6.8, 8.0, and 8.7 seconds. The time interval vs. source-depth curves of Figure 22 appear to be most appropriate for this source-station combination, but only the first two observed phases fit the curves of Figure 22. It was found, however, that a slight modification in the assumed crustal structure resulted in a good fit for all phases. An increase of 5 km in the crustal thickness of the western province and an increase of 3 km in the crustal thickness of the eastern province brought each of the seven recorded phases into alignment with theoretically predicted phases. The revised time interval vs. source-depth curves are given in Figure 37, and the observed arrival time sequence is shown by the circles for the value $h = 4\frac{1}{2}$ km. Figure 38 shows the vertical and in-line horizontal records from the station HLY with the phase identifications as determined from Figure 37. The new crustal sections have the same velocities as given in Figure 5, but the western section (in the region of the earthquake) is now 28 km thick and the eastern section (under

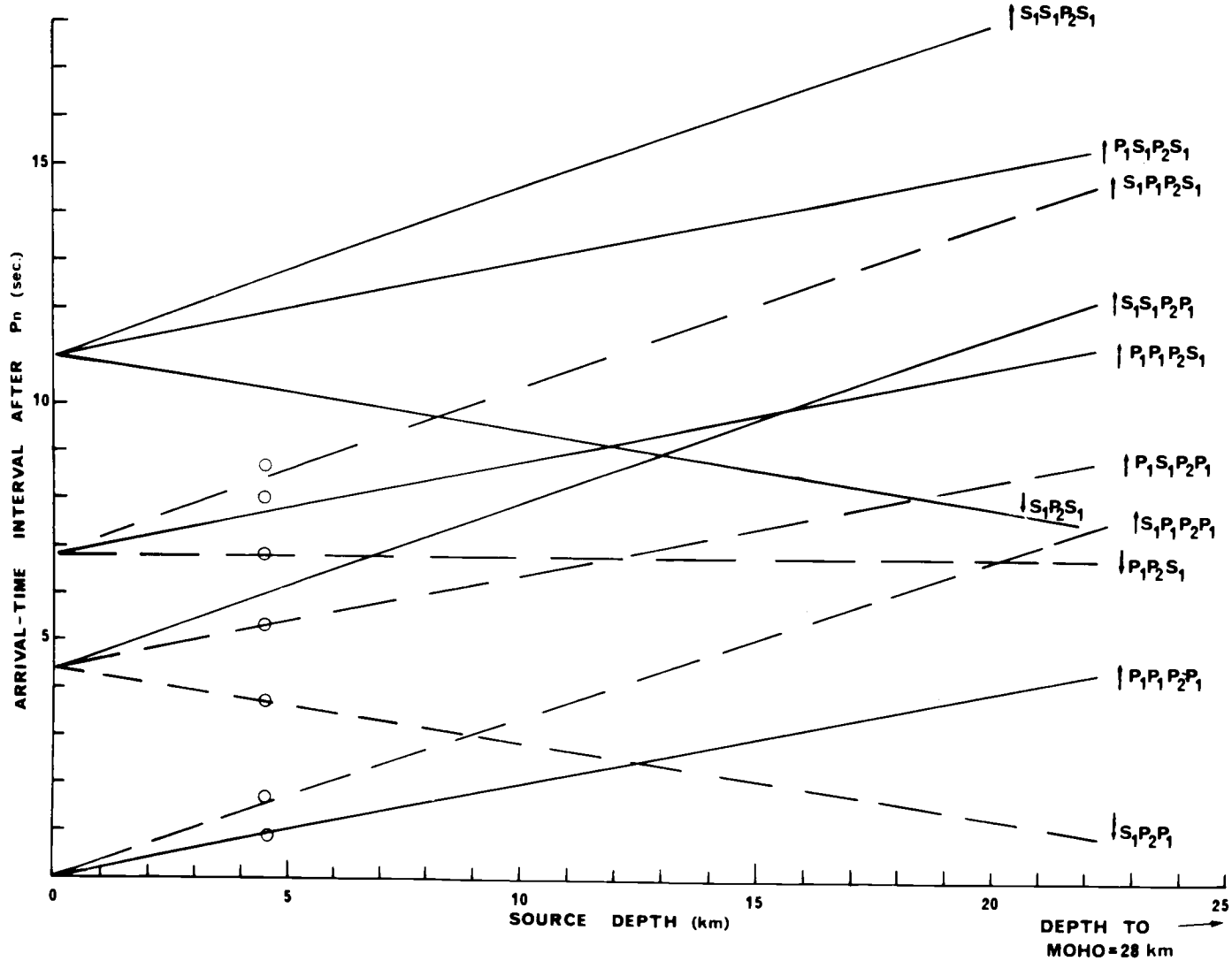

Figure 37. Revision of Figure 22 resulting from an increase of 5 km in the crustal thickness of the western province and an increase of 3 km in the eastern province.

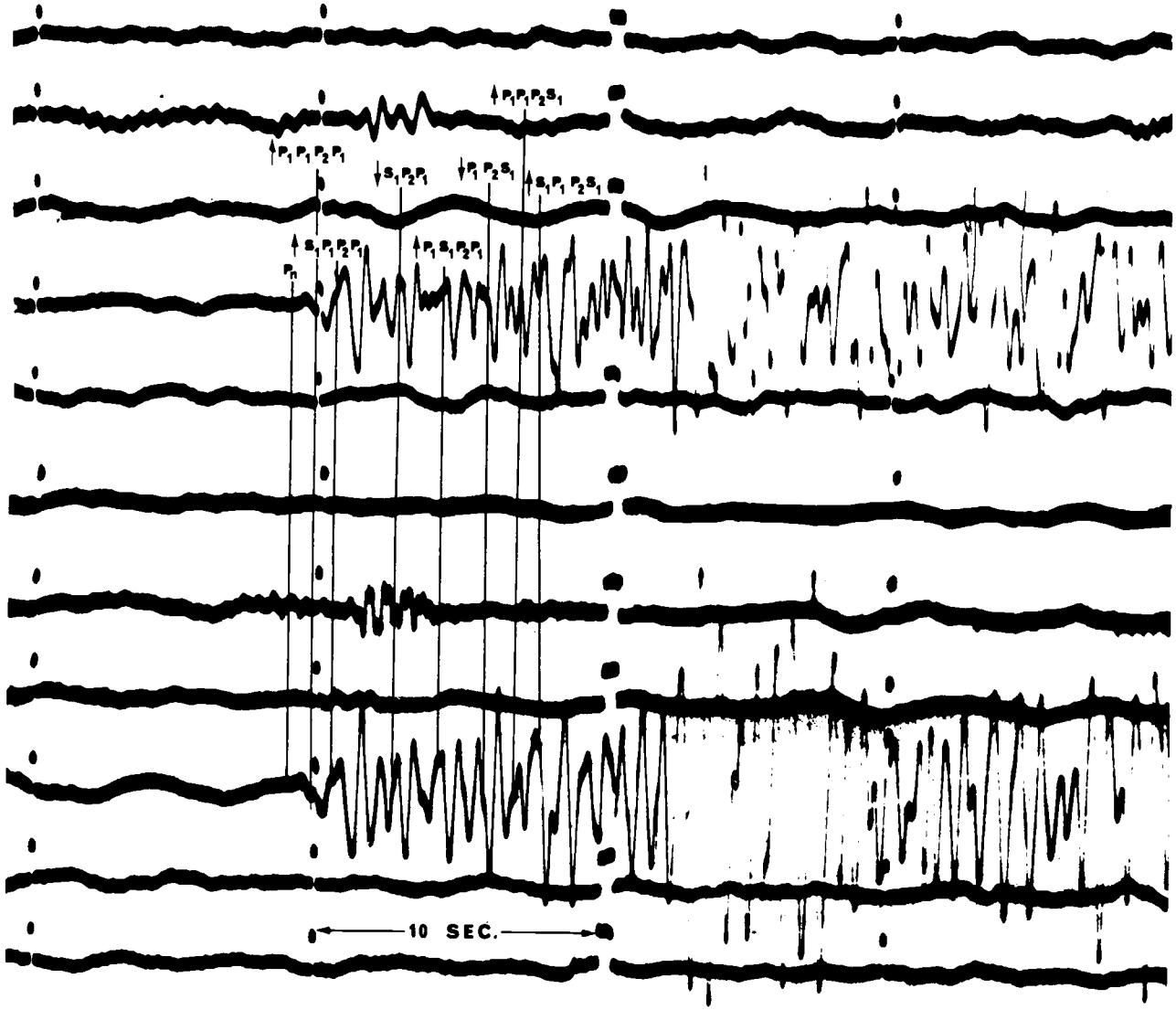

Figure 38. Head wave interpretation of the January 24, 1963 earthquake as recorded at HLY.

the station HLY) is now 45 km thick. The earthquake epicenter was near 122° W longitude, and the crustal thickness of 28 km as is required in order to explain the phases by the head wave model--without altering the velocities as determined by refraction studies--is remarkably consistent with Figure 4.

It is seen from Figure 38 that the wave $\uparrow P_1 P_1 P_2 P_1$ was identified at HLY. From Table 6 this implies a source radiation pattern such that $\uparrow P$ has about ten times the amplitude of $\downarrow P$ towards HLY. The wave interpreted as $\downarrow P_1 P_2 S_1$ has an amplitude which is larger relative to P_n than the theoretical value, but this amplitude discrepency is attributed to a small P_n amplitude caused by the interference of P_n and $\uparrow P_1 P_1 P_2 P_1$. This overlapping of the first phases also accounts for the apparent long period onset of the earthquake.

Figure 39 displays the vertical records from stations at two other azimuths from this same earthquake. The time intervals as taken from the HLY records for the phases $\uparrow P_1 P_1 P_2 P_1$, $\uparrow S_1 P_1 P_2 P_1$, $\downarrow S_1 P_2 P_1$ and $\uparrow P_1 S_1 P_2 P_1$ are indicated on each seismogram of Figure 39. The time intervals for these phases are dependent only upon the source depth and crustal structure in the source region and should be the same for all stations. Some of these phases may become more dominant or may disappear at certain azimuths, depending upon the radiation pattern of the earthquake. The time intervals between

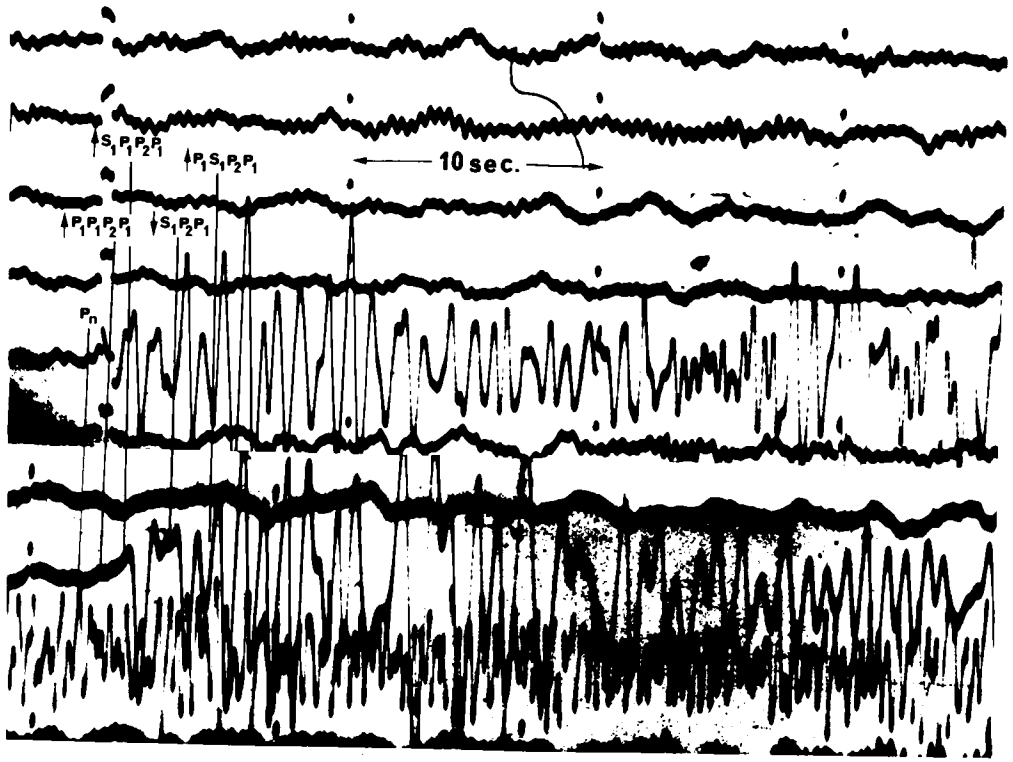

SHORT-PERIOD VERTICAL SEISMOGRAMS RECORDED AT WINNEMUCCA (TOP, 455K) AND MINA (BOTTOM, 593K), NEVADA, FROM THE JANUARY 24, 1963 EARTHQUAKE LOCATED SE OF SEATTLE. DISTANCE AND AZIMUTHS TO STATIONS ARE:

WINNEMUCCA	768KM	151°
MINA	1060KM	167°

Figure 39. Short-period vertical seismograms of the earthquake of January 24, 1963 as recorded at MNA and WMC. The relative arrival times marked on the records were taken directly from the record of Figure 38.

P_n and the phases $\downarrow P_1P_2S_1$, $\uparrow P_1P_1P_2S_1$, and $\uparrow S_1P_1P_2P_1$ depend upon the crustal structure under the station.

It is seen from Figure 39 that all recorded arrivals at stations WMC and MNA can be correlated with arrivals observed on the HLY seismograms. The seismograms of Figure 39 indicate that the azimuth to the station MNA is along a null direction for the P_n radiation from this source. The arrival times of station converted waves could not be determined for seismograms of Figure 39 as the phases following $\uparrow P_1S_1P_2P_1$ interfere with each other. This overlapping of phases at larger epicentral distances appears to be due to an increase in recorded periods. The frequently observed increased period with increasing epicentral distance presents a major obstacle to the application of this technique. It should be possible to obviate these difficulties through the use of pulse-shortening techniques, such as the deconvolution filters employed in seismic reflection shooting. These techniques require extensive digital processing of the data, however, and were not used here.

The other earthquakes listed in Table 3 were analyzed using arguments similar to those presented above. The interpretations which could be obtained are given below.

December 27, 1963

The analysis produced h = 7 km, based upon an $\uparrow S_1P_1P_2P_1$

interpretation of the second arrival at BLL and TON. The records were not of good quality.

January 6, 1963

The depth of h = 5 km was determined by an $\uparrow S_1P_1P_2P_1$ interpretation of the second arrival and an $\downarrow S_1P_2P_1$ interpretation of a very large third arrival at 5 seconds after P_n on the WMC records.

January 27, 1963

The best interpretation gave h = 16 km, based upon the LON records showing three waves following P_n, whose amplitude ratios to that of P_n were $\frac{1}{2}$, 2, and 4, respectively, and whose arrival times after P_n were 2.6, 3.5, and 5.1 seconds. These waves were interpreted to be $\uparrow P_1P_1P_2P_1$, $\downarrow S_1P_2P_1$ and $\uparrow S_1P_1P_2P_1$, respectively.

August 22, 1963

The results of this analysis produced h = 5 km, based on an $\uparrow S_1P_1P_2P_1$ interpretation of the second arrival at ARC, MIN, WMC, and HLY. P_n registered as a small but clear wave (see Figure 13), and the records took on the appearance of a ringing marine refraction record upon the arrival of $\uparrow S_1P_1P_2P_1$. The S to P reflection is from the ocean floor, and it is this encounter with the water

layer which sets up the reverberations.

The other oceanic shocks listed in Table 2 were recorded with periods which are too long to allow for the determination of more than one second arrival. Also, the limited azimuthal station coverage did not permit the first arrivals to be picked as the P_n wave.

CONCLUSIONS

The following are concluded from this investigation:

1. The Post-P_n phases (appearing on seismograms for about 10 seconds after P_n) can not be explained as: (a) instrumental effects, (b) signal-generated noise, (c) converted waves at intercrustal discontinuities, (d) aftershocks, or (e) "stopping" or "breakout" phases, because the amplitudes compared to P_n are too large. Similarly, these second arrivals can not be explained as (a) large-angle sub-Moho reflections, (b) slightly different travel paths from P_n, or (c) aftershocks, "stopping" or "breakout" phases, because azimuthal variations in the first motions of these phases relative to those of P_n are not consistent with such mechanisms.

2. The nature of the Post-P_n waves originating from shocks within the crust can be explained theoretically, and verified on earthquake seismograms, as head waves which have been reflected at the earth's surface (above the source) or were converted at the Moho. For certain radiation patterns and azimuthal directions, the waves following P_n that are usually recorded with large amplitude include $\uparrow S_1P_1P_2P_1$ (sP_n), $\downarrow S_1P_2P_1$, and $\uparrow S_1P_1P_2S_1$. Waves with smaller amplitudes (often not recorded) include $\uparrow P_1P_1P_2P_1$ (pP_n), $\downarrow P_1P_2S_1$, and $\uparrow P_1S_1P_2P_1$.

Theoretically possible waves which are always small or negligible, and therefore not applicable for interpretive purposes, include $\downarrow S_1P_2S_1$, $\uparrow P_1S_1P_2S_1$, $\uparrow P_1P_1P_2S_1$, $\uparrow S_1S_1P_2P_1$, and $\uparrow S_1S_1P_2S_1$.

3. The consistency in the predicted head waves with those observed on seismograms during the first 10 seconds after the arrival of P_n is strong support for the assumption that P_n is a head wave.

4. The good agreement between synthetic seismograms, assuming head wave interpretations for Post-P_n waves and a single source motion of short duration, with actual seismograms, provides evidence that an earthquake source can indeed be represented by a single pulse motion.

5. The P_x wave of Gutenberg can be explained by head wave theory as either $\uparrow S_1P_1P_2P_1$ (sP_n) or $\downarrow S_1P_2P_1$ waves, and perhaps in a few cases as $\uparrow P_1P_1P_2P_1$. P_x does not distinguish between these phases.

6. By proper identification of the second arrival head waves, various ones of these waves can be used to determine focal depths of small shocks located within the crust and recorded at only a few (even one) station. The focal depths can be determined with rather unexpected accuracy; the accuracy of the velocity structure in the crust and upper mantle being the

controlling factors. Identification of the second arrival head waves for focal depth determinations ($\uparrow S_1P_1P_2P_1$, $\downarrow S_1P_2P_1$, and $\uparrow S_1P_1P_2S_1$) can be made most reliably at epicentral distances between 150 and 1000 km, with best results obtained at distances greater than 350 km. These focal depth determinations are independent of origin times and do not require a close network of stations.

7. Focal depths of earthquakes in the Pacific Northwest states have been determined, using head wave theory and a single layer crust over a mantle having velocities previously determined, as follows:

Date	Epicenter	Focal Depth
August 23, 1962	Crescent City, California	h = $5\frac{1}{2}$ km
November 6, 1962	Portland, Oregon	h = 10 km
January 24, 1963	Seattle, Washington	h = $4\frac{1}{2}$ km
December 27, 1963	Kings Valley, Oregon	h = 7 km
January 6, 1963	S. W. Montana	h = 5 km
January 27, 1963	Central Idaho	h = 16 km
August 22, 1963	Off Southern Oregon	h = 5 km

8. Crustal thicknesses in the vicinity of a source (above the Moho) and a station (at distances of 150 to 1000 km) can be determined (or modified) from time differences between P_n and the properly identified subsequent head waves. This was illustrated by the analysis of the shock of January 24, 1963.

The crustal thickness was found to be 28 km under the epicenter and 45 km under the station HLY (the model used assumed 23 km and 42 km respectively). The analysis could conceivably be extended beyond that used in this study to a two or even three layer crust.

9. A limiting factor in applying the head wave model to interpreting Post-P_n phases is the overlapping of phases owing to the relatively long periods of each phase. This factor makes the head wave model more appropriate to determining focal depths of crustal shocks in continental more than in oceanic provinces. However, where separation of overriding phases is required, mathematical filtering methods can be applied or higher frequency seismometers used.

BIBLIOGRAPHY

Andreev, S. S. 1957. A study of the plutonic structure of the earth's crust using PS exchange waves recorded during earthquakes. Bulletin of the Academy of Sciences of the U. S. S. R., no. 1, p. 22-31. (Geophysics Series) (Translated from Izvestiia Akademiia Nauk S. S. S. R. Seriia Geofizicheskaia)

Andreev, S. S. and N. V. Shebalin. 1957. The use of short period seismograms for isolating exchange waves on traces of distant earthquakes. Bulletin of the Academy of Sciences of the U. S. S. R., no. 7, p. 109-112. (Geophysics Series) (Translated from Izvestiia Akademiia Nauk S. S. S. R. Seriia Geofizicheskaia)

Berg, J. W., Jr., K. F. Cook and H. D. Nerans, Jr. 1959. Seismic studies of crustal structure in the eastern Basin and Range province. (Abstract) Bulletin of the Geologic Society of America 70:1709.

Berg, J. W., Jr. and L. T. Long. 1966. Characteristics of refracted arrivals of seismic waves. Journal of Geophysical Research 71:2583-2589.

Brekhovskikh, L. M. 1960. Waves in layered media, tr. by D. Lieherman, ed. by R. T. Beyer. New York, Academic. 561 p.

Bullen, K. E. 1963. An introduction to the theory of seismology. 3d ed. London, Cambridge University. 381 p.

Chiburis, E. F. 1965. Crustal structure in the Pacific Northwest states from phase-velocity dispersion of seismic surface waves. Ph. D. thesis. Corvallis, Oregon State University, 170 numb. leaves.

Cook, K. L., S. T. Algermissen and J. K. Costain. 1962. The status of PS converted waves in crustal studies. Journal of Geophysical Research 67:4769-4778.

Dehlinger, P. 1964. Second semiannual technical report for 15 September 1963 to 14 March 1964. Seismicity of Oregon. Corvallis, Oregon State University, Dept. of Oceanography. 14 p. (Contract no. AF(628)-2778)

Dehlinger, P., E. F. Chiburis and M. M. Collver. 1965. Local travel-time curves and their geologic implications for the Pacific Northwest states. Bulletin of the Seismological Society of America 55:587-607.

Dehlinger, P. and W. S. French. 1965. Investigations of the nature of Post-P_n waves. (Abstract) Transactions of the American Geophysical Union 46:156.

Dehlinger, P., R. W. Couch and M. Gemperle. 1968. Continental and oceanic structure from the Oregon coast westward across the Juan de Fuca Ridge. Canadian Journal of Earth Sciences 5:1079-1090.

Dobrin, M. B., R. F. Simon and P. L. Lawrence. 1951. Rayleigh waves from small explosions. Transactions of the American Geophysical Union 32:822-831.

Ewing, M., W. S. Jardetzky and F. Press. 1957. Elastic waves in layered media. New York, McGraw-Hill. 380 p.

Grant, F. S. and G. F. West. 1965. Interpretation theory in applied geophysics. New York, McGraw-Hill. 583 p.

Gutenberg, B. 1951. Revised travel times in southern California. Bulletin of the Seismological Society of America 41:143-163.

Gutenberg, B. 1959. Physics of the earth's interior. New York, Academic. 240 p.

Hagedoorn, J. G. 1964. The elusive first arrival. Geophysics 29: 806-813.

Hagiwara, T. 1958. A note on the theory of the electromagnetic seismograph. Bulletin of the Earthquake Research Institute (Tokyo University) 36:139-164.

Hall, D. H. and W. C. Brisbin. 1965. Crustal structures from converted head waves in central western Manitoba. Geophysics 30:1053-1067.

Heelan, P. A. 1953. On the theory of head waves. Geophysics 18: 871-893.

James, D. E. and J. S. Steinhart. 1966. Structure beneath the continents: A critical review of explosion studies 1960-1965. In: The earth beneath the continents, ed. by Steinhart, J. S. and T. J. Smith. Washington, D.C. p. 293-333. (American Geophysical Union. Monograph 10)

Key, F. A. 1967. Signal generated noise recorded at the Eskdalemuir seismometer array station. Bulletin of the Seismological Society of America 57:27-37.

Kondorskaya, N. V. 1956. Identification of the sP wave in shallow earthquakes, and its use in determining the depth of focus. Trudy Instituta Geofiziki. Akademiya Nauk S. S. S. R. 36:35-47.

Lapwood, E. R. 1949. The disturbance due to a line source in a semi-infinite elastic medium. Philosophical Transactions of the Royal Society of London 242:63-100.

Matuzawa, T., K. Hasegawa and S. Haeno. 1928. On the fore-runners of earthquake motions of certain earthquakes. Bulletin of the Earthquake Research Institute (Tokyo University) 4:85-106.

Matuzawa, T., K. Yamada and T. Suziki. 1929. On the fore-runners of earthquake motions. The second paper. Bulletin of the Earthquake Research Institute (Tokyo University) 7: 241-260.

McEvilly, T. V. 1966. The earthquake sequence of November 1964 near Corralitos, California. Bulletin of the Seismological Society of America 56:755-773.

Mikumo, T. 1962. Mechanisms of local earthquakes in Kwanto region, Japan, derived from the amplitude relation of P and S waves. Bulletin of the Earthquake Research Institute (Tokyo University) 40:399-424.

Nakamura, Y. 1966. Multi-reflected head waves in a single-layered medium. Geophysics 31:927-939.

Newlands, M. 1952. The disturbance due to a line source in a semi-infinite elastic medium with a single surface layer. Philosophical Transactions of the Royal Society of London 245: 213-308.

Pakiser, L. C. and D. P. Hill. 1963. Crustal structure in Nevada and southern Idaho from nuclear explosions. Journal of Geophysical Research 68:5757-5766.

Richter, C. F. 1958. Elementary seismology. San Francisco, Freeman. 768 p.

Ryall, A. 1962. The Hebgen Lake, Montana, earthquake of August 18, 1959: P waves. Bulletin of the Seismological Society of America 52:235-271.

Sarmah, Suryya Kanta. 1967. Attenuation of compressional waves in the earth's mantle. Ph. D. thesis. Corvallis, Oregon State University. 80 numb. leaves.

Savage, J. D. 1965. The stopping phase of seismograms. Bulletin of the Seismological Society of America 55:47-58.

Schwind, J. J., J. W. Berg, Jr. and L. L. Cook. 1960. PS converted waves from large explosions. Journal of Geophysical Research 65:3817-3824.

Shor, G. G., Jr., P. Dehlinger, K. K. Kirk and W. S. French. 1968. Seismic refraction studies off Oregon and northern California. Journal of Geophysical Research 73:2175-2194.

Tatel, H. E. 1954. Note on the nature of a seismogram-II. Journal of Geophysical Research 59:289-294.

Tatel, H. E. and M. A. Tuve. 1955. Seismic exploration of a continental crust. In: A symposium on the crust of the earth, ed. by A. Poldervaart. Washington, D. C. p. 35-50. (Geological Society of America. Special Paper 62)

Thiruvathukal, John Varkey. 1968. Regional geology of Oregon. Ph. D. thesis. Corvallis, Oregon State University. 92 numb. leaves.

Turcotte, F. T. 1964. Epicenters and focal depths in the Hollister region of central California. Ph. D. thesis. Berkeley, University of California. 129 numb. leaves.

Udias, A. 1965. A study of the aftershocks and focal mechanism of the Salinas-Watsonville earthquakes of August 31 and September 14, 1963. Bulletin of the Seismological Society of America 55:85-106.

Wyss, M. and J. N Brune. 1967. Alaska earthquake of 28 March 1964: A complex multiple rupture. Bulletin of the Seismological Society of America 57:1126.

APPENDICES

APPENDIX I.

NEWLANDS' POTENTIAL AND DISPLACEMENT EQUATIONS

The expressions for the various potentials and corresponding displacements as derived by Newlands (1952) are photographically reproduced below. A few typographical errors were present in Newlands' paper. The following corrections should be made. A factor of $1/F_o$ is missing in the expressions for ${}_s\psi^{(2)}_{a_2}$, ${}_sU^{(2)}_{a_2}$ (under ${}_s\psi^{(2)}_{a_2}$) and ${}_pU^{(9)}_{a_2}$ (under ${}_p\psi^{(9)}_{a_2}$). The term ${}_s\phi^{(3)}_{a_2}$ has its superscript misprinted. All of the W components for the ${}_p\psi$ contributions from Γ_{a_2} have the wrong algebraic signs. The exponent of "i" in ${}_p\psi^{(2)}_{a_2}$ should be 3 rather than 3/2. In addition, the second subscript on the brackets in the displacement equations for the ${}_s\phi$ and ${}_s\psi$ contributions from Γ_{a_2} are unnecessary. The equations were checked for accuracy and are otherwise correct.

${}_p\phi$ contributions from Γ_{α_2}

$$\begin{cases} {}_p\phi^{(2)}_{\alpha_2} \doteq \dfrac{-16\sqrt{(2\pi i^3)}\,\alpha_2^8(2/\alpha_2^2-1/\beta_1^2)^2}{\widehat{\beta_1\alpha_2}[x\alpha_2-2H\widehat{\beta_1\alpha_2}-(h+z)\,\widehat{\alpha_1\alpha_2}]^{\frac{1}{2}}}\left[\dfrac{1}{F_0^2}\left(\dfrac{T_1}{S_0}-\dfrac{T_0S_1}{S_0^2}\right)\right]_{\alpha_2}\omega^{-\frac{1}{2}}\exp\{i\omega\tau\}, \\ {}_pU^{(2)}_{\alpha_2} \doteq \dfrac{-32\sqrt{2}\,i\,\alpha_2^7(2/\alpha_2^2-1/\beta_1^2)^2}{\widehat{\beta_1\alpha_2}[x\alpha_2-2H\widehat{\beta_1\alpha_2}-(h+z)\,\widehat{\alpha_1\alpha_2}]^{\frac{1}{2}}}\left[\dfrac{1}{F_0^2}\left(\dfrac{T_1}{S_0}-\dfrac{T_0S_1}{S_0^2}\right)\right]_{\alpha_2}\tau^{\frac{1}{2}}H(\tau) \doteq {}_pW^{(2)}_{\alpha_2}\times\widehat{\alpha_1\alpha_2}/\alpha_2, \end{cases}$$

where $$\tau = t-x/\alpha_2-2H/\widehat{\beta_1\alpha_2}-(h+z)/\widehat{\alpha_1\alpha_2};$$

$$\begin{cases} {}_p\phi^{(3)}_{\alpha_2} \doteq \dfrac{4\sqrt{(2\pi i)}\,\alpha_2^5\,\widehat{\alpha_1\alpha_2}(2/\alpha_2^2-1/\beta_1^2)}{\widehat{\beta_1\alpha_2}[x\alpha_2-(H+h-z)\,\widehat{\alpha_1\alpha_2}-H\widehat{\beta_1\alpha_2}]^{\frac{1}{2}}}\left[\dfrac{1}{F_0}\left(\dfrac{Y_1}{S_0}-\dfrac{Y_0S_1}{S_0^2}\right)\right]_{\alpha_2}\omega^{-\frac{1}{2}}\exp\{i\omega\tau\}, \\ {}_pU^{(3)}_{\alpha_2} \doteq \dfrac{8\sqrt{2}\,\alpha_2^4\,\widehat{\alpha_1\alpha_2}(2/\alpha_2^2-1/\beta_1^2)}{\widehat{\beta_1\alpha_2}[x\alpha_2-(H+h-z)\,\widehat{\alpha_1\alpha_2}-H\widehat{\beta_1\alpha_2}]^{\frac{1}{2}}}\left[\dfrac{1}{F_0}\left(\dfrac{Y_1}{S_0}-\dfrac{Y_0S_1}{S_0^2}\right)\right]_{\alpha_2}\tau^{\frac{1}{2}}H(\tau) \doteq -{}_pW^{(3)}_{\alpha_2}\times\widehat{\alpha_1\alpha_2}/\alpha_2, \end{cases}$$

where $$\tau = t-x/\alpha_2-(H+h-z)/\widehat{\alpha_1\alpha_2}-H/\widehat{\beta_1\alpha_2};$$

$$\begin{cases} {}_p\phi^{(4)}_{\alpha_2} \doteq \dfrac{4\sqrt{(2\pi i)}\,\alpha_2^5\,\widehat{\alpha_1\alpha_2}(2/\alpha_2^2-1/\beta_1^2)}{\widehat{\beta_1\alpha_2}[x\alpha_2-(H-h+z)\,\widehat{\alpha_1\alpha_2}-H\widehat{\beta_1\alpha_2}]^{\frac{1}{2}}}\left[\dfrac{1}{F_0}\left(\dfrac{Y_1}{S_0}-\dfrac{Y_0S_1}{S_0^2}\right)\right]_{\alpha_2}\omega^{-\frac{1}{2}}\exp\{i\omega\tau\}, \\ {}_pU^{(4)}_{\alpha_2} \doteq \dfrac{8\sqrt{2}\,\alpha_2^4\,\widehat{\alpha_1\alpha_2}(2/\alpha_2^2-1/\beta_1^2)}{\widehat{\beta_1\alpha_2}[x\alpha_2-(H-h+z)\,\widehat{\alpha_1\alpha_2}-H\widehat{\beta_1\alpha_2}]^{\frac{1}{2}}}\left[\dfrac{1}{F_0}\left(\dfrac{Y_1}{S_0}-\dfrac{Y_0S_1}{S_0^2}\right)\right]_{\alpha_2}\tau^{\frac{1}{2}}H(\tau) \doteq {}_pW^{(4)}_{\alpha_2}\times\widehat{\alpha_1\alpha_2}/\alpha_2, \end{cases}$$

where $$\tau = t-x/\alpha_2-(H-h+z)/\widehat{\alpha_1\alpha_2}-H/\widehat{\beta_1\alpha_2};$$

$$\begin{cases} {}_p\phi^{(5)}_{\alpha_2} \doteq \dfrac{-8\sqrt{(2\pi i)}\,\alpha_2^5\,\widehat{\alpha_1\alpha_2}(2/\alpha_2^2-1/\beta_1^2)}{\widehat{\beta_1\alpha_2}[x\alpha_2-(H+h+z)/\widehat{\alpha_1\alpha_2}-H\widehat{\beta_1\alpha_2}]^{\frac{1}{2}}}\left[\dfrac{F_0}{F_0^2}\left(\dfrac{Y_1}{S_0}-\dfrac{Y_0S_1}{S_0^2}\right)\right]_{\alpha_2}\omega^{-\frac{1}{2}}\exp\{i\omega\tau\}, \\ {}_pU^{(5)}_{\alpha_2} \doteq \dfrac{-16\sqrt{2}\,\alpha_2^4\,\widehat{\alpha_1\alpha_2}(2/\alpha_2^2-1/\beta_1^2)}{\widehat{\beta_1\alpha_2}[x\alpha_2-(H+h+z)/\widehat{\alpha_1\alpha_2}-H\widehat{\beta_1\alpha_2}]^{\frac{1}{2}}}\left[\dfrac{F_0}{F_0^2}\left(\dfrac{Y_1}{S_0}-\dfrac{Y_0S_1}{S_0^2}\right)\right]_{\alpha_2}\tau^{\frac{1}{2}}H(\tau) \doteq {}_pW^{(5)}_{\alpha_2}\times\widehat{\alpha_1\alpha_2}/\alpha_2, \end{cases}$$

where $$\tau = t-x/\alpha_2-(H+h+z)/\widehat{\alpha_1\alpha_2}-H/\widehat{\beta_1\alpha_2};$$

$$\begin{cases} {}_p\phi^{(6)}_{\alpha_2} \doteq \sqrt{(2\pi i^3)}\,\widehat{\alpha_1\alpha_2}\,\alpha_2^2[x\alpha_2-(2H-h-z)\,\widehat{\alpha_1\alpha_2}]^{-\frac{1}{2}}\left[\dfrac{W_1}{S_0}-\dfrac{W_0S_1}{S_0^2}\right]_{\alpha_2}\omega^{-\frac{1}{2}}\exp\{i\omega\tau\}, \\ {}_pU^{(6)}_{\alpha_2} \doteq 2\sqrt{2i}\,\widehat{\alpha_1\alpha_2}\,\alpha_2[x\alpha_2-(2H-h-z)\,\widehat{\alpha_1\alpha_2}]^{-\frac{1}{2}}\left[\dfrac{W_1}{S_0}-\dfrac{W_0S_1}{S_0^2}\right]_{\alpha_2}\tau^{\frac{1}{2}}H(\tau) \doteq -{}_pW^{(6)}_{\alpha_2}\times\widehat{\alpha_1\alpha_2}/\alpha_2, \end{cases}$$

where $$\tau = t-x/\alpha_2-(2H-h-z)/\widehat{\alpha_1\alpha_2};$$

$$\begin{cases} {}_p\phi^{(7)}_{\alpha_2} \doteq -\sqrt{(2\pi i^3)}\,\widehat{\alpha_1\alpha_2}\,\alpha_2^2[x\alpha_2-(2H+h-z)\,\widehat{\alpha_1\alpha_2}]^{-\frac{1}{2}}\left[\dfrac{F_0}{F_0}\left(\dfrac{W_1}{S_0}-\dfrac{W_0S_1}{S_0^2}\right)\right]_{\alpha_2}\omega^{-\frac{1}{2}}\exp\{i\omega\tau\}, \\ {}_pU^{(7)}_{\alpha_2} \doteq -2\sqrt{2i}\,\widehat{\alpha_1\alpha_2}\,\alpha_2[x\alpha_2-(2H+h-z)\,\widehat{\alpha_1\alpha_2}]^{-\frac{1}{2}}\left[\dfrac{F_0}{F_0}\left(\dfrac{W_1}{S_0}-\dfrac{W_0S_1}{S_0^2}\right)\right]_{\alpha_2}\tau^{\frac{1}{2}}H(\tau) \doteq -{}_pW^{(7)}_{\alpha_2}\times\widehat{\alpha_1\alpha_2}/\alpha_2, \end{cases}$$

where $$\tau = t-x/\alpha_2-(2H+h-z)/\widehat{\alpha_1\alpha_2};$$

$$\begin{cases} {}_p\phi^{(8)}_{\alpha_2} \doteq -\sqrt{(2\pi i^3)}\,\widehat{\alpha_1\alpha_2}\,\alpha_2^2[x\alpha_2-(2H-h+z)\,\widehat{\alpha_1\alpha_2}]^{-\frac{1}{2}}\left[\dfrac{F_0}{F_0}\left(\dfrac{W_1}{S_0}-\dfrac{W_0S_1}{S_0^2}\right)\right]_{\alpha_2}\omega^{-\frac{1}{2}}\exp\{i\omega\tau\}, \\ {}_pU^{(8)}_{\alpha_2} \doteq -2\sqrt{2i}\,\widehat{\alpha_1\alpha_2}\,\alpha_2[x\alpha_2-(2H-h+z)\,\widehat{\alpha_1\alpha_2}]^{-\frac{1}{2}}\left[\dfrac{F_0}{F_0}\left(\dfrac{W_1}{S_0}-\dfrac{W_0S_1}{S_0^2}\right)\right]_{\alpha_2}\tau^{\frac{1}{2}}H(\tau) \doteq {}_pW^{(8)}_{\alpha_2}\times\widehat{\alpha_1\alpha_2}/\alpha_2, \end{cases}$$

where $$\tau = t-x/\alpha_2-(2H-h+z)/\widehat{\alpha_1\alpha_2};$$

$$\begin{cases} {}_p\phi^{(9)}_{\alpha_2} = \sqrt{(2\pi i^3)}\,\widehat{\alpha_1\alpha_2}\,\alpha_2^2[x\alpha_2-(2H+h+z)\,\widehat{\alpha_1\alpha_2}]^{-\frac{1}{2}}\left[\dfrac{F_0^2}{F_0^2}\left(\dfrac{W_1}{S_0}-\dfrac{W_0S_1}{S_0^2}\right)\right]_{\alpha_2}\omega^{-\frac{1}{2}}\exp\{i\omega\tau\}, \\ {}_pU^{(9)}_{\alpha_2} = 2\sqrt{2i}\,\widehat{\alpha_1\alpha_2}\,\alpha_2[x\alpha_2-(2H+h+z)\,\widehat{\alpha_1\alpha_2}]^{-\frac{1}{2}}\left[\dfrac{F_0^2}{F_0^2}\left(\dfrac{W_1}{S_0}-\dfrac{W_0S_1}{S_0^2}\right)\right]_{\alpha_2}\tau^{\frac{1}{2}}H(\tau) \doteq {}_pW^{(9)}_{\alpha_2}\times\widehat{\alpha_1\alpha_2}/\alpha_2, \end{cases}$$

where $$\tau = t-x/\alpha_2-(2H+h+z)/\widehat{\alpha_1\alpha_2}.$$

${}_p\psi$ *contributions from* Γ_{α_2}

$$\begin{cases} {}_p\psi^{(2)}_{\alpha_2} \doteq \dfrac{-4\sqrt{(2\pi i^{\frac{1}{2}})}\,\alpha_2^5(2/\alpha_2^2-1/\beta_1^2)}{[x\alpha_2-(2H-z)\,\widehat{\beta_1\alpha_2}-h\widehat{\alpha_1\alpha_2}]^{\frac{1}{2}}}\left[\dfrac{1}{F_0}\left(\dfrac{T_1}{S_0}-\dfrac{T_0S_1}{S_0^2}\right)\right]_{\alpha_2}\omega^{-\frac{1}{2}}\exp\{i\omega\tau\}, \\ {}_pU^{(2)}_{\alpha_2} \doteq \dfrac{8\sqrt{2i}\,\alpha_2^5(2/\alpha_2^2-1/\beta_1^2)}{\widehat{\beta_1\alpha_2}[x\alpha_2-(2H-z)\,\widehat{\beta_1\alpha_2}-h\widehat{\alpha_1\alpha_2}]^{\frac{1}{2}}}\left[\dfrac{1}{F_0}\left(\dfrac{T_1}{S_0}-\dfrac{T_0S_1}{S_0^2}\right)\right]_{\alpha_2}\tau^{\frac{1}{2}}H(\tau) \doteq -{}_pW^{(2)}_{\alpha_2}\times\alpha_2/\widehat{\beta_1\alpha_2}, \end{cases}$$

where $$\tau = t-x/\alpha_2-(2H-z)/\widehat{\beta_1\alpha_2}-h/\widehat{\alpha_1\alpha_2};$$

$$\begin{cases} {}_p\psi^{(3)}_{\alpha_2} \doteq \dfrac{4\sqrt{(2\pi i^3)}\,\alpha_2^5(2/\alpha_2^2-1/\beta_1^2)}{[x\alpha_2-(2H+z)\,\widehat{\beta_1\alpha_2}-h\widehat{\alpha_1\alpha_2}]^{\frac{1}{2}}}\left[\dfrac{F_0}{F_0^2}\left(\dfrac{T_1}{S_0}-\dfrac{T_0S_1}{S_0^2}\right)\right]_{\alpha_2}\omega^{-\frac{1}{2}}\exp\{i\omega\tau\}, \\ {}_pU^{(3)}_{\alpha_2} \doteq \dfrac{8\sqrt{2i}\,\alpha_2^5(2/\alpha_2^2-1/\beta_1^2)}{\widehat{\beta_1\alpha_2}[x\alpha_2-(2H+z)\,\widehat{\beta_1\alpha_2}-h\widehat{\alpha_1\alpha_2}]^{\frac{1}{2}}}\left[\dfrac{F_0}{F_0^2}\left(\dfrac{T_1}{S_0}-\dfrac{T_0S_1}{S_0^2}\right)\right]_{\alpha_2}\tau^{\frac{1}{2}}H(\tau) \doteq {}_pW^{(3)}_{\alpha_2}\times\alpha_2/\widehat{\beta_1\alpha_2}, \end{cases}$$

where $$\tau = t-x/\alpha_2-(2H+z)/\widehat{\beta_1\alpha_2}-h/\widehat{\alpha_1\alpha_2};$$

$$\begin{cases} {}_p\psi^{(4)}_{\alpha_2} \doteq \dfrac{\sqrt{(2\pi i)}\,\alpha_2^2\,\widehat{\alpha_1\alpha_2}}{[x\alpha_2-(H-h)\,\widehat{\alpha_1\alpha_2}-(H-z)\,\widehat{\beta_1\alpha_2}]^{\frac{1}{2}}}\left[\dfrac{Y_1}{S_0}-\dfrac{Y_0S_1}{S_0^2}\right]_{\alpha_2}\omega^{-\frac{1}{2}}\exp\{i\omega\tau\}, \\ {}_pU^{(4)}_{\alpha_2} \doteq \dfrac{-2\sqrt{2}\,\widehat{\alpha_1\alpha_2}\,\alpha_2^2}{\widehat{\beta_1\alpha_2}[x\alpha_2-(H-h)\,\widehat{\alpha_1\alpha_2}-(H-z)\,\widehat{\beta_1\alpha_2}]^{\frac{1}{2}}}\left[\dfrac{Y_1}{S_0}-\dfrac{Y_0S_1}{S_0^2}\right]_{\alpha_2}\tau^{\frac{1}{2}}H(\tau) \doteq -{}_pW^{(4)}_{\alpha_2}\times\alpha_2/\widehat{\beta_1\alpha_2}, \end{cases}$$

where $$\tau = t-x/\alpha_2-(H-h)/\widehat{\alpha_1\alpha_2}-(H-z)\,\widehat{\beta_1\alpha_2};$$

$$\left|\begin{aligned}
{}_{\beta}V^{(5)}_{\alpha_2} &\doteq \frac{-\sqrt{(2\pi i)}\,\alpha_2^2\widehat{\alpha_1\alpha_2}}{[x\alpha_2-(H-h)\,\widehat{\alpha_1\alpha_2}-(H+z)\,\widehat{\beta_1\alpha_2}]^{\frac{1}{2}}}\left[\frac{F_0}{F_0}\left(\frac{Y_1}{S_0}-\frac{Y_0S_1}{S_0^2}\right)\right]_{\alpha_2}\omega^{-\frac{1}{2}}\exp\{i\omega\tau\},\\
{}_{\beta}U^{(5)}_{\alpha_2} &\doteq \frac{-2\sqrt{2}\,\widehat{\alpha_1\alpha_2}\,\alpha_2^2}{\widehat{\beta_1\alpha_2}[x\alpha_2-(H-h)\,\widehat{\alpha_1\alpha_2}-(H+z)\,\widehat{\beta_1\alpha_2}]^{\frac{1}{2}}}\left[\frac{F_0}{F_0}\left(\frac{Y_1}{S_0}-\frac{Y_0S_1}{S_0^2}\right)\right]_{\alpha_2}\tau^{\frac{1}{2}}H(\tau)\doteq {}_{\beta}W^{(5)}_{\alpha_2}\times\alpha_2/\widehat{\beta_1\alpha_2},
\end{aligned}\right.$$

where $$\tau = t-x/\alpha_2-(H-h)/\widehat{\alpha_1\alpha_2}-(H+z)/\widehat{\beta_1\alpha_2};$$

$$\left|\begin{aligned}
{}_{\beta}V^{(6)}_{\alpha_2} &\doteq \frac{-\sqrt{(2\pi i)}\,\alpha_2^2\widehat{\alpha_1\alpha_2}}{[x\alpha_2-(H+h)\,\widehat{\alpha_1\alpha_2}-(H-z)\,\widehat{\beta_1\alpha_2}]^{\frac{1}{2}}}\left[\frac{F_0}{F_0}\left(\frac{Y_1}{S_0}-\frac{Y_0S_1}{S_0^2}\right)\right]_{\alpha_2}\omega^{-\frac{1}{2}}\exp\{i\omega\tau\},\\
{}_{\beta}U^{(6)}_{\alpha_2} &\doteq \frac{2\sqrt{2}\,\widehat{\alpha_1\alpha_2}\,\alpha_2^2}{\widehat{\beta_1\alpha_2}[x\alpha_2-(H+h)\,\widehat{\alpha_1\alpha_2}-(H-z)\,\widehat{\beta_1\alpha_2}]^{\frac{1}{2}}}\left[\frac{F_0}{F_0}\left(\frac{Y_1}{S_0}-\frac{Y_0S_1}{S_0^2}\right)\right]_{\alpha_2}\tau^{\frac{1}{2}}H(\tau)\doteq -{}_{\beta}W^{(6)}_{\alpha_2}\times\alpha_2/\widehat{\beta_1\alpha_2},
\end{aligned}\right.$$

where $$\tau = t-x/\alpha_2-(H+h)/\widehat{\alpha_1\alpha_2}-(H-z)/\widehat{\beta_1\alpha_2};$$

$$\left|\begin{aligned}
{}_{\beta}V^{(7)}_{\alpha_2} &\doteq \frac{\sqrt{(2\pi i)}\,\alpha_2^2\widehat{\alpha_1\alpha_2}}{[x\alpha_2-(H+h)\,\widehat{\alpha_1\alpha_2}-(H+z)\,\widehat{\beta_1\alpha_2}]^{\frac{1}{2}}}\left[\left(\frac{F_0^2}{F_0^2}-\frac{16\alpha_2^6(2/\alpha_2^2-1/\beta_1^2)^2}{\widehat{\alpha_1\alpha_2}\widehat{\beta_1\alpha_2}F_0^2}\right)\left(\frac{Y_1}{S_0}-\frac{Y_0S_1}{S_0^2}\right)\right]_{\alpha_2}\omega^{-\frac{1}{2}}\exp\{i\omega\tau\},\\
{}_{\beta}U^{(7)}_{\alpha_2} &\doteq \frac{2\sqrt{2}\,\widehat{\alpha_1\alpha_2}\,\alpha_2^2}{\widehat{\beta_1\alpha_2}[x\alpha_2-(H+h)\,\widehat{\alpha_1\alpha_2}-(H+z)\,\widehat{\beta_1\alpha_2}]^{\frac{1}{2}}}\left[\left(\frac{F_0^2}{F_0^2}-\frac{16\alpha_2^6(2/\alpha_2^2-1/\beta_1^2)^2}{\widehat{\alpha_1\alpha_2}\widehat{\beta_1\alpha_2}F_0^2}\right)\left(\frac{Y_1}{S_0}-\frac{Y_0S_1}{S_0^2}\right)\right]_{\alpha_2}\tau^{\frac{1}{2}}H(\tau)\\
&\quad\doteq {}_{\beta}W^{(7)}_{\alpha_2}\times\alpha_2/\widehat{\beta_1\alpha_2},
\end{aligned}\right.$$

where $$\tau = t-x/\alpha_2-(H+h)/\widehat{\alpha_1\alpha_2}-(H+z)/\widehat{\beta_1\alpha_2};$$

$$\left|\begin{aligned}
{}_{\beta}V^{(8)}_{\alpha_2} &\doteq \frac{-4\sqrt{(2\pi i^3)}\,\alpha_2^5(2/\alpha_2^2-1/\beta_1^2)}{[x\alpha_2-(2H-h)\,\widehat{\alpha_1\alpha_2}-z\widehat{\beta_1\alpha_2}]^{\frac{1}{2}}}\left[\frac{1}{F_0}\left(\frac{W_1}{S_0}-\frac{W_0S_1}{S_0^2}\right)\right]_{\alpha_2}\omega^{-\frac{1}{2}}\exp\{i\omega\tau\},\\
{}_{\beta}U^{(8)}_{\alpha_2} &\doteq \frac{-8\sqrt{2}\,i\,\alpha_2^5(2/\alpha_2^2-1/\beta_1^2)}{\widehat{\beta_1\alpha_2}[x\alpha_2-(2H-h)\,\widehat{\alpha_1\alpha_2}-z\widehat{\beta_1\alpha_2}]^{\frac{1}{2}}}\left[\frac{1}{F_0}\left(\frac{W_1}{S_0}-\frac{W_0S_1}{S_0^2}\right)\right]_{\alpha_2}\tau^{\frac{1}{2}}H(\tau)\doteq {}_{\beta}W^{(8)}_{\alpha_2}\times\alpha_2/\widehat{\beta_1\alpha_2},
\end{aligned}\right.$$

where $$\tau = t-x/\alpha_2-(2H-h)/\widehat{\alpha_1\alpha_2}-z/\widehat{\beta_1\alpha_2};$$

$$\left|\begin{aligned}
{}_{\beta}V^{(9)}_{\alpha_2} &\doteq \frac{4\sqrt{(2\pi i^3)}\,\alpha_2^5(2/\alpha_2^2-1/\beta_1^2)}{[x\alpha_2-(2H+h)\,\widehat{\alpha_1\alpha_2}-z\widehat{\beta_1\alpha_2}]^{\frac{1}{2}}}\left[\frac{F_0}{F_0^2}\left(\frac{W_1}{S_0}-\frac{W_0S_1}{S_0^2}\right)\right]_{\alpha_2}\omega^{-\frac{1}{2}}\exp\{i\omega\tau\},\\
{}_{\beta}U^{(9)}_{\alpha_2} &\doteq \frac{8\sqrt{2}\,i\,\alpha_2^5(2/\alpha_2^2-1/\beta_1^2)}{\widehat{\beta_1\alpha_2}[x\alpha_2-(2H+h)\,\widehat{\alpha_1\alpha_2}-z\widehat{\beta_1\alpha_2}]^{\frac{1}{2}}}\left[\frac{F_0}{F_0}\left(\frac{W_1}{S_0}-\frac{W_0S_1}{S_0^2}\right)\right]_{\alpha_2}\tau^{\frac{1}{2}}H(\tau)\doteq {}_{\beta}W^{(9)}_{\alpha_2}\times\alpha_2/\widehat{\beta_1\alpha_2},
\end{aligned}\right.$$

where $$\tau = t-x/\alpha_2-(2H+h)/\widehat{\alpha_1\alpha_2}-z/\widehat{\beta_1\alpha_2}.$$

${}_s\phi$ contributions from Γ_{α_2}

$$\begin{cases} {}_s\phi^{(2)}_{\alpha_2} \doteq \dfrac{4\sqrt{(2\pi i^3)}\,\alpha_2^5(2/\alpha_2^2-1/\beta_1^2)}{[x\alpha_2-z\widehat{\alpha_1\alpha_2}-(2H-h)\widehat{\beta_1\alpha_2}]^{\frac{1}{2}}}\left[\frac{T_1}{S_0}-\frac{T_0S_1}{S_0^2}\right]_{\alpha_2}\omega^{-\frac{1}{2}}\exp\{i\omega\tau\}, \\ {}_sU^{(2)}_{\alpha_2} \doteq \dfrac{8\sqrt{2}\,i\,\alpha_2^4(2/\alpha_2^2-1/\beta_1^2)}{[x\alpha_2-z\widehat{\alpha_1\alpha_2}-(2H-h)\widehat{\beta_1\alpha_2}]^{\frac{1}{2}}}\left[\frac{T_1}{S_0}-\frac{T_0S_1}{S_0^2}\right]_{\alpha_2,0}\tau^{\frac{1}{2}}H(\tau) \doteq {}_sW^{(2)}_{\alpha_2}\times\widehat{\alpha_1\alpha_2}/\alpha_2, \end{cases}$$

where $$\tau = t-x/\alpha_2-z/\widehat{\alpha_1\alpha_2}-(2H-h)/\widehat{\beta_1\alpha_2};$$

and similarly

$${}_s\phi^{(2)}_{\alpha_2} \doteq (-1)\times\ldots,\quad {}_sU^{(3)}_{\alpha_2} \doteq (-1)\times\ldots,\quad {}_sW^{(3)}_{\alpha_2} \doteq (-1)\times\ldots,$$

with $(2H+h)$ for $(2H-h)$ and $[(T_1/S_0-T_0S_1/S_0^2)\,\overline{F}_0/F_0]$ for $[T_1/S_0-T_0S_1/S_0^2]$:

$$\begin{cases} {}_s\phi^{(4)}_{\alpha_2} \doteq \dfrac{-\sqrt{(2\pi i)}\,\widehat{\alpha_1\alpha_2}\,\alpha_2^2}{[x\alpha_2-(H-z)\widehat{\alpha_1\alpha_2}-(H-h)\widehat{\beta_1\alpha_2}]^{\frac{1}{2}}}\left[\frac{Y_1}{S_0}-\frac{Y_0S_1}{S_0^2}\right]_{\alpha_2}\omega^{-\frac{1}{2}}\exp\{i\omega\tau\}, \\ {}_sU^{(4)}_{\alpha_2} \doteq \dfrac{-2\sqrt{2}\,\widehat{\alpha_1\alpha_2}\,\alpha_2}{[x\alpha_2-(H-z)\widehat{\alpha_1\alpha_2}-(H-h)\widehat{\beta_1\alpha_2}]^{\frac{1}{2}}}\left[\frac{Y_1}{S_0}-\frac{Y_0S_1}{S_0^2}\right]_{\alpha_2,0}\tau^{\frac{1}{2}}H(\tau) \doteq -{}_sW^{(4)}_{\alpha_2}\times\widehat{\alpha_1\alpha_2}/\alpha_2, \end{cases}$$

where $$\tau = t-x/\alpha_2-(H-z)/\widehat{\alpha_1\alpha_2}-(H-h)/\widehat{\beta_1\alpha_2};$$

and similarly

$${}_s\phi^{(5)}_{\alpha_2} \doteq (-1)\times\ldots,\quad {}_sU^{(5)}_{\alpha_2} \doteq (-1)\times\ldots,\quad {}_sW^{(5)}_{\alpha_2} \doteq (-1)\times\ldots,$$

with $(H+h)$ for $(H-h)$ and $[(Y_1/S_0-Y_0S_1/S_0^2)\,\overline{F}_0/F_0]$ for $[Y_1/S_0-Y_0S_1/S_0^2]$,

$${}_s\phi^{(6)}_{\alpha_2} \doteq (-1)\times\ldots,\quad {}_sU^{(6)}_{\alpha_2} \doteq (-1)\times\ldots,\quad {}_sW^{(6)}_{\alpha_2} \doteq (+1)\times\ldots,$$

with $(H+z)$ for $(H-z)$ and $[(Y_1/S_0-Y_0S_1/S_0^2)\,\overline{F}_0/F_0]$ for $[Y_1/S_0-Y_0S_1/S_0^2]$,

$${}_s\phi^{(7)}_{\alpha_2} \doteq (+1)\times\ldots,\quad {}_sU^{(7)}_{\alpha_2} \doteq (+1)\times\ldots,\quad {}_sW^{(7)}_{\alpha_2} \doteq (-1)\times\ldots,$$

with $(H+h)$ for $(H-h)$, $(H+z)$ for $(H-z)$

and

$[(Y_1/S_0-Y_0S_1/S_0^2)\,(\overline{F}_0^2/F_0^2-16\{2/\alpha_2^2-1/\beta_1^2\}^2\,\alpha_2^6/\widehat{\alpha_1\alpha_2}\widehat{\beta_1\alpha_2}F_0^2)]$ for $[Y_1/S_0-Y_0S_1/S_0^2]$;

$$\begin{cases} {}_s\phi^{(8)}_{\alpha_2} \doteq \dfrac{4\sqrt{(2\pi i^3)}\,(2/\alpha_2^2-1/\beta_1^2)\,\alpha_2^5}{[x\alpha_2-(2H-z)\widehat{\alpha_1\alpha_2}-h\widehat{\beta_1\alpha_2}]^{\frac{1}{2}}}\left[\frac{1}{\overline{F}_0}\left(\frac{W_1}{S_0}-\frac{W_0S_1}{S_0^2}\right)\right]_{\alpha_2}\omega^{-\frac{1}{2}}\exp\{i\omega\tau\}, \\ {}_sU^{(8)}_{\alpha_2} \doteq \dfrac{8\sqrt{2}\,i\,(2/\alpha_2^2-1/\beta_1^2)\,\alpha_2^4}{[x\alpha_2-(2H-z)\widehat{\alpha_1\alpha_2}-h\widehat{\beta_1\alpha_2}]^{\frac{1}{2}}}\left[\frac{1}{\overline{F}_0}\left(\frac{W_1}{S_0}-\frac{W_0S_1}{S_0^2}\right)\right]_{\alpha_2,0}\tau^{\frac{1}{2}}H(\tau) \doteq -{}_sW^{(8)}_{\alpha_2}\times\widehat{\alpha_1\alpha_2}/\alpha_2, \end{cases}$$

where $$\tau = t-x/\alpha_2-(2H-z)/\widehat{\alpha_1\alpha_2}-h/\widehat{\beta_1\alpha_2};$$

and similarly

$${}_s\phi^{(9)}_{\alpha_2} \doteq (-1)\times\ldots,\quad {}_sU^{(9)}_{\alpha_2} \doteq (-1)\times\ldots,\quad {}_sW^{(9)}_{\alpha_2} \doteq (+1)\times\ldots,$$

with $(2H+z)$ for $(2H-z)$ and $[\overline{F}_0/F_0^2]$ for $[1/F_0]$.

${}_s\Psi$ contributions from Γ_{α_2}

$$\begin{cases} {}_s\Psi^{(2)}_{\alpha_2} \doteq \dfrac{-16\sqrt{(2\pi i^3)}\,\alpha_2^8(2/\alpha_2^2-1/\beta_1^2)^2}{\widehat{\alpha_1\alpha_2}[x\alpha_2-2H\widehat{\alpha_1\alpha_2}-(h+z)\widehat{\beta_1\alpha_2}]^{\frac{1}{2}}}\left[\dfrac{1}{F_0}\left(\dfrac{W_1}{S_0}-\dfrac{W_0S_1}{S_0^2}\right)\right]_{\alpha_2}\omega^{-\frac{1}{2}}\exp\{i\omega\tau\}, \\ {}_sU^{(2)}_{\alpha_2} \doteq \dfrac{-32\sqrt{2}\,i\,\alpha_2^8(2/\alpha_2^2-1/\beta_1^2)^2}{\widehat{\alpha_1\alpha_2}\widehat{\beta_1\alpha_2}[x\alpha_2-2H\widehat{\alpha_1\alpha_2}-(h+z)\widehat{\beta_1\alpha_2}]^{\frac{1}{2}}}\left[\dfrac{1}{F_0}\left(\dfrac{W_1}{S_0}-\dfrac{W_0S_1}{S_0^2}\right)\right]_{\alpha_2,0}\tau^{\frac{1}{2}}H(\tau) \doteq -{}_sW^{(2)}_{\alpha_2}\times\widehat{\alpha_1\alpha_2}/\alpha_2, \end{cases}$$

where $$\tau = t-x/\alpha_2-2H/\widehat{\alpha_1\alpha_2}-(h+z)/\widehat{\beta_1\alpha_2},$$

$$\begin{cases} {}_s\Psi^{(3)}_{\alpha_2} \doteq \dfrac{4\sqrt{(2\pi i)}\,\alpha_2^5(2/\alpha_2^2-1/\beta_1^2)}{[x\alpha_2-H\widehat{\alpha_1\alpha_2}-(H+h-z)\widehat{\beta_1\alpha_2}]^{\frac{1}{2}}}\left[\dfrac{1}{F_0}\left(\dfrac{Y_1}{S_0}-\dfrac{Y_0S_1}{S_0^2}\right)\right]_{\alpha_2}\omega^{-\frac{1}{2}}\exp\{i\omega\tau\}, \\ {}_sU^{(3)}_{\alpha_2} \doteq \dfrac{-8\sqrt{2}\,\alpha_2^5(2/\alpha_2^2-1/\beta_1^2)}{\widehat{\beta_1\alpha_2}[x\alpha_2-H\widehat{\alpha_1\alpha_2}-(H+h-z)\widehat{\beta_1\alpha_2}]^{\frac{1}{2}}}\left[\dfrac{1}{F_0}\left(\dfrac{Y_1}{S_0}-\dfrac{Y_0S_1}{S_0^2}\right)\right]_{\alpha_2,0}\tau^{\frac{1}{2}}H(\tau) = {}_sW^{(3)}_{\alpha_2}\times\widehat{\alpha_1\alpha_2}/\alpha_2, \end{cases}$$

where $$\tau = t-x/\alpha_2-H/\widehat{\alpha_1\alpha_2}-(H+h-z)/\widehat{\beta_1\alpha_2},$$

and similarly
$${}_s\Psi^{(4)}_{\alpha_2} \doteq (+1)\times\ldots,\quad {}_sU^{(4)}_{\alpha_2} \doteq (-1)\times\ldots,\quad {}_sW^{(4)}_{\alpha_2} \doteq (+1)\times\ldots,$$
with $$(H-h+z) \quad \text{for} \quad (H+h-z),$$
$${}_s\Psi^{(5)}_{\alpha_2} \doteq (-2)\times\ldots,\quad {}_sU^{(5)}_{\alpha_2} \doteq (+2)\times\ldots,\quad {}_sW^{(5)}_{\alpha_2} \doteq (-2)\times\ldots,$$
with $$(H+h+z) \text{ for } (H+h-z) \quad \text{and} \quad [\overline{F_0}/F_0^2] \text{ for } [1/F_0];$$

$$\begin{cases} {}_s\Psi^{(6)}_{\alpha_2} \doteq \dfrac{\sqrt{(2\pi i^3)}\,\alpha_2^2\widehat{\beta_1\alpha_2}}{[x\alpha_2-(2H-h-z)\widehat{\beta_1\alpha_2}]^{\frac{1}{2}}}\left[\dfrac{T_1}{S_0}-\dfrac{T_0S_1}{S_0^2}\right]_{\alpha_2}\omega^{-\frac{1}{2}}\exp\{i\omega\tau\}, \\ {}_sU^{(6)}_{\alpha_2} \doteq \dfrac{-2\sqrt{2}\,i\,\alpha_2^2}{[x\alpha_2-(2H-h-z)\widehat{\beta_1\alpha_2}]^{\frac{1}{2}}}\left[\dfrac{T_1}{S_0}-\dfrac{T_0S_1}{S_0^2}\right]_{\alpha_2,0}\tau^{\frac{1}{2}}H(\tau) \doteq {}_sW^{(6)}_{\alpha_2}\times\alpha_2/\widehat{\beta_1\alpha_2}, \end{cases}$$

where $$\tau = t-x/\alpha_2-(2H-h-z)/\widehat{\beta_1\alpha_2},$$

and similarly
$${}_s\Psi^{(7)}_{\alpha_2} \doteq (-1)\times\ldots,\quad {}_sU^{(7)}_{\alpha_2} \doteq (-1)\times\ldots,\quad {}_sW^{(7)}_{\alpha_2} \doteq (-1)\times\ldots,$$
with $$(2H+h-z) \quad \text{for} \quad (2H-h-z)$$
and $$[(T_1/S_0-T_0S_1/S_0^2)\,\overline{F}_0/F_0] \quad \text{for} \quad [T_1/S_0-T_0S_1/S_0^2],$$
$${}_s\Psi^{(8)}_{\alpha_2} \doteq (-1)\times\ldots,\quad {}_sU^{(8)}_{\alpha_2} \doteq (+1)\times\ldots,\quad {}_sW^{(8)}_{\alpha_2} \doteq (-1)\times\ldots,$$
with $$(2H-h+z) \quad \text{for} \quad (2H-h-z)$$
and $$[(T_1/S_0-T_0S_1/S_0^2)\,\overline{F}_0/F_0] \quad \text{for} \quad [T_1/S_0-T_0S_1/S_0^2],$$
$${}_s\Psi^{(9)}_{\alpha_2} \doteq (+1)\times\ldots,\quad {}_sU^{(9)}_{\alpha_2} \doteq (-1)\times\ldots,\quad {}_sW^{(9)}_{\alpha_2} \doteq (+1)\times\ldots,$$
with $$(2H+h+z) \quad \text{for} \quad (2H-h-z)$$
and $$[(T_1/S_0-T_0S_1/S_0^2)\,\overline{F}_0^2/F_0^2] \quad \text{for} \quad [T_1/S_0-T_0S_1/S_0^2].$$

APPENDIX II

COMPUTER PROGRAM

This program calculates the amplitude ratios of the vertical components of the various phases of Figure 17 to the vertical component of P_n and the amplitude ratios of the horizontal components of the phases of Figure 17 to the horizontal component of P_n. The program is written in FORTRAN for use on a CDC 3300 computer and was written to handle three crustal structures at a time.

Input

Card 1. FORMAT (5F10.2) - layer parameters for the first crustal section in the order H, P_1, S_1, P_2, S_2.

Card 2 FORMAT (5F10.2) - layer parameters for the second crustal section.

Card 3 FORMAT (5F10.2) - layer parameters for the third crustal section.

Output

The output consists of the amplitude ratios for epicentral distances from 200 to 1000 km calculated for each 100 km interval. Also, for each epicentral distance, the ratios are calculated for source depths of from .1H to .9H at intervals of .1H (H = crustal thickness). The output is in the printed form.

The FORTRAN listings for this program follows:

```
$ IPUD  1                    0
$
$
      PROGRAM MATRIX
  200 FORMAT(15H LAYER MATRICES)
  201 FORMAT(38H HEAD WAVE AND REFLECTION COEFFICIENTS)
  100 FORMAT(1H ,5HP1 = ,F5.2/6H S1 = ,F5.2/6H P2 = ,F5.2/6H S2 = ,F5.2/
     18H RH01 = ,F5.2/8H RH02 = ,F5.2///)
  101 FORMAT(1H ,5HS0 = ,F9.3/6H S1 = ,F9.3/6H W0 = ,F9.3/6H W1 = ,F9.3/
     16H T0 = ,F9.3/6H T1 = ,F9.3/6H Y0 = ,F9.3/6H Y1 = ,F9.3/
     26H F0 = ,F9.3/7H F0B = ,F9.3///)
  102 FORMAT(1H ,6HHPP = ,F9.3/7H HPS = ,F9.3/7H HSS = ,F9.3/7H HSP = ,
     1F9.3/7H RPP = ,F9.3/7H RPS = ,F9.3/7H RSP = ,F9.3/7H RSS = ,F9.3)
  300 FORMAT(33H TOTAL PN VERTICAL    AMPLITUDE = ,E9.2)
  301 FORMAT(33H TOTAL PN HORIZONTAL AMPLITUDE = ,E9.2)
  302 FORMAT(41H THE NORMALIZED HORIZONTAL AMPLITUDES ARE///
     112H P1P2S1    = ,F7.3/12H S1P2S1    = ,F7.3/12H S1P2P1    = ,F7.3/
     212H P1P1P2P1  = ,F7.3/12H P1P1P2S1  = ,F7.3/12H P1S1P2P1  = ,F7.3/
     312H P1S1P2S1  = ,F7.3/12H S1P1P2P1  = ,F7.3/12H S1P1P2S1  = ,F7.3/
     412H S1S1P2P1  = ,F7.3/12H S1S1P2S1  = ,F7.3)
  303 FORMAT(41H THE NORMALIZED VERTICAL   AMPLITUDES ARE///
     112H P1P2S1    = ,F7.3/12H S1P2S1    = ,F7.3/12H S1P2P1    = ,F7.3/
     212H P1P1P2P1  = ,F7.3/12H P1P1P2S1  = ,F7.3/12H P1S1P2P1  = ,F7.3/
     312H P1S1P2S1  = ,F7.3/12H S1P1P2P1  = ,F7.3/12H S1P1P2S1  = ,F7.3/
     412H S1S1P2P1  = ,F7.3/12H S1S1P2S1  = ,F7.3)
  500 FORMAT(46H THE FOLLOWING RESULTS ARE FOR SOURCE DEPTH = ,F6.1)
  501 FORMAT(23H EPICENTRAL DISTANCE = ,F7.1)
  520 FORMAT(5F10.2)
      DO 600 K=1,3
      READ 520,H,P1,S1,P2,S2
      D1=.374*(1.+P1)
      D2=.374*(1.+P2)
      R1=D1*S1*S1
      R2=D2*S2*S2
      PP=P1*P2/SQRT(P2*P2-P1*P1)
      S1P=S1*P2/SQRT(P2*P2-S1*S1)
      S2P=S2*P2/SQRT(P2*P2-S2*S2)
      VP=P2/PP
      VS=S1P/P2
      A11=P2/PP
      A12=-1.
      A13=-1.
      A21=-2.*P2/PP
      A22=2.-(P2*P2)/(S1*S1)
      A23=(2.-(P2*P2)/(S2*S2))*R2/R1
      A31=A22
      A32=-2.*P2/S1P
      A33=2.*P2*R2/(S2P*R1)
      B11=-1.
      B12=P2/S1P
      B13=-P2/S2P
      B21=A11
      B22=-1.
      B23=-1.
```

```
 B31=A21
 B32=A22
 B33=A23
 DS0=-(-A11*A22*A33+A11*A32*A23+A21*A12*A33-A21*A32*A13+A31*A12*A23
1-A31*A22*A13)-A23*(B11*B22*B33-B11*B32*B23+B21*B12*B33-B21*B32*B13
2-B31*B12*B23+B31*B22*B13)
 A11=-A11
 A21=-A21
 B21=-B21
 B31=-B31
 W0 =-(-A11*A22*A33+A11*A32*A23+A21*A12*A33-A21*A32*A13+A31*A12*A23
1-A31*A22*A13)-A23*(B11*B22*B33-B11*B32*B23+B21*B12*B33-B21*B32*B13
2-B31*B12*B23+B31*B22*B13)
 A11=-A11
 A21=-A21
 B21=-B21
 B31=-B31
 A32=-A32
 B12=-B12
 T0 =-(-A11*A22*A33+A11*A32*A23+A21*A12*A33-A21*A32*A13+A31*A12*A23
1-A31*A22*A13)-A23*(B11*B22*B33-B11*B32*B23+B21*B12*B33-B21*B32*B13
2-B31*B12*B23+B31*B22*B13)
 A32=-A32
 B12=-B12
 C11=B11
 C12=B12
 C13=B13
 C21=A21
 C22=A22
 C23=A23
 C31=A31
 C32=A32
 C33=A33
 D11=B11
 D12=B12
 D13=B13
 D21=A11
 D22=A12
 D23=A13
 D31=A31
 D32=A32
 D33=A33
 DS1=C11*C22*C33-C11*C32*C23+C21*C12*C33
1-C21*C32*C13+C31*C12*C23-C31*C22*C13+(2.*R2/R1)*(D11*D22*D33
2-D11*D32*D23+D21*D12*D33-D21*D32*D13+D31*D12*D23-D31*D22*D13)
 C21=-C21
 D21=-D21
 W1 =C11*C22*C33-C11*C32*C23+C21*C12*C33
1-C21*C32*C13+C31*C12*C23-C31*C22*C13+(2.*R2/R1)*(D11*D22*D33
2-D11*D32*D23+D21*D12*D33-D21*D32*D13+D31*D12*D23-D31*D22*D13)
 C21=-C21
 D21=-D21
 C12=-C12
 C32=-C32
```

```
      D12=-D12
      D32=-D32
      T1 =C11*C22*C33-C11*C32*C23+C21*C12*C33
     1-C21*C32*C13+C31*C12*C23-C31*C22*C13+(2.*R2/R1)*(D11*D22*D33
     2-D11*D32*D23+D21*D12*D33-D21*D32*D13+D31*D12*D23-D31*D22*D13)
      C12=-C12
      C32=-C32
      D12=-D12
      D32=-D32
      E11=-A11
      E12=A11
      E13=-1.
      E21=-A21
      E22=A21
      E23=A23
      E31=A31
      E32=A31
      E33=A33
      F11=-1.
      F12=-1.
      F13=B13
      F21=E11
      F22=E12
      F23=E13
      F31=E21
      F32=E22
      F33=E23
      YO=-(-E11*E22*E33-E11*E32*E23+E21*E12*E33+E21*E32*E13
     1+E31*E12*E23-E31*E22*E13)+E23*(F11*F22*F33-F11*F32*F23
     2-F21*F12*F33-F21*F32*F13+F31*F12*F23+F31*F22*F13)
      G11=F11
      G12=F12
      G13=F13
      G21=E21
      G22=E22
      G23=E23
      G31=E31
      G32=E32
      G33=E33
      H11=F11
      H12=F12
      H13=F13
      H21=F21
      H22=F22
      H23=F23
      H31=E31
      H32=E32
      H33=E33
      Y1=(+G11*G22*G33+G11*G32*G23-G21*G12*G33+G21*G32*G13
     1-G31*G12*G23-G31*G22*G13)+(2.*R2/R1)*(-H11*H22*H33
     2-H11*H32*H23+H21*H12*H33-H21*H32*H13+H31*H12*H23+H31*H22*H13)
      FO=(2.-P2*P2/(S1*S1))*(2.-P2*P2/(S1*S1))+4.*P2*P2/(PP*S1P)
      FOB=(2.-P2*P2/(S1*S1))*(2.-P2*P2/(S1*S1))-4.*P2*P2/(PP*S1P)
      PRINT 100,P1,S1,P2,S2,D1,D2
```

```
PRINT 200,
PRINT 101,DSO,DS1,WO,W1,TO,T1,YO,Y1,FO,FOB
HPP=-PP*P2*P2*(W1/DSO-WO*DS1/(DSO*DSO))/P1
HPS=-PP*P2*P2*(Y1/DSO+YO*DS1/(DSO*DSO))/S1
HSS=S1P*P2*P2*(T1/DSO-TO*DS1/(DSO*DSO))/S1
HSP=-PP*P2*P2*(Y1/DSO+YO*DS1/(DSO*DSO))/P1
RPP=-FOB/FO
RPS=(P1/S1)*4.*P2*P2*P2*(2./(P2*P2)-1./(S1*S1))/(PP*FO)*(-1.)
RSP=-(S1/P1)*4.*P2*P2*P2*(2./(P2*P2)-1./(S1*S1))/(S1P*FO)
RSS=+FOB/FO
PRINT 201,
PRINT 102,HPP,HPS,HSS,HSP,RPP,RPS,RSP,RSS
HP=P1/P2
HS=S1/S1P
RE=S1P*P1/(S1*PP)
RH=PP*S1/(P1*S1P)
DO 600 J=2,10
BBB=J
X=100.*BBB
DO 600 I=1,5
CCC=I
D=H*(.2*CCC-.1)
PRINT 500,D
PRINT 501,X
AL1=X*P2-(2.*H-D)*PP
BL1=AL1**1.5
CL1=AL1/P2
U11=HPP*HP/BL1
U12=HPP*RPP*HP/BL1
U13=HPP*RPS*HS/BL1
AL2=X*P2-(H-D)*PP-H*S1P
BL2=AL2**1.5
CL2=AL2/P2
U21=HPS*HS/BL2
U22=HPS*RSP*HP/BL2
U23=HPS*RSS*HS/BL2
AL3=X*P2-(2.*H-D)*S1P
BL3=AL3**1.5
CL3=AL3/P2
U31=HSS*HS/BL3
U32=HSS*RSP*HP/BL3
U33=HSS*RSS*HS/BL3
AL4=X*P2-H*PP-(H-D)*S1P
BL4=AL4**1.5
CL4=AL4/P2
U41=HSP*HP/BL4
U42=HSP*RPP*HP/BL4
U43=HSP*RPS*HS/BL4
AL5=X*P2-(2.*H+D)*PP
BL5=AL5**1.5
CL5=AL5/P2
U51=RPP*U11*BL1/BL5
U52=RPP*U12*BL1/BL5
U53=RPP*U13*BL1/BL5
```

```
AL6=X*P2-(H+D)*PP-H*S1P
BL6=AL6**1.5
CL6=AL6/P2
U61=RPP*U21*BL2/BL6
U62=RPP*U22*BL2/BL6
U63=RPP*U23*BL2/BL6
AL7=X*P2-(H+D)*PP-H*S1P
BL7=AL7**1.5
CL7=AL7/P2
U71=RPS*RH*U41*BL4/BL7
U72=RPS*RH*U42*BL4/BL7
U73=RPS*RH*U43*BL4/BL7
AL8=X*P2-2.*H*S1P-D*PP
BL8=AL8**1.5
CL8=AL8/P2
U81=RPS*RH*U31*BL3/BL8
U82=RPS*RH*U32*BL3/BL8
U83=RPS*RH*U33*BL3/BL8
AL9=X*P2-2.*H*PP-D*S1P
BL9=AL9**1.5
CL9=AL9/P2
U91=-1.*RSP*RE*U11*BL1/BL9
U92=-1.*RSP*RE*U12*BL1/BL9
U93=-1.*RSP*RE*U13*BL1/BL9
AL10=X*P2-H*PP-(H+D)*S1P
BL10=AL10**1.5
CL10=AL10/P2
U101=-1.*RSP*RE*U21*BL2/BL10
U102=-1.*RSP*RE*U22*BL2/BL10
U103=-1.*RSP*RE*U23*BL2/BL10
AL11=X*P2-H*PP-(H+D)*S1P
BL11=AL11**1.5
CL11=AL11/P2
U111=-1.*RSS*U41*BL4/BL11
U112=-1.*RSS*U42*BL4/BL11
U113=-1.*RSS*U43*BL4/BL11
AL12=X*P2-H*PP-(H+D)*S1P
BL12=AL12**1.5
CL12=AL12/P2
U121=-1.*RSS*U31*BL3/BL12
U122=-1.*RSS*U32*BL3/BL12
U123=-1.*RSS*U33*BL3/BL12
U1=U11+U12+U13
AU2=(U21+U22+U23)/U1
AU3=(U31+U32+U33)/U1
AU4=(U41+U42+U43)/U1
AU5=(U51+U52+U53)/U1
AU6=(U61+U62+U63)/U1
AU7=(U71+U72+U73)/U1
AU8=(U81+U82+U83)/U1
AU9=(U91+U92+U93)/U1
AU10=(U101+U102+U103)/U1
AU11=(U111+U112+U113)/U1
AU12=(U121+U122+U123)/U1
```

```
      W1=U11*VP-U12*VP+U13*VS
      AW2=(-U21*VS-U22*VP+U23*VS)/W1
      AW3=(-U31*VS-U32*VP+U33*VS)/W1
      AW4=(+U41*VP-U42*VP+U43*VS)/W1
      AW5=(+U51*VP-U52*VP+U53*VS)/W1
      AW6=(-U61*VS-U62*VP+U63*VS)/W1
      AW7=(+U71*VP-U72*VP+U73*VS)/W1
      AW8=(-U81*VS-U82*VP+U83*VS)/W1
      AW9=(+U91*VP-U92*VP+U93*VS)/W1
      AW10=(-U101*VS-U102*VP+U103*VS)/W1
      AW11=(+U111*VP-U112*VP+U113*VS)/W1
      AW12=(-U121*VS-U122*VP+U123*VS)/W1
      PRINT 300,W1
      PRINT 303,AW2,AW3,AW4,AW5,AW6,AW7,AW8,AW9,AW10,AW11,AW12
      PRINT 301,U1
  600 PRINT 302,AU2,AU3,AU4,AU5,AU6,AU7,AU8,AU9,AU10,AU11,AU12
      END
      EOF
27554515
    0288
```